Universitat de Barcelona
Departament de Física Fonamental
Facultat de Física

Spherical Gravitational Wave Detectors

José Antonio Ortega Ruiz
April 14th, 1997

Summary

Chapter 1

Introduction

1.1 Historical context

The General theory of Relativity, proposed by A. Einstein in 1916 [44], supposed a breakthrough in our conceptual understanding of physical phenomena and their interrelationship with space and time. The new, active part played by space–time in the description of gravitational interactions demanded not only a radical departure from Newtonian conceptions, but also the introduction of a new mathematical language—differential geometry—which eventually spread across many other branches of fundamental physics.

General Relativity offered a theoretical framework of great conceptual richness, which was the outcome of basically only three clear–cut, elegant principles: general covariance, principle of equivalence and geodesic postulate. In his seminal work of 1916, Einstein also presented *observational* implications of General Relativity, explaining the well–known but ill–understood anomalies in the motion of the perihelion of Mercury, and predicting new phenomena—bending of light rays—which soon had a striking experimental confirmation in Eddington's observations of solar eclipses [40, 99]. A third effect predicted by Einstein—red shift of spectral lines—also received partial confirmation from experiment in those early years [99], although it was not unambiguously observed until the experiments of Pound and Rebka in the sixties [100]. These three effects conform the so–called classical tests of General Relativity.

In spite of its initial success, observational General Relativity fell in what has been called a 'hibernation' period between 1920 and 1960. While theorists were faced with mathematical complexity of the non–linear Einstein equations, the field of experimental

gravitation seemed to be exhausted. For, their conceptual divergency notwithstanding, Einstein's and Newton's theories lead to virtually the same predictions when dealing with weak gravitational fields, such as the Earth's or the Solar system's. Apart from the aformentioned three *classical* effects, relativistic corrections to Newtonian mechanics laid far beyond observation.

Among these 'unobservable' consequences of General Relativity was one more of Einstein's earlier predictions: the existence of gravitational waves, ensuing from the finite velocity of propagation of gravitational interactions. As he himself pointed out [45, 46], the linearized equations of the gravitational field admit radiative solutions, analogous to those describing electromagnetic waves in Maxwell's theory, and propagating with the velocity of light. Einstein was also able to show that gravitational waves have two physical degrees of freedom and to compute the power radiated by non–self–gravitating, slow–motion masses. This calculation made evident the extreme weakness of any likely gravitational waves bathing the Earth from any astronomical source known at that time, and put out of the question their generation in laboratory. Thus, this subject became exclusively a matter of theoretical discussion for many years. Weyl [128] and Eddington [42] elaborated on Einstein's initial work, giving a full description of the linear theory of gravitational waves by the mid twenties. The issue of radiation emission by self–gravitating systems was first tackled successfully by Landau and Lifshitz in 1941 [73]. It was not until the work by Bondi [17] in 1957 that gravitational waves were generally accepted as a potentially measurable physical phenomenon, implying energy transport, instead of the mere coordinate effect suggested by other authors. Later work in the sixties, due largely to Hartle and Brill [19] and to Isaacson [65, 66], finally provided a solid mathematical basis to describe the energy transport by gravitational waves.

It was at this period that Weber started his pioneering work on resonant gravitational wave detectors. His original idea [122] was to measure the oscillations induced in a rigid solid by a passing gravitational wave. After making a first attempt at a theoretical description of the interaction between elastic solids and weak gravitational radiation [123], Weber undertook to set up an actual resonant antenna at the University of Maryland. It consisted of a 1.2 ton aluminium bar at room temperature, whose vibrations were monitored with the aid of piezoelectric transducers. Observations were performed with this single antenna during the period 1963–1968 [124, 125], and, afterwards, a second cylinder at the Argonne National Laboratory of Chicago permitted coincidence experiments between the opposite ends of a 1000 km baseline. In 1969, Weber announced positive results of these experiments [126]. This gave rise to great excitement, which translated

Experiment	Location	Mass (kg)	T (K)	Date	Sensit.
CRAB	Tokyo	1200	4.2	1991	2×10^{-22}
EXPLORER	Geneva	2300	2.5	July 90	7×10^{-19}
NAUTILUS	Rome	2300	0.1	94–95	$3{\times}10^{-18}$
ALTAIR	Rome	390	4.2	-	-
AURIGA	Legnaro	2300	0.1	1995	-
ALLEGRO	Louisiana	2300	4.2	June 91	7×10^{-19}
NIOBE	Perth	1500	4.2	June 1993	7×10^{-19}
Moscow Univ.	Moscow	1500	290	1993	7×10^{-17}

Table 1.1. *Resonant cylindrical antennæ worldwide. We give the mass of the detector, its operating temperature, the date since they are taking data and their sensitivity in terms of the minimum detectable gravitational wave amplitude for a 1 ms burst. The high sensitivity of the CRAB antenna is attained only for monocromatic sources.*

into the construction of cylindrical bar antennæ by other groups, aimed at the confirmation of Weber's observations. In the end, however, none of the groups operating with detectors of Weber's type could report evidence on the existence of gravitational waves [52, 36, 13]. These negative results, together with astronomical observations, made clear the need of technological improvements in the antenna design in order to attain higher sensitivities. Thus, in the late seventies, other experimental researchers got involved in building 'second generation' gravitational antennæ, which offered better performance by means of three important improvements. First, the use of cryogenic techniques allowed lowering the temperature of the bars down to 4 K. In second term, the suspension system and vibration isolation of the antennæ were carefully redesigned. And, finally, the introduction of resonant transducers matched to the normal vibrations of the cylinder, and the use of low noise amplifiers, greatly improved the readout system. During the eighties, these second generation detectors were perfected, and nowadays there are several resonant bars worldwide (see table 1.1), taking data for sustained periods of time and even operating in coincidence.

A second type of detectors were also considered in the seventies, namely, laser–interferometer detectors. The first, small–scale prototype was constructed by Forward in

1972 [49], and by the mid eighties improved prototypes were also constructed in Munich, Glasgow, Caltech and MIT, working at amplitude sensitivities around 2000 times better than that of Forward's first prototype.

In spite of this great technological effort, gravitational waves have not yet been detected by means of Earth–based detectors. Nevertheless, Hulse and Taylor's observations of the binary pulsar PSR B1913+16 since its discovery in 1975[63] have provided the first experimental confirmation of some of the predictions of gravitational wave physics. PSR 1913+16 is a binary system where relativistic effects are within experimental range. In fact, the decay of its orbital period, owing, according to General Relativity, to emission of gravitational radiation, can be directly measured. Comparison of the observed values with the predicted delay due to gravitational wave emission, shows that Einstein's theory passes the test with a fractional accuracy better than 0.4%. The clock–comparison experiment for PSR 1913+16 thus provides direct experimental proof that changes in gravity propagate at the speed of light, thereby creating a dissipative mechanism in an orbiting system [115, 64].

The strong experimental evidence provided by Hulse and Taylor's observations on the existence of gravitational waves suggests that the negative results of present gravitational wave antennæ ensue from their being not sensitive enough. Therefore, further improvements are needed in order to reach the required sensitivities. Projected large–scale Earth–based interferometers LIGO [1] and VIRGO [53] having km–long arms, or the ambitious space–based interferometer project LISA [106] would, if finally made operative, be able to detect gravitational radiation bathing the Earth according to current theoretical views. On the other hand, resonant detectors are also expected to push forward their sensitivity threshold with the aid of ultracryogenics and SQUID technologies.

There is, however, a different way of making a step further in order to improve the sensitivity of resonant detectors: *the introduction of a better suited geometry, namely,* spherical *geometry*.

Spherical detectors were soon recognized by Forward [48] to offer better detection capabilities than cylindrical bars: they are omnidirectional and have at least five modes of vibration coupling to gravitational waves. Further theoretical work by Wagoner and Paik [119] also showed that the sensitivity of a sphere is slightly better than that of a cylinder of equal mass. However, the possibility of building spherical resonant antennæ was disregarded by experimental researchers until the last decade. Currently, though, the experience accumulated over more than 25 years of development work with cylinders has given the experimentalists the necessary confidence to reconsider the spherical an-

tenna project. As a matter of fact, a number of groups worlwide are currently commited to a development of spherical gravitational wave detectors, from both theoretical and experimental points of view. Also, small prototypes of truncated icosahedral detectors have been already built and operated at room temperature at Lousiana State University. When finally operative, spherical detectors would moreover offer the possibility of interesting coincidence experiments with other types of detector.

Summing up, spherical resonant gravitational detectors appear as a promising, feasible and challenging possibility of direct detection of gravitational waves in the near, or at least not too distant, future.

1.2 Overview of this essay

The aim of this thesis is to contribute to the development of spherical resonant gravitational wave antennæ from a theoretical point of view. If we are to monitor the sphere's surface displacements searching for gravitationally induced disturbances, the first question to address is what will these displacements look like. A short, theoretically–minded answer is: the sphere's displacements will be given by the solution of the requisite equations of motion.

Within the framework of General Relativity, these equations are obtained from the generalized conservation law for the energy–momentum tensor describing the solid. The problem of determining this tensor for elastic and viscoelastic solids has been extensively treated in the literature [97, 87, 22]. As the stresses into a rigid solid are the outcome of the *changes in the distance* between its particles, care must be taken to define in a covariant way the state of deformation of the body at hand. Once this has been acomplished, we can write down the conservation equation in the weak field limit—for we expect any gravitational wave reaching the Earth to be extremely weak—, and *in terms of coordinate displacements*—for these are the quantities to be eventually measured in an experimental layout. Owing to the non–tensorial character of coordinate position, the final equations of motion are not gauge invariant. For instance, when spelled out for a TT system, the take the form of those of a *free* Newtonian solid. This fact has lead some authors to the conclusion that gravitational waves do not couple with homogeneous rigid solids [39, 23]. We argue, however, that a better suited coordinate sytem to describe our actual measurements is the well–known normal frame. It is shown that in such a system the effect of a passing gravitational waves shows as a tidal driving term in the Newtonian

equations of motion.

Admittedly, the question of whether the quasi–Minkowskian normal frame actually describes our experimental layouts is an open one; but we shall not go into a detailed discussion of this issue here. Rather, we assume in the following that the "correct" form of the equations of motion is the one obtained in this frame, and analyse the consequences ensuing from such assumption. As is often the case with theoretical controversy, experience will eventually provide a check on our conceptions.

Hence, not very surprisingly, the study of the behaviour of viscoelastic solids acted upon by gravitational waves demands an analysis of their Newtonian equations of motion, which we undertake in chapters 3 and 4. The problem of determining the normal modes of vibration of an elastic solid sphere is among the classical ones in elasticity treatises (see, e.g. [80]), but we offer a thorough analysis of this issue in modern notation, and extend classical results to the interesting case of a *hollow sphere*. A complete study of the assymptotic properties of the spectrum of spherical bodies is also given. Moreover, we take advantage of the theory of linear operators in Hilbert spaces to reformulate the problem in a compact and elegant form. This allows an easier handling of the somewhat cumbersome algebra involved, and also our original perturbative treatment of the small deviations from spherical symmetry originating in the suspension of the detector in the terrestrial gravitational field. Closed expressions for the perturbations of the spectrum are found for an arbitrary surface suspension. Finally, by way of example, we explicitly compute the threefold splitting of the fundamental mode of a sphere hung by means of axisymmetric tensions applied on a small circular cap.

Real bodies are not perfectly elastic, though. They undergo dissipative processes transforming ordered, macroscopic motions (such as normal vibrations) into disordered, molecular motion (that is, heat). This process is sometimes modelled introducing, by hand, a damping factor $\exp(-\omega t/Q)$ in the periodic time–dependence of elastic normal modes. This approach demands the introduction of experimental values of the quality factor Q at each frequency considered, as they provide no means to their calculation from a finite set of parameters characterizing the solid. In chapter 4, we overcome this problem by the introduction of a theoretical model describing both the elastic behaviour of the small deformations of the solid, and the dissipation processes which it undergoes. The classical theory of viscoelasticity offers a wide variety of possible models, each one starting from a given constitutive relationship between the stress and strain tensors. We solve in detail the simplest ones for the solid sphere, assuming small viscosity (i.e. high quality factor). We show that the viscoelasticity equations of motion for these models

admit free solutions with the time dependence $\exp(-\omega t/Q)\sin\omega t$, where ω is a frequency of the elastic solid's spectrum.

The explicit form obtained for Q as a function of frequency opens the possibility of experimental checking of the proposed models, because the quality factor has an immediate observational meaning—it gives the mechanical bandwith of the solid's vibrations. Moreover, we show how the simple models dealt with can be generalized to more sophisticated ones, in case the former would be found unsuitable to fit actual measurements. In any case, they provide a theoretical framework encompassing both the elastic and viscous properties of rigid bodies, allowing thus a rigourous treatment of the effect of gravitational waves on real bodies.

In chapter 5, we finally address the problem of solving the equations of motion of (visco)elastic solids acted upon by a driving force. Our objective is twofold. First of all, explicit expressions for the displacements ensuing from the interaction between a (visco)elastic solid and a external general force are given. Spelling out these expressions for a *tidal* driving force, we obtain a precise description of the kind of deformations that we should expect as the outcome of a passing gravitational wave. In second term, the power absorbed by the solid can be directly computed, and, thence, we can obtain the absorption cross–section, $\sigma_{\rm abs}$, of spherical gravitational wave detectors. This concept—a familiar one in many branches of physics; e.g., scattering of electromagnetic waves or neutron absorption— provides a quantitative measure of the detector's sensitivity.

Two properties of our solution to the equations of motion are worth noting. Elastic and Kelvin–Voigt viscoelastic solids undergo forced displacements *which can be expressed in terms of purely elastic normal modes*, regardless the concrete form of the driving force. On the other hand, when specializing to a tidal one, we find that gravitational waves can possibly excite only quadrupole spheroidal modes with polarization $m = \pm 2$, this fact allowing the possibility of strong experimental vetoes on the correctness of General Relativity.

In our subsequent study of the solid sphere's sensitivity, we recover the known results regarding its good performance at the fundamental mode. But also special attention is paid to the potential use of spherical bodies *as a two–frequency detector*, a possibility overlooked in previous work on the subject. As we have already pointed out in [27], the sphere's sensitivity at is second quadrupole frequency *is still higher* than that of a cylinder's fundamental mode operating in the same frequency range. In fact, for typical bars, the corresponding sphere having the same fundamental frequency has an energy sensitivity over 20 times better, and its second mode absorbs over 15 times more energy

than the fundamental mode of the cylinder—always assuming optimal orientation of the latter.

It is also shown how the good sensitivity of the sphere at its second mode can be used to reduce the number of components of a xylophone of spherical detectors aimed at wideband coverage.

To close the list of the advantges offered by spherical geometry, we must mention the sphere's omnidirectionality, and its having five modes at each frequency coupling to gravitational waves. These properties are not shared by single cylidrincal detectors or interferometers. Multiple arrays of such detectors are needed to meet the properties which a single sphere has on its own.

On the other hand, hollow spheres present new capabilities on their own. Although their sensitivity is always below that of a solid sphere of equal mass at its fundamental mode, we have discovered that the cross–section of a hollow sphere's second mode increases with the ratio between its inner and outer radii. Indeed, the detector's sensitivity becomes *larger* at the *second* mode than it is at the first. It always keeps below that of a solid sphere, but we have the additional advantage that, for a given mass, *thinner shells have lower resonance frequencies*. It is shown that a thin hollow sphere can operate with high sensitivity at a (remakably low) frequency of 200–300 Hz *and* at a frequency around 1 kHz. This opens the possibility of resonant detectors operating at low frequencies, typically covered by interferometers, and, therefore, of coincidence experiments between the two types of antenna.

The last chapter of this thesis briefly touches on some issues which lay somewhat out of its natural scope, but which are nevertheless of great practical importance. Thus, the chapter opens with a brief discussion of the deconvolution problem for spherical detectors, following previous work by Wagoner and Paik [119]. It is shown that measurements taken at five points of the antenna's surface allow, assuming General Relativity, the determination of the gravitational wave incidence direction and of its 'plus' and 'cross' amplitudes up to a polarisation angle. In section 6.2 we discuss how a two–sphere observatory provides this missing information, and how it can be used to determine the velocity of propagation of gravitational waves. Chapter 6 closes with a brief catalogue of likely sources of gravitational radiation and a discussion of their detectability by a spherical antenna. Specially interesting is the ability of a thin shell to monitor coalescing binaries at two frequencies of their inspiralling motion, which would provide a way of computing the coalescence time of such systems.

Finally, we have collected in appendices A and B some lengthy algebra appearing

in the derivations of chapters 3 through 5, while appendix C gives the description and source code of a C–library developed to perform the numerical work needed in many calculations (e.g., computation of eigenfrequencies, calculation of sensitivities, etc.).

1.3 Notation and linear gravitational waves

Through this essay we shall use the following notation.

- Four–dimensional magnitudes will be typed in italics, with greek indices ranging from 0 to 3; e.g. u_μ, $A^{\alpha\beta}_{\mu\nu}$, etc.

- The metric tensor of space–time is denoted $g_{\mu\nu}$, and has signature -+++. Minkowski's metric is denoted $\eta_{\mu\nu} = \mathrm{diag}\{-1, 1, 1, 1\}$.

- Partial differentiation with respect to x^μ is denoted $\partial/\partial x^\mu$, ∂_μ or by means of a subscript $(_{,\mu})$.

- Lie derivative with respect a vector field u_μ is denoted $\mathcal{L}_u$.

- Covariant differentation is denoted by ∇_μ or a semicolon $_{;\mu}$.

- Parenthesis indicate symmetrization, e.g. $A_{(\mu\nu)} \equiv (A_{\mu\nu} + A_{\nu\mu})/2$.

- Boldface letters denote three–dimensional Cartesian vectors; e.g. $\mathbf{x}$, $\mathbf{s}$. Cartesian vector indices are denoted by latin letters (i, j, ...), and are raised and lowered with the diagonal metric $\delta_{ij} = \delta^{ij} = \mathrm{diag}\{1, 1, 1\}$.

- ∇, without subindices, denotes the Cartesian nabla operator, i.e. $\nabla \equiv (\partial_x, \partial_y, \partial_z)$.

- Einstein summation convention is used. For Cartesian tensors, contraction is indicated by covariant indices; e.g. s_{kk} denotes summation over the repeated index k.

- Levi–Civita's totally skewsymmetric tensor is denoted ϵ_{ijk}, with $\epsilon_{123} \equiv 1$.

- Cartesian dot product: $\mathbf{a} \cdot \mathbf{b} \equiv a_i b_i$.

- Cartesian vector product: $(\mathbf{a} \times \mathbf{b})_i \equiv \epsilon_{ijk} a_j b_k$.

- c is the velocity of light, and G the Newtonian gravitational constant.

We shall also assume that gravitational waves are correctly described by the linearized Einstein equations. We give here a very brief review of the standard theory [127, 93, 121].

In a properly chosen coordinate system, gravitational radiation appears as a linear deviation $h_{\mu\nu}$ from flat space–time:

$$g_{\mu\nu}(x) = \eta_{\mu\nu} + h_{\mu\nu}(x) \quad , \qquad |h_{\mu\nu}(x)| \ll 1 \tag{1.1}$$

Here $h_{\mu\nu}$ satifies the linearized Einstein equations

$$\Box \bar{h}_{\mu\nu} - \bar{h}_{\mu}{}^{\sigma}{}_{,\sigma\nu} - \bar{h}_{\nu}{}^{\sigma}{}_{,\sigma\mu} + \bar{h}^{\rho\sigma}{}_{,\rho\sigma}\, \eta_{\mu\nu} = -\frac{16\pi G}{c^4}\, T_{\mu\nu} \tag{1.2}$$

where

$$\bar{h}_{\mu\nu} \equiv h_{\mu\nu} - \frac{1}{2}\, h\, \eta_{\mu\nu} \quad , \qquad h \equiv \eta^{\mu\nu}\, h_{\mu\nu} \tag{1.3}$$

and $T_{\mu\nu}$ denotes the source's energy–momentum tensor. These equations are invariant under first–order coordinate transformations preserving (1.1). These are of the form

$$x'^{\mu} = x^{\mu} + \epsilon^{\mu}(x) \tag{1.4}$$

where $\partial_\nu \epsilon^\mu(x) = o(h)$. Gauge freedom can be used to impose a supplementary condition on $h_{\mu\nu}$. We shall always use the *Hilbert gauge*

$$\bar{h}^{\mu\nu}{}_{,\nu} = 0 \tag{1.5}$$

for which the equations of motion reduce to the wave equation

$$\Box \bar{h}_{\mu\nu} = -\frac{16\pi G}{c^4}\, T_{\mu\nu} \tag{1.6}$$

We have still the possibility of further gauge transformations leaving invariant equations (1.5) and (1.6). They are given by any set of functions $\epsilon^\mu(x)$ satisfying $\Box \epsilon_\mu = 0$. In the absence of sources, it can be shown that it is always possible to choose a coordinate system (the transverse–traceless, or TT–system) in which the gravitational wave reduces to the canonical form:

$$h_{\mu\nu}(\mathbf{x}, t) = \begin{pmatrix} 0 & 0 & 0 & 0 \\ 0 & h_+(\mathbf{x}, t) & h_\times(\mathbf{x}, t) & 0 \\ 0 & h_\times(\mathbf{x}, t) & -h_+(\mathbf{x}, t) & 0 \\ 0 & 0 & 0 & 0 \end{pmatrix} \tag{1.7}$$

Chapter 2

Interaction of gravitational waves with elastic and viscoelastic bodies

2.1 Introduction

The use of elastic resonant detectors of gravitational radiation demands a thorough analysis of the way in which an impinging gravitational wave interacts with the elastic antenna. Thus, a generalization of the classical theory of elastic media within the framework of General Relativity is needed, once the mathematical description of (weak) gravitational waves has been stated. Such generalization has been carried through by several authors (see [22, 23, 61, 85, 97, 113], and references therein), with different levels of mathematical rigour, but leading to the same equations of motion for a solid elastic body which undergoes small deformations in the presence of gravitational fields. We present here a brief survey of these theories, stressing their application to the case of weak gravitational fields, and the physical interpretation given to the resulting equations of motion in terms of measurable displacements.

The resonant detectors are not perfectly elastic bodies, and they undergo dissipation processes which damp their elastic vibrations. This internal friction is modelled classically by means of the so–called viscoelastic models, which combine the elastic properties of deformable solids with that of a viscous flow. We present a brief review of the classical theory, and generalize it to the relativistic case of interaction with a gravitational wave.

2.2 Classical theories

2.2.1 Classical elasticity

In the Newtonian theory of elasticity [98, 80], the state of strain of a deformable body is described by the strain tensor, s_{ij}, which gives the change in the distance between two close particles of the elastic medium after deformation. Thus, if $\mathbf{x}$ and $\mathbf{x}+d\mathbf{x}$ are the positions of two particles of the medium before deformation, their distance being then $ds^2 = dx_i dx_i$, after deformation the distance between them will be

$$ds'^2 = ds^2 + 2\, s_{ij} dx_i dx_j. \tag{2.1}$$

When using cartesian coordinates, if $\mathbf{s}(\mathbf{x})$ is the field of displacements (i.e., the position of the particle changes from $\mathbf{x}$ to $\mathbf{x}+\mathbf{s}$) the strain tensor is given, up to second order in s, by

$$s_{ij} = s_{(i,j)}. \tag{2.2}$$

On the other hand, the dynamics of the body is described by its stress tensor, σ_{ij}, $\sigma_{ij}n_j$ being the force per unit area acting on a surface element with normal $\mathbf{n}$. Due to angular momentum conservation, σ_{ij} is symmetric. The equations of motion are then

$$\rho \frac{\partial^2 s_i}{\partial\, t^2} = \frac{\partial \sigma_{ij}}{\partial\, x^j} + f_i, \tag{2.3}$$

$\mathbf{f}$ being the force per unit mass due to external fields acting on the elastic body. The above system of partial differential equations is subjected to the following boundary conditions on the surface of the elastic body:

$$\sigma_{ij} n_j = S_j, \tag{2.4}$$

where $\mathbf{S}$ stands for the surface tractions on the body's surface. In order to have a system of differential equations for the displacements, a relation between stress and strain must be set. Most materials show a linear dependence (Hooke's law) of the form

$$\sigma_{ij} = C_{ij}^{lm} s_{lm}, \tag{2.5}$$

where C_{ij}^{lm} are constants with the following symmetries:

$$C_{ij}^{lm} = C_{lm}^{ij} = C_{lm}^{ji}, \tag{2.6}$$

known as Voigt symmetries in the literature. Thus, a linear elastic body is in general characterized by 21 independent parameters. In the special case of homogeneous,

isotropic media, only two constants, the Lamé coefficients, are needed, and Hooke's law has the simple form

$$\sigma_{ij} = \lambda\, s_{kk}\delta_{ij} + 2\,\mu\, s_{ik}. \tag{2.7}$$

Then, the equations of motion can be written

$$\rho\frac{\partial^2 \mathbf{s}}{\partial\, t^2} = (\lambda+\mu)\nabla(\nabla\cdot\mathbf{s}) + \mu\nabla^2\mathbf{s} + \mathbf{f}, \tag{2.8}$$

with boundary conditions:

$$\lambda(\nabla\cdot\mathbf{s})\mathbf{n} + 2\mu(\mathbf{n}\cdot\nabla)\mathbf{s} + \mu\,\mathbf{n}\times(\nabla\times\mathbf{s}) = \mathbf{S}, \tag{2.9}$$

to be satisfied on the body's surface, which has normal vector $\mathbf{n}$.

2.2.2 Classical viscoelasticity

The theory of deformable solids presented in the previous section takes into account only purely conservative processes, and no energy loses are allowed by the equations of motion. The total mechanical energy is conserved, and transformations between potential elastic energy and kinetic energy are the only energy transfers permitted within the framework of classical elasticity. In fact, the theory of linear elasticity can be conceptually viewed as a generalization of Hooke's law for one–dimensional springs to three–dimensional continua. Following this parallelism, we shall consider one–dimensional mechanical models presenting internal friction which will be later generalized to describe rigid solids undergoing dissipation, giving rise to the so–called *viscoelastic* models for deformable solids [16, 31, 60]. While the elastic component of our mechanical model will be a linear spring satisfying Hooke's law, the internal friction shall be modelled by a dashpot (see figure 2.1), that is, a piston immersed in a viscous fluid giving rise to a frictional force proportional to velocity. Thus, if s stands for the displacement of the piston when a uniaxial tension σ is applied to the free ends of the dashpot, the following equation holds:

$$\sigma = \eta\dot{s}, \tag{2.10}$$

where a dot denotes time derivative, and η is a parameter characterizing the dashpot's viscosity. The spring shall be characterized by the restitution constant E appearing in Hooke's law, which, in terms of the spring's elongation s when it is under a tension σ, is written as:

$$\sigma = E\, s. \tag{2.11}$$

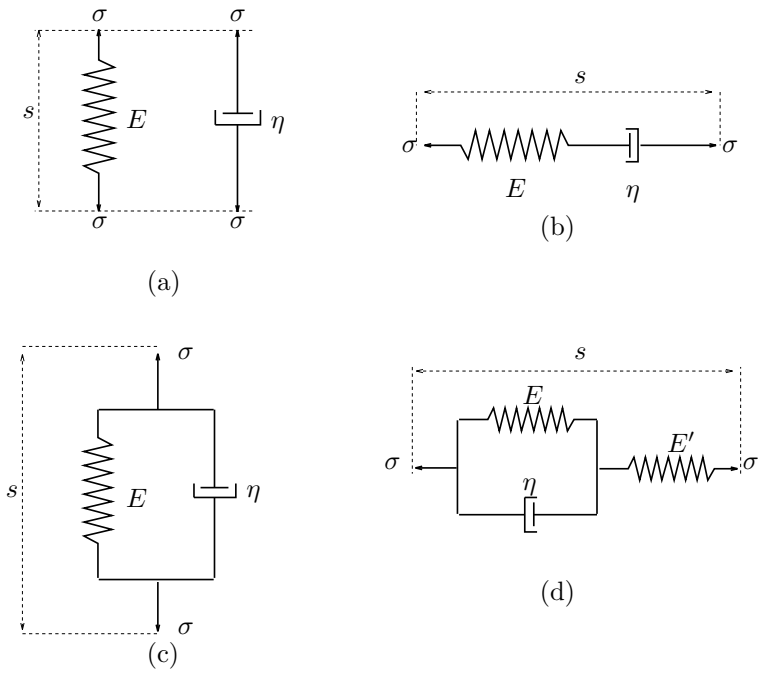

Figure 2.1. *One–dimensional mechanical models for linear viscoelastic solids. Their building blocks are the Hookean spring and the viscous dashpot represented in figure (a). Figure (b) represents the Maxwell model, in (c) the Kelvin–Voigt model is depicted, and figure (d) shows the Standard Linear Model.*

In order to build a one–dimensional viscoelastic model, the aforementioned components can be combined in a variety of ways. We shall limit ourselves here to the three simplest models (Kelvin-Voigt, Maxwell and Standard Linear Model), which are represented in figure 2.1. Our aim will be to obtain an equation relating the stress and strain tensors (known as *constitutive equation*), which will play the part of the linear Hooke's law (2.7) for elastic bodies.

The Maxwell model consists of a dashpot in series with a spring. When a tension is applied to the free ends of the spring and the dashpot, it is instantaneously deformed (elastic response); if the tension is mantained, the deformation increases due to the viscous flow of the piston in the dashpot. Thus, this model has the capability of unlimited deformation under finite stress, and it would be not suitable for describing real solids under constant stress. Nevertheless, when free vibrations are considered, the model presents sensible properties, as we shall see in chapter 4, where it is applied to a solid

sphere (see [55] for an extensive analysis of the properties of this and the following models in the one–dimensional case). The total displacement of the model, s, will be given by addittion of the dashpot's and the spring's displacements (say s_e and s_d), so that the constitutive equation for a Maxwell solid is given by

$$\dot{s} = \dot{s}_e + \dot{s}_d = E^{-1}\dot{\sigma} + \eta^{-1}\sigma. \tag{2.12}$$

The corresponding generalization to a three-dimensional solid is readily obtained from the above equation:

$$\partial_t \sigma_{ij} + D_{ij}^{lm}\sigma_{lm} = C_{ij}^{lm}\partial_t \mathbf{s}_{ij}, \tag{2.13}$$

where C_{ij}^{lm} and D_{ij}^{lm} are constant tensors with the Voigt symmetries (2.6). Thus, a Maxwell solid will be parametrized by 42 coefficients. In the special case of isotropy and homogeneity, the number of independent parameters reduces to four, and the constitutive equation can be written as

$$\partial_t \sigma_{ij} + \alpha\,\sigma_{kk}\delta_{ij} + \beta\,\sigma_{ij} = \partial_t\,\left(\lambda\, s_{kk}\,\delta_{ij} + 2\mu\, s_{ij}\right), \tag{2.14}$$

where, besides the usual Lamé coefficients, we have introduced two new positive constants, α and β, describing the effects of internal friction.

The second model to be considered consists of a dashpot in parallel with a spring (figure 2.1(c)), and is known in the literature as the Kelvin–Voigt model. A constant strain applied to its free ends produces no instantaneous elastic response, due to the presence of the dashpot, but an asymptotically constant elongation which is recovered after an eventually infinite time lapse since the tension is removed (such viscoelastic contraction is not present in the Maxwell model). To obtain the constitutive equation for this model, one simply needs to take into account that the total stress σ is given by the addition of the tensions at which each element is submitted, while both undergo the same displacement. Thus,

$$\sigma = \sigma_e + \sigma_d = E\,s + \eta\,\dot{s}, \tag{2.15}$$

and the corresponding constitutive relation between the stress and strain tensors of a Kelvin-Voigt three–dimensional solid shall take the form

$$\sigma_{ij} = \left(C_{ij}^{lm} + C_{ij}^{\prime lm}\partial_t\right) s_{lm}, \tag{2.16}$$

where, again, the constant tensors C_{ij}^{lm} and $C_{ij}^{\prime lm}$ both satisfy equation (2.6). Their 42 independent components are reduced to 4 for an isotropic, homogeneous body, whose

constitutive equation can be written as

$$\sigma_{ij} = (\lambda + \lambda'\partial_t)\, s_{kk}\delta_{ij} + 2\,(\mu + \mu'\partial_t)\, s_{ij}, \tag{2.17}$$

the new positive constants λ' and μ' describing the effects of viscosity.

We shall still consider a third model, consisting of three elements: two springs and a dashpot. It is called Standard Linear model (or three–element model [16, 60]) and is obtained by the association in series of a Kelvin–Voigt model and a spring (figure 2.1(d)). This more involved layout is used frequently to model viscoleastic solids under certain regimes, for it exhibits a behaviour closer to that of real bodies [16, 55]. Nevertheless, it will be shown in chapter 4 that, under the assumption of small internal friction, it happens to be equivalent to a Kelvin–Voigt solid. To obtain the constitutive equation of the Standard Linear model, it suffices to consider that its two aforementioned constituents are under the same tension σ, and that the total displacement s is given by the addition of that of the Kelvin-Voigt element and that of the spring. It is then straightforward to derive the relation

$$(E + E')\sigma + \eta\dot{\sigma} = EE's + E\eta\dot{s}. \tag{2.18}$$

The generalization of the above equation to three–dimensional solids gives us a constitutive relation depending on 63 real parameters, namely:

$$\sigma_{ij} + E^{lm}_{ij}\partial_t\sigma_{lm} = \left(C^{lm}_{ij} + C'^{lm}_{ij}\partial_t\right)\, s_{lm}, \tag{2.19}$$

whose isotropic, homogeneous version reduces to a six–parametric relation of the form

$$\sigma_{ij} + \partial_t\left(\alpha\,\sigma_{kk}\delta_{ij} + 2\beta\,\sigma_{ij}\right) = (\lambda + \alpha'\partial_t)\, s_{kk}\delta_{ij} + 2(\mu + \beta'\partial_t)\, s_{ij}. \tag{2.20}$$

Once the constitutive relation between stress and strain has ben stated, the classical theory of viscoelasticity makes use of the Newtonian equation of motion (2.3) with the boundary conditions (2.4). The construction of solutions to such equations for the elastic and viscoelastic cases, as well as possible generalizations, shall be dealt with in following chapters. Before that, we must proceed to the formulation of these classical theories whithin the framework of General Relativity, in order to know under which circumstances the Newtonian theory is still reliable to account for the interaction of a rigid solid with gravitational waves.

2.3 Relativistic theory of elasticity

2.3.1 Nonlinear theory

Within the framework of General Relativity, we shall work on a 4-dimensional, smooth manifold, V_4, representing the space-time continuum, and endowed with a non-degenerate, pseudo-riemannian metric $g_{\mu\nu}$. An elastic body will be represented by a time-like congruence, which in local coordinates may be written as

$$x^\mu = X^\mu(\tau, \boldsymbol{\alpha}), \tag{2.21}$$

where X^μ are smooth functions of proper time, τ, and three Lagrangian coordinates α^A, labelling the particles of the elastic body[1]. Equations (2.21) can be viewed as a map between the space-time manifold and the product manifold $\mathbb{R} \times \mathcal{B}_3$, $\mathcal{B}_3$ being a three-dimensional manifold whose points represent the positions of the particles of the elastic body at some initial state. This map must be invertible, so that we can write

$$\tau = \mathcal{A}^0(x) \qquad\qquad \alpha^B = \mathcal{A}^B(x), \tag{2.22}$$

for properly chosen functions $\mathcal{A}^0, \mathcal{A}^A$. We can also introduce the Jacobian matrices (X_0^μ, X_A^μ) and $(\mathcal{A}_\mu^0, \mathcal{A}_\mu^A)$ with the usual definition:

$$\begin{aligned} X_0^\mu &\equiv \frac{\partial X^\mu}{\partial \tau} & X_A^\mu &\equiv \frac{\partial X^\mu}{\partial \alpha^A} \\ \mathcal{A}_\mu^0 &\equiv \frac{\partial \mathcal{A}^0}{\partial x^\mu} & \mathcal{A}_\mu^A &\equiv \frac{\partial \mathcal{A}^A}{\partial x^\mu} \end{aligned} \tag{2.23}$$

and which are inverse matrices:

$$X_0^\mu \mathcal{A}_\nu^0 + X_B^\mu \mathcal{A}_\nu^B = \delta_\nu^\mu \tag{2.24}$$

$$\mathcal{A}_\mu^0 X_0^\mu = 1 \qquad \mathcal{A}_\mu^0 X_B^\mu = 0 \qquad \mathcal{A}_\mu^C X_B^\mu = \delta_B^C, \tag{2.25}$$

As usual, we introduce the normalised velocity vector field:

$$u^\mu \equiv \frac{dX^\mu}{d\tau} \qquad\qquad u^\mu u_\mu = -c^2. \tag{2.26}$$

The interaction between the particles of the elastic body will be described by a second-rank, symmetric energy-momentum tensor, $T_{\mu\nu}$, which satisfies the conservation equations

$$\nabla^\mu T_{\mu\nu} = 0. \tag{2.27}$$

[1] Uppercase indices run from 1 to 3, and will always be attached to magnitudes defined in the Lagrangian manifold of the particles of the body.

Assuming no heat conduction, i.e., supposing the deformation is an adiabatic process, we can split the energy-momentum tensor into its components along the four-velocity and those orthogonal to it as follows:

$$T_{\mu\nu} = \rho(1 + c^{-2}\epsilon)u_\mu u_\nu - \sigma_{\mu\nu} \qquad \sigma_{\mu\nu}u^\mu = 0. \tag{2.28}$$

Here, ρ stands for the rest mass density, while ϵ is the internal energy per unit mass, which in our case will be potencial elastic energy. The symmetric, purely spatial tensor $\sigma_{\mu\nu}$ plays the part of the classical stress tensor discussed in the previous section. Introducing the projector onto the orthogonal subspace to the flow-lines,

$$P^\nu_\mu \equiv \delta^\nu_\mu + \frac{1}{c^2}u_\mu u^\nu, \tag{2.29}$$

equations (2.27) can be split into an energy conservation equation (mass conservation, $\nabla_\mu(\rho\, u^\mu) = 0$, is assumed):

$$\rho\, u^\mu \nabla_\mu \epsilon = \sigma_{\mu\nu}\nabla^\mu u^\nu, \tag{2.30}$$

and an equation for the acceleration of the world-lines,

$$\rho(1 + c^{-2}\epsilon)u^\mu \nabla_\mu u_\nu = P^\mu_\nu \nabla^\alpha \sigma_{\alpha\mu}, \tag{2.31}$$

analogous to the classical equation (2.3), when no external forces are considered (we note that (2.31) represents three independent equations, as it involves only magnitudes orthogonal to u^μ). As in the case of Newtonian formulation, we need a relation between the stress tensor and the state of deformation of the body, as described by the vector field $\mathbf{u}$ or, equivalently, by the congruence (2.21). The spatial distance between nearby particles of the solid is given by the induced metric $P_{\mu\nu}$, but, to define a strain tensor in the fashion of equation (2.1), we need to introduce a *reference* spatial metric, $P^{(0)}_{AB}$, giving us the distances between the particles before deformation. The strain tensor can then be defined analogously to the classical case as

$$u_{AB} \equiv \frac{1}{2}\left(P_{\mu\nu}X^\mu_A X^\nu_B - P^{(0)}_{AB}\right). \tag{2.32}$$

Then, $\Delta(\tau, \boldsymbol{\alpha}) = 2u_{AB}d\alpha^A d\alpha^B$ will be the variation of the distance between the particles labelled by Lagrangian coordinates $\boldsymbol{\alpha}$ and $\boldsymbol{\alpha} + d\boldsymbol{\alpha}$ at proper time τ. This variation can also be expressed in terms of space-time coordinates as $\Delta(x) = 2u_{\mu\nu}dx^\mu dx^\nu$, where

$$u_{\mu\nu} = \frac{1}{2}\left(P_{\mu\nu} - P^{(0)}_{CD}\mathcal{A}^C_\mu \mathcal{A}^D_\nu\right) \equiv \frac{1}{2}\left(P_{\mu\nu} - P^{(0)}_{\mu\nu}\right), \tag{2.33}$$

is the relativistic, space-time counterpart of the classical strain tensor (by construction, $u_{\mu\nu}$ is also a purely spatial tensor). $P^{(0)}_{\mu\nu}$ plays the role of an intrinsic thermodinamical variable characterizing the elastic body, with the only *a priori* restriction of being invariant along the flow-lines, i.e.,

$$\mathcal{L}_u P^{(0)}_{\mu\nu} = 0, \tag{2.34}$$

which is also Born's condition for rigid motion [107, 109]. This approach must face the conceptual difficulty of giving a way for determining the intrinsic metric of the body, $P^{(0)}_{AB}$. While Carter and Quintana [23] simply set $P^{(0)}_{\mu\nu} = 0$ with no argument other than convenience, Hernández [61] suggests that it could be measured when the body is in equilibrium and in a zone with no gravitational fields. As pointed out by Winicour and Glass [57], this method will not be operative when the body, in its *natural* state, is not an elastic solid, as will probably be the case when dealing with strong gravitational fields. Nevertheless, in the case of a linear gravitational wave superposed to a static background, the intrinsic metric of the elastic body can be defined easily as the induced spatial metric corresponding to the static metric describing the background (see next section). This approach amounts to considering the proper spatial distance between the particles of the elastic body as the natural magnitude to define strain, instead of the gauge-dependent difference of coordinate positions used in the Newtonian theory, a choice which seems the natural one within the theoretical framework of General Relativity. Once a definition of strain has been given, the relativistic generalization of Hooke's Law is straightforward:

$$\sigma_{\mu\nu} = C^{\alpha\beta}_{\mu\nu}\, u_{\alpha\beta}, \tag{2.35}$$

where $C^{\alpha\beta}_{\mu\nu}$ must be purely spatial and have the Voigt symmetries (2.6), so that we have again 21 independent constants fully describing an elastic body. For the homogenous, isotropic case, these constants are reduced to the Lamé coefficients λ and μ, and (cf. (2.7)):

$$C^{\alpha\beta}_{\mu\nu} = \lambda\, g^{\alpha\beta} g_{\mu\nu} + 2\,\mu\, \delta^{(\alpha}_{\mu} \delta^{\beta)}_{\nu}. \tag{2.36}$$

Now we could go on to introduce the above relations into the equations of motion, and obtain the exact non-linear equations governing the motion of an elastic body in a gravitational field, that must be suplemented with Einstein equations for the metric $g_{\mu\nu}$. Such a developement can be found, e.g., in the early work of Souriau [113], or in the equivalent formalisms of Carter [23, 21, 22] and Maugin [87]. But, as the gravitational fields of the Earth, and that of a hypothetical gravitational wave impinging the Earth are

weak, we are not interested in the full non-linear theory, and in the next section we shall consider the particular case of a test elastic body interacting with a linear gravitational wave, along the lines of previous work by Maugin [85] and Papapetrou [97].

Before that, we must mention a different approach to the theory of strain, termed theory of *hypoelasticity* [57], and introduced by Synge [114] and Papapetrou [97]. These authors avoid the definition of the strain tensor (and, therefore, of an intrinsic metric of the body), and make use of the *rate of change of strain* tensor, $e_{\mu\nu}$, given by the well-known expression

$$e_{\mu\nu} \equiv \frac{1}{2}\mathcal{L}_u P_{\mu\nu} = P^{\alpha}_{\mu} P^{\beta}_{\nu} \nabla_{(\alpha} u_{\beta)}, \tag{2.37}$$

and a generalized Hooke's law relating rate of change of strain and rate of change of stress:

$$\mathcal{L}_u \sigma_{\mu\nu} = C^{\alpha\beta}_{\mu\nu} e_{\alpha\beta}. \tag{2.38}$$

We note that the above expression is a straightforward consequence of our previous definition of strain (2.33) and Hooke's law (2.35), and, therefore, hypoelasticity contains as a special case our previous theory of elasticity. In fact, they only differ in quantities whose Lie derivative is null, such as the intrinsic metric $P^{(0)}_{\mu\nu}$. This metric appears, so to speak, as a *constant of integration* in hypoelasticity, so that we would be faced again with the problem of its determination. Most authors circumvent this problem by treating always with Lie derivatives of the equations of motion, making the calculations rather cumbersome. Thus, we shall prefer treating directly with the previously outlined theory of strain, which will allow, in the next section, a derivation of the differential equations for the particle displacements clearer and quicker than those found in the literature [97, 85, 23].

2.3.2 Weak field limit

We shall focus now our attention in the particular case of a resonant detector on the Earth which interacts with an impinging gravitational wave. This particularization will allow some simplifying assumptions that will make easier the application of the formalism outlined in the preceeding section. These assumptions are the following:

1. The elastic body can be considered as a test body, i.e., its energy-momemtum tensor does not appear as a source in Einstein equations for the metric.

2. The background metric will be a solution to the linearized Einstein vacuum equations, representing a weak gravitational wave, plus a weak static field representing

the Earth's gravitational field. Thus, we shall write it as

$$g_{\mu\nu} = \eta_{\mu\nu} + \gamma_{\mu\nu} + h_{\mu\nu} \tag{2.39}$$

in a properly chosen coordinate system. Here, η is the Minkowski metric, γ stands for a static solution (e.g., Schwarzschild's) with Killing timelike vector ∂_t (that is, $\partial_t \gamma_{\mu\nu} = 0$), and h is a linear gravitational wave sweeping the detector, which will be assumed different from zero only in a given time lapse. Non-linear terms involving self-interaction of the gravitational field will be discarded, as both γ and h are small, although the static field will be greater than the gravitational wave:

$$\eta_{\mu\nu} \gg \gamma_{\mu\nu} \gg h_{\mu\nu}. \tag{2.40}$$

3. The displacements that the particles of the elastic body undergo, as well as their velocities, are small. The elastic body will be assumed in equilibrium in the static gravitational field before the gravitational wave arrives. The congruence (2.21) will be given by the following equations:

$$x^0 = ct \qquad\qquad x^i = x^i_{(0)} + s^i(t), \tag{2.41}$$

$x^i_{(0)}$ being the particle's position before the arrival of the gravitational wave. In the notation of the previous section, we can choose the Lagrangian coordinates simply as $\alpha^A = \delta^A_i x^i_{(0)}$.

Under these assumptions, we can compute the equations of motion up to first order in the small quantities

$$h, \quad s^i/L, \quad V^i/c \approx o(1), \tag{2.42}$$

L being the typical size of the detector, and $V^i \equiv s^i_{,t}$, the particle's velocity. Hence, we shall drop out any term quadratic in the above quantities, as well as any product of a first order quantity by γ.

The inverse transformations (2.22) between Lagrangian and space-time coordinates will be the following:

$$\tau = \mathcal{A}^0(x) = c^{-1} \int^t \sqrt{-g_{\mu\nu} V^\mu V^\nu}\, dt = \int^t \left(1 - \frac{h_{00}}{2} - \frac{\gamma_{00}}{2}\right) dt \tag{2.43}$$

$$\alpha^A = \mathcal{A}^A(x) = x^i \delta^A_i - s^i(t) \delta^A_i, \tag{2.44}$$

where we have defined $V^0 \equiv c$. Equation (2.43), which follows from the definition of proper time, allows a direct calculation of the velocity four-vector, yielding:

$$u^0 = c\frac{dt}{d\,\tau} = c\left(1 + \frac{\gamma_{00}}{2} + \frac{h_{00}}{2}\right) \qquad u^i = u^0 V^i/c = V^i \tag{2.45}$$

$$u_0 = -c\left(1 - \frac{\gamma_{00}}{2} - \frac{h_{00}}{2}\right) \qquad u_i = c(\gamma_{0i} + h_{0i}) + V_i. \tag{2.46}$$

The orthogonal projector and induced metric of the solid body, $P_{\mu\nu}$, is then:

$$P_{00} = 0 \qquad P_{0i} = -c^{-1}V_i \qquad P_{ij} = g_{ij}. \tag{2.47}$$

Before the arrival of the gravitational wave, we have simply $\boldsymbol{u} = \partial_0$, and $g_{\mu\nu} = \eta_{\mu\nu} + \gamma_{\mu\nu}$. The spatial metric corresponding to the orthogonal subspaces $x^0 = 0$ is then given by the well-known expression (see [73], x84):

$$g_{ij} - \frac{g_{0i}g_{0j}}{g_{00}},$$

whence the intrinsic reference metric is

$$P^{(0)}_{AB} = \delta^i_A \delta^j_B (\delta_{ij} + \gamma_{ij}). \tag{2.48}$$

In order to compute the strain tensor (2.33), we need, finally, the Jacobian matrix of the transformation (2.44), which is easily computed to give:

$$\mathcal{A}^A_i = \delta^A_i - \delta^A_j s^j{}_{,i} \qquad \mathcal{A}^A_0 = -\delta^A_j \frac{V^j}{c}. \tag{2.49}$$

Using now in the definition (2.33) for the strain tensor the relations (2.47), (2.48) and (2.49), we obtain

$$u_{ij} = s_{(i,j)} + \frac{1}{2}h_{ij}, \tag{2.50}$$

the other components of $u_{\mu\nu}$ being null (as expected, for $u_{\mu\nu}$ is by definition a spatial tensor). Comparing this equation with the Newtonian one (2.2), we see that the relativistic theory introduces the variation, h_{ij}, of the background metric into the calculation of the distance increments, as well as the coordinate displacements. In fact, equation (2.33) implies that the proper spatial distance between particles is the quantity that measures strain, and, as should be expected, u_{ij} is a gauge-invariant quantity. This seems to be a conceptually sound definition of strain whithin a metric theory of the gravitational field, and reassures the previous formalism. Using Hooke's law, we can now write down the stress tensor for a homogeneous, isotropic body (which, again, shall be purely spatial) as

$$\sigma_{ij} = \lambda\, u_{kk}\delta_{ij} + 2\mu\, u_{ij} = \sigma^{(N)}_{ij} + \sigma^{(R)}_{ij}, \tag{2.51}$$

where we have introduced the notation

$$\sigma_{ij}^{(N)} \equiv \lambda\, s_{kk}\delta_{ij} + 2\mu\, s_{ij} \tag{2.52}$$

$$\sigma_{ij}^{(R)} \equiv \frac{\lambda}{2} h_{kk}\delta_{ij} + \mu\, h_{ij} \tag{2.53}$$

for the Newtonian and purely relativistic parts of the stress tensor.

Let us turn our attention to the conservation equation. The energy conservation equation (2.30) becomes

$$\rho\frac{\partial \epsilon}{\partial t} = \sigma_{ij}\nabla^i u^j, \tag{2.54}$$

which shows that the energy density is a second order quantity. On the other hand, the spatial part of the covariant derivative of $\boldsymbol{u}$ is simply the Lie derivative of the strain tensor (cf. (2.37)), and we can rewrite the above equation as

$$\rho\frac{\partial \epsilon}{\partial t} = \sigma_{ij}\mathcal{L}_u u^{ij}. \tag{2.55}$$

The Lie derivative of an arbitrary second rank tensor $A^{\mu\nu}$ is, by definition,

$$\mathcal{L}_u A^{\mu\nu} \equiv u^\alpha \partial_\alpha A^{\mu\nu} - A^{\alpha\mu}\partial_\alpha u^\nu - A^{\alpha\nu}\partial_\alpha u^\mu,$$

whence, whenever $A^{\mu\nu}$ is a first order quantity, we have simply

$$\mathcal{L}_u A^{\mu\nu} = \frac{\partial A^{\mu\nu}}{\partial t}. \tag{2.56}$$

Thus, the mass conservation equation (2.55) finally becomes

$$\rho\frac{\partial \epsilon}{\partial t} = \sigma_{ij}\frac{\partial u^{ij}}{\partial t}. \tag{2.57}$$

Due to the fact that σ_{ij} is linear in the strain tensor, the preceeding equation can be immediately integrated to give the elastic potential energy density:

$$\epsilon = \frac{1}{2\rho}\sigma_{ij}u^{ij} + \epsilon_0, \tag{2.58}$$

where ϵ_0 is an arbitrary function of the point which is time independent an gives the initial potential energy stored in the elastic body.

To first order, the covariant divergence of the stress tensor appearing in the equation for the acceleration (2.31) reduces to the Minkowskian one, as the terms involving products of the stress tensor by Christoffel symbols will all be second order. Hence,

$$P_i^\mu \nabla^\nu \sigma_{\nu\mu} = \sigma_{ij,j}. \tag{2.59}$$

On the other hand, the first order expression for the acceleration will be

$$a^i = u^\mu \nabla_\mu u^i = \frac{\partial^2 s^i}{\partial t^2} + c^2 \Gamma^i_{00}, \tag{2.60}$$

where Γ^i_{00} is a Christoffel symbol, and again we have discarded second order terms of the form (ΓV) and (ΓV^2) in the fully covariant expression for the acceleration. Equations (2.59) and (2.60) finally give us the desired equations of motion for an elastic body interacting with a linear gravitational wave:

$$\frac{\partial^2 s_i}{\partial t^2} - \frac{1}{\rho}\frac{\partial \sigma^{(N)}_{ij}}{\partial x^j} = \frac{1}{\rho}\frac{\partial \sigma^{(R)}_{ij}}{\partial x^j} - c^2 \Gamma^i_{00}. \tag{2.61}$$

2.3.3 Discussion

The equations just obtained for the displacements are expressed in terms of gauge-dependent quantities, as should be expected from the fact that the values taken by s^i will depend on the coordinate system chosen to express them. We have the freedom to use any coordinate system in which the metric can be cast in the form (2.39), and satisfying the Hilbert gauge for the gravitational wave h. In each one of these systems, the relativistic driving terms $\sigma^{(R)}$ and $c^2\Gamma^i_{00}$ will take a given value, and will give rise to different coordinate displacements. Thus, in the transverse, traceless gauge usually employed to describe gravitational waves (see preceeding chapter), $\Gamma^i_{00} = 0$, and, using the TT properties of $h_{\mu\nu}$ in this gauge, we have

$$\sigma^{(R)}_{ik,k} = \mu_{,k} h_{ik}, \tag{2.62}$$

which is different from zero only when the shear modulus μ has inhomogenities. Hence, for a homogenous body, a TT-observer will see no coupling between the elastic vibrations and the gravitational wave *by purely measuring the displacements*. Let us emphasize this last fact, because this absence of coupling in the differential equation for the coordinate displacements does *not* imply, from our point of view, an absence of interaction between the elastic body and the gravitational wave. Even the TT-observer would be able to detect such an interaction provided he or she has a way to measure the potencial energy of the body, which, according to equation (2.58) varies as the wave passes the detector. Moreover, it is at least arguable that displacement measurements for detectors located on the Earth must be referred to the TT coordinate system. It seems more natural to assume that such measurements are taken in a normal coordinate system, which is the locally Newtonian one. This system is of the type required in our calculations, and its

connection with the TT-coordinate system has been thoroughly studied in the literature [47, 84]. Normal coordinates are attached to a freely falling object, and are valid at distances which are small when compared with the radius of curvature.[2] In this system the metric takes the form [83]

$$\begin{aligned} g_{00} &= -1 + R_{0i0j}x^i x^j \\ g_{0i} &= \frac{2}{3}R_{0jik}x^j x^k \\ g_{ij} &= \delta_{ij} + \frac{1}{3}R_{ikjl}x^k x^l \end{aligned} \tag{2.63}$$

where the Riemann tensor $R_{\mu\nu\alpha\beta}$ is calculated at the detector's center of mass. These formulæ are accurated up to second order in $(x/\mathcal{R})^2$, with $\mathcal{R}$ the radius of curvature. We are thus interested in the computation of the Riemann tensor for the case of a gravitational wave. But, as this tensor is gauge invariant, we can directly pick the TT-expressions calculated in the previous chapter, and therefore

$$R_{0i0j} = -\frac{1}{2c^2}\frac{\partial^2 h_{ij}^{TT}}{\partial\, t^2}, \tag{2.64}$$

all the other components being zero. In this equation, h_{ij}^{TT} denote the metric potentials measured in a transverse, traceless gauge. Hence, in a normal coordinate system, the metric corresponding to a gravitational wave takes the simple form

$$g_{\mu\nu} = \eta_{\mu\nu} + \delta^0_\mu \delta^0_\nu\, R_{0i0j}x^i x^j. \tag{2.65}$$

Thus, the relativistic driving terms appearing in the equations of motion have the following values:

$$\Gamma^i_{00} = R_{0i0j}x^j \qquad\qquad \sigma^{(R)}_{ij} = 0, \tag{2.66}$$

and we have the following differental equation for the displacements:

$$\frac{\partial^2 s_i}{\partial\, t^2} - \frac{(\lambda+\mu)}{\rho}\frac{\partial}{\partial\, x^i}\frac{\partial s^k}{\partial\, x^k} - \frac{\mu}{\rho}\frac{\partial}{\partial\, x_k}\frac{\partial s_i}{\partial\, x^k} = -c^2 R_{0i0j}x^j, \tag{2.67}$$

which is valid only in a normal reference frame. Hence, in these coordinates, the effect of the gravitational wave on the displacements appears in the familiar form of geodesic deviation used by different authors based upon heuristical arguments [76, 123]. Our derivation justifies their approach, and shows that it is compatible with the assumed absence of interaction predicted by other authors from the vanishing of the driving terms in the TT-gauge [39, 57, 23].

[2] In our case, this amounts to saying that the detector's size is small compared to the wavelength of h, which shall always be the case for realistic resonant detectors.

2.4 Relativistic theory of viscoelasticity

The relativistic theory of viscoelasticity is developed along the same lines of relativistic elasticity [11, 86]. In fact, we have already defined all the requisite quantities: the strain tensor (2.33) and its rate of change (2.37). The difference between elastic and viscoelastic solids, as was the case in the classical theory, depends on the way in which the state of deformation of the body at hand gives rise to a distribution of stress inside it. While for an elastic body this was described by Hooke's law as given by equation (2.35) or (2.38), for a viscoelastic solid we must take into account the combined effects of strain and rate of strain, as both happen to cause internal stresses. In general, we can generalize the classical constitutive equations discussed in x2.2.2 to a covariant formulation of the form

$$\left(\delta^{\alpha}_{\mu}\delta^{\beta}_{\nu} + D^{\alpha\beta}_{\mu\nu}\mathcal{L}_u\right)\sigma_{\alpha\beta} = \left(C^{\alpha\beta}_{\mu\nu} + C'^{\alpha\beta}_{\mu\nu}\mathcal{L}_u\right)u_{\alpha\beta}, \tag{2.68}$$

where the purely spatial tensors D, C and C' have the Voigt symmetries (2.6). The above equation must be used together with the equations of motion (2.30) and (2.31) to solve the full non–linear problem in the General Relativistic case. However, we shall be, again, mainly interested in the weak field limit. In this approximation, which we have studied in detail in x2.3.2, the four–dimensional quantities appearing in the general constitutive equation (2.68) are transformed according to the following rules:

$$u_{\mu\nu} \rightarrow s_{ij} + \frac{h_{ij}}{2}, \tag{2.69}$$

where the metric potentials h_{ij} vanish when measured in a Fermi coordinate system, and

$$\mathcal{L}_u u_{\mu\nu} \rightarrow \partial_t u_{ij}, \tag{2.70}$$

(cf. equation (2.56)). Therefore, in the weak field limit, the four–dimensional constitutive equation (2.68) reduces to the classical expressions already given in x2.2.2. On the other hand, the equations of motion can be written as

$$\frac{\partial^2 s_i}{\partial t^2} - \frac{1}{\rho}\frac{\partial \sigma_{ij}}{\partial x^j} = -c^2 R_{0i0j}x^j, \tag{2.71}$$

when expressed in a Fermi coordinate system (cf. the discussion of previous section). Hence, when measuring displacements in such system, the relativistic equations of motion for a viscoelastic solid will be identical to the classical ones with a tidal driving term.

Chapter 3

Normal modes of vibration for spherical solids

3.1 Introduction

In this chapter, we shall focus our attention in the idealized case of a free, elastic body with spherical symmetry and subject to neither external forces nor surface tractions. The time–dependent, periodic deformations that such a body can undergo are known as *normal modes of vibration*. A complete analysis of the normal modes of vibration of spherically symmetric elastic bodies is presented, giving the mathematical basis for the construction of the general solution to the equations of motion. Normal modes of vibration are the building blocks to understanding and constructing the field of deformations which an elastic solid undergoes as a result of any driving force, and, as we shall see, permit us a natural separation of the spin features of any forced solution. As gravitational waves have well-defined spin properties, they will excite only those modes with requisite ones. Thus, a sound knowledge of both the mathematical and physical properties of normal modes happens to be paramount in our understanding of the performance of spherical elastic bodies as antennæ of gravitational radiation. Once these properties have been stated, we apply them, in chapter 5, to the solution of the equations of motion for a *tidal-like* driving term, always assuming spherical symmetry, and to the calculation of absorption cross-sections.

Most of the results presented in this chapter can be found (for the case of the solid sphere) in classical books and papers on elasticity [68, 71, 72, 80], or modern research

papers [119, 76, 5, 89, 88], but, to our knowledge, there is no complete survey of this subject in the literature. Thus, our aim is to present here a comprehensive derivation and analysis of this matter with a view to its application to the problem of detection of gravitational radiation, as well as to generalize the known calculations (which are always referred to solid spheres) to the interesting case of a hollow, elastic sphere. Spherical symmetry will allow us, with the help of a little numerical work, to completely solve the rather cumbersome set of differential equations and boundary conditions appearing in the classical theory of elasticity, and to bring up the nice mathematical structure underlying it.

Nevertheless, exact spherical symmetry would be seldom present in real cases. For instance, the suspension of a rigid elastic sphere in the static gravitational field of the Earth will give rise to its shape deformation. In order to compute how small deviations from spherical shape and/or homogeneity affect the solid's spectrum, we close this chapter with a perturbation squeme for the equations of elasticity. By way of example, we calculate the threefold splitting of the fundamental mode of a hung sphere.

Also, the reformulation of the elasticity equations introduced to tackle this problem, will be used in chapter 5 to find the solution to the forced equations of motion.

3.2 General elastic solid

Through this and the following chapters, we shall deal with homogeneous, isotropic elastic bodies with constant density ρ, and which undergo small deformations following the linear Hooke's law. Thus, their elastic properties shall be fully described by two constant Lamé coefficients, λ and μ. As showed in the preceeding chapter, the field of displacements $\mathbf{s}(\mathbf{x}, t)$ induced by a gravitational wave impinging on such a solid, when measured in a normal coordinate system, is given by the solution to the following set of partial differential equations:

$$\rho \frac{\partial^2 \mathbf{s}}{\partial t^2} - (\lambda + \mu)\nabla (\nabla \cdot \mathbf{s}) - \mu \nabla^2 \mathbf{s} = \mathbf{f}(\mathbf{x}, t), \tag{3.1}$$

satisfying, on the body's surface, suitable boundary conditions. In the above equations, $\mathbf{f}$ stands for the body force density induced by the passing gravitational wave (cf. the discussion in previous chapter).

Before proceeding to the solution of the equations of motion, we shall deal with the periodic, separable solutions to the homogeneous counterpart of (3.1), i.e., with solutions

of the form

$$\mathbf{s}(\mathbf{x}, t) = e^{i\omega t}\mathbf{s}(\mathbf{x}), \tag{3.2}$$

where the spatial part $\mathbf{s}(\mathbf{x})$ satifies the eigenvalue equation

$$(\lambda + \mu)\nabla(\nabla \cdot \mathbf{s}) + \mu\nabla^2\mathbf{s} = -\rho\omega^2\mathbf{s}, \tag{3.3}$$

as well as homogeneous boundary conditions. These solutions, known as *normal modes of vibration*, describe the unforced oscillations of an elastic body, and will be used in chapter 5 as the basis to constructing the general solution to (3.1), and to compute the sensitivity of spherical detectors to gravitational waves. We will also show in chapter 4 that they appear again in the description of quasi–normal modes of vibration of viscoelastic bodies.

In order to solve equation (3.3), we shall split the vector field $\mathbf{s}(\mathbf{x})$ into its irrotational and divergence-free components, termed, respectively, longitudinal and transverse components:

$$\mathbf{s} = \mathbf{s}_t + \mathbf{s}_l, \qquad \nabla \cdot \mathbf{s}_t = 0, \qquad \nabla \times \mathbf{s}_l = 0. \tag{3.4}$$

Introducing this splitting into equation (3.3), we get

$$(\lambda + \mu)\nabla(\nabla \cdot \mathbf{s}_l) + \mu\nabla^2(\mathbf{s}_l + \mathbf{s}_t) = -\rho\omega^2(\mathbf{s}_l + \mathbf{s}_t), \tag{3.5}$$

and, taking the divergence of the above relationship, the following relation follows:

$$\nabla \cdot \left[(\lambda + 2\mu)\nabla^2\mathbf{s}_l + \rho\omega^2\mathbf{s}_l\right] = 0.$$

Thus, the vector between square brackets has null divergence and rotational, and, therefore, must vanish everywhere. This yields a Helmholtz equation for $\mathbf{s}_l$:

$$\nabla^2\mathbf{s}_l + q^2\mathbf{s}_l = 0 \qquad \left(q^2 \equiv \frac{\rho\omega^2}{\lambda + 2\mu}\right). \tag{3.6}$$

As regards the transverse part, taking the rotational of equation (3.5) and using the fact that both the rotational of a gradient and the rotational of $\mathbf{s}_l$ are null, we are left also with a Helmholtz equation for $\mathbf{s}_t$:

$$\nabla^2\mathbf{s}_t + k^2\mathbf{s}_t = 0 \qquad \left(k^2 \equiv \frac{\rho\omega^2}{\mu}\right). \tag{3.7}$$

Thus, $\mathbf{s}_l$ and $\mathbf{s}_t$ represent wave motions propagating, respectively, with speeds $v_l = \sqrt{\mu/\rho}$ and $v_t = \sqrt{(\lambda + 2\mu)/\rho}$. It is also worth noting the following relation, which is valid for any elastic solid:

$$\frac{q}{k} = \frac{v_t}{v_l} = \sqrt{\frac{\mu}{\lambda + 2\,\mu}}. \tag{3.8}$$

The transverse and longitudinal solutions can be constructed (see, e.g., [5] or [76]) using two scalar functions, $\phi(\mathbf{x};q)$ and $\varphi(\mathbf{x};k)$, which are solutions of equations:

$$\nabla^2\phi(\mathbf{x};q)+q^2\phi(\mathbf{x};q)=0 \qquad \nabla^2\varphi(\mathbf{x};k)+k^2\varphi(\mathbf{x};k)=0, \tag{3.9}$$

and applying to them differential operators which commute with the Laplacian operator and which give rise to transverse and longitudinal independent vectors when applied to a scalar function. For the longitudinal part, the obvious choice is the gradient:

$$\mathbf{s}_l=\nabla\phi, \tag{3.10}$$

The suitable choice for the case of the transverse solution is the well–known "angular momentum" operator $\mathbf{L}=-i\,\mathbf{x}\times\nabla$, and, in order to obtain a third independent solution, the operator $\nabla\times\mathbf{L}$[1]. We shall have then two transverse solutions, $\mathbf{s}_t$ and $\mathbf{s}_{t'}$ given by the following expressions:

$$\mathbf{s}_t=i\,\nabla\times\mathbf{L}\varphi \tag{3.11}$$

$$\mathbf{s}_{t'}=i\,\mathbf{L}\varphi, \tag{3.12}$$

The final solution shall therefore be expressed as a linear combination of the form:

$$\begin{aligned}\mathbf{s}(\mathbf{x}) &= \frac{C_l}{q}\,\mathbf{s}_l+\frac{C_t}{k}\,\mathbf{s}_t+C_{t'}\mathbf{s}_{t'}\\ &= \frac{C_l}{q}\nabla\phi(\mathbf{x};q)+i\frac{C_t}{k}\nabla\times\mathbf{L}\varphi(\mathbf{x};k)+i\,C_{t'}\mathbf{L}\varphi(\mathbf{x};k),\end{aligned} \tag{3.13}$$

with the constants C_t, $C_{t'}$, C_l having dimensions of length and chosen, together with k, so that the boundary conditions are satisfied.

Up to now, the method exposed is general enough to be applied, in principle, to any homogeneous, isotropic elastic solid, and, in fact, to the construction of solutions to equation (3.3) satisfying arbitrary boundary conditions. Nevertheless, normal modes of vibration are, by definition, bound to satisfy the homogenous conditions

$$\lambda\,(\nabla\cdot\mathbf{s})\,\mathbf{n}+2\mu\,\mathbf{n}\cdot\nabla\mathbf{s}+\mu\,\mathbf{n}\times(\nabla\times\mathbf{s})=0, \tag{3.14}$$

on the body's surface, which endow normal modes of vibration with some interesting and well–known properties: they are orthogonal, and admit only real eigenfrequencies.

In the following two sections, we shall carry out the explicit calculation of the normal modes when spherical symmetry is also assumed.

[1] That this is in fact the case, will be proved *a posteriori* by the actual construction of the solutions (cf. next section).

3.3 Solid sphere

3.3.1 Form of the solutions and boundary conditions

Let us consider the case of a solid sphere of radius R and constant density ρ. Using spherical coordinates (r, θ, ϕ), the regular solutions of equations (3.9) are

$$\phi_{lm}(r,\theta,\phi) = j_l(qr)Y_{lm}(\theta,\phi), \qquad \varphi_{lm}(r,\theta,\phi) = j_l(kr)Y_{lm}(\theta,\phi), \tag{3.15}$$

where j_l stands for the spherical Bessel functions of the first kind,

$$j_l(z) = (-)^l z^l \left(\frac{1}{z}\frac{d}{dz}\right)^l \frac{\sin z}{z}, \tag{3.16}$$

which are regular at the origin, and Y_{lm} are spherical harmonics (we follow the usual conventions for special functions; see, e.g., [2, 59]). As usual, here l denotes a multipolar integer index running from zero to infinity, while m can take any integer value from $-l$ to l.

Using the expressions (3.15) and the definitions given in the previous section, we can proceed to the computation of the longitudinal and transverse solutions as expressed in spherical coordinates. Somewhat cumbersome algebra, involving vector differential operators as $\mathbf{L}$ or ∇, is needed in the calculation. Thus, we give it in Appendix A.1.1, where it is shown that the irrotational and divergence–free components of $\mathbf{s}$ can be finally written

$$\mathbf{s}_l(r,\theta,\phi) = \frac{dj_l(qr)}{d\,r}\, Y_{lm}\,\mathbf{n} - \frac{j_l(qr)}{r}\, i\,\mathbf{n}\times\mathbf{L}Y_{lm}\,. \tag{3.17}$$

$$\mathbf{s}_t(r,\theta,\phi) = -l(l+1)\frac{j_l(kr)}{r}\, Y_{lm}\,\mathbf{n} + \left(\frac{j_l(kr)}{r} + \frac{dj_l(kr)}{d\,r}\right) i\,\mathbf{n}\times\mathbf{L}Y_{lm}\,. \tag{3.18}$$

$$\mathbf{s}_{t'}(r,\theta,\phi) = j_l(kr)\, i\,\mathbf{L}Y_{lm}\,. \tag{3.19}$$

We note that the expressions derived for the longitudinal and transverse parts of the normal modes are expressed naturally in terms of the orthogonal triad

$$(\, Y_{lm}\,\mathbf{n}\,,\, i\,\mathbf{n}\times\mathbf{L}Y_{lm}\,,\, i\,\mathbf{L}Y_{lm}\,),$$

which depends only on angular coordinates, and is a basis of the vector fields on the unit sphere S^2. They are termed *pure-spin vector harmonics* in [116] and they stem from linear combinations of the usual vector spherical harmonics (see, e.g., [43], page 82). As well as being orthogonal in each point, they have the following normalization over S^2:

$$\int_{S^2} (\, Y_{lm}\mathbf{n}\,)\cdot(\, Y_{l'm'}\mathbf{n}\,)^* d\Omega = \delta_{ll'}\delta_{mm'}$$

$$\int_{S^2}(\,i\,\mathbf{n}\times\mathbf{L}Y_{lm}\,)\cdot(\,i\,\mathbf{n}\times\mathbf{L}Y_{l'm'}\,)^{*}d\Omega = l(l+1)\delta_{ll'}\delta_{mm'}$$
$$\int_{S^2}(\,i\mathbf{L}Y_{lm})\cdot(\,i\mathbf{L}Y_{l'm'}\,)^{*}d\Omega = l(l+1)\delta_{ll'}\delta_{mm'}, \tag{3.20}$$

where the asterisk denotes complex conjugation, and $d\Omega = \sin^2\theta\, d\theta\, d\phi$. The explicit representation in terms of this basis given by equations (3.17), (3.19) and (3.18) also shows that $\mathbf{s}_l$, $\mathbf{s}_t$, and $\mathbf{s}_{t'}$ are linearly independent, so that their linear combination (3.13) yields the general solution to equation (3.3).

In order to determine completely each normal mode we must find the relation between the constants C_t, $C_{t'}$, C_l, q and k which complies with the boundary conditions (3.14). These boundary conditions can be written as

$$\frac{C_l}{q}\boldsymbol{b}[\mathbf{s}_l] + \frac{C_t}{k}\boldsymbol{b}[\mathbf{s}_t] + C_{t'}\boldsymbol{b}[\mathbf{s}_{t'}] = 0 \qquad \text{at } r = R, \tag{3.21}$$

where we have introduced the linear differential operator $\boldsymbol{b}[.]$, whose action on a vectorial field $\boldsymbol{a}$ is defined by

$$\boldsymbol{b}[\boldsymbol{a}] \equiv \lambda\,(\nabla\cdot\boldsymbol{a})\mathbf{n} + 2\mu\,\partial_r\boldsymbol{a} + \mu\mathbf{n}\times(\nabla\times\boldsymbol{a}). \tag{3.22}$$

Here, use has been made of the fact that $\mathbf{n} = \boldsymbol{x}/x$ and, therefore, $\mathbf{n}\cdot\nabla = \partial_r$. Computing the result of applying $\boldsymbol{b}$ to the longitudinal and transverse solutions given above involves again rather lengthy algebra. Thus, we shall give the details of the computation in the appendix (cf. Appendix A.1.2), and quote here simply the results:

$$\begin{aligned}
\boldsymbol{b}[\mathbf{s}_l] &= \left[2\mu\frac{d^2 j_l(qr)}{d\,r^2} - \lambda\,q^2 j_l(qr)\right] Y_{lm}\,\mathbf{n} - 2\mu\frac{d}{dr}\left(\frac{j_l(qr)}{r}\right) i\,\mathbf{n}\times\mathbf{L}Y_{lm}\,,\\
\boldsymbol{b}[\mathbf{s}_{t'}] &= -\mu\,r\frac{d}{dr}\left(\frac{j_l(kr)}{r}\right) i\,\mathbf{L}Y_{lm}\,,\\
\boldsymbol{b}[\mathbf{s}_t] &= -2\mu\,l(l+1)\frac{d}{dr}\left(\frac{j_l(kr)}{r}\right) Y_{lm}\,\mathbf{n}\\
&\quad +\mu\left[\frac{d^2 j_l(kr)}{d\,r^2} - (l+2)(l-1)\frac{j_l(kr)}{r^2}\right] i\,\mathbf{n}\times\mathbf{L}Y_{lm}\,.
\end{aligned} \tag{3.23}$$

Inserting the above equations into (3.21), and taking into account the orthogonality of the vector spherical harmonics involved, the boundary conditions can be cast as the following system of linear equations for the constants C_l, C_t and $C_{t'}$:

$$\begin{pmatrix} \beta_4(qR) & -l(l+1)\frac{k}{q}\beta_1(kR) & 0\\ -\beta_1(qR) & \frac{k}{q}\beta_3(kR) & 0\\ 0 & 0 & -\frac{k}{q}\,kR\,\beta_1(kR)\end{pmatrix}\begin{pmatrix} C_l\\ C_t\\ C_{t'}\end{pmatrix} = 0, \tag{3.24}$$

where, to ease the notation, we have introduced the following set of auxiliary functions:

$$\begin{aligned}
\beta_1(z) &\equiv \frac{d}{dz}\left(\frac{j_l(z)}{z}\right) \\
\beta_2(z) &\equiv \frac{d^2 j_l(z)}{d\,z^2} \\
\beta_3(z) &\equiv \frac{1}{2}\left[\beta_2(z) + (l+2)(l-1)\,\frac{j_l(z)}{z^2}\right] \\
\beta_4(z) &\equiv \beta_2(z) - \frac{\lambda}{2\mu} j_l(z).
\end{aligned} \tag{3.25}$$

The homogeneous system (3.24) will admit non-trivial solutions only in the case that the determinant of its 3×3 matrix of coefficients is null. When the elastic properties of the material (i.e. the quotient λ/μ) are given, this matrix is a function only of the non-dimensional parameter kR, because, by definition, $k^2 = q^2\,(2 + \lambda/\mu)$ (cf. (3.8)). Thus, imposing the condition of compatibility to the linear system (3.24) will provide a trascendental equation to be satisfied by kR, which has a numerable infinity of real solutions, and which will give the eigenfrequencies of each normal mode via the relation $\omega = k\,v_t$. The fact that the spectrum is real and numerable can be proved within the standard theory of self-adjoint operators on Hilbert spaces. In fact, equations (3.3) and (3.14) define a well-posed eigenvalue problem (of the elliptic type, see [35]) on the Hilbert space of integrable vector fields with support in the interior of a sphere and measure of integration ρ.

The compatibility condition of the homogeneous system (3.24) can be written as

$$\det\begin{pmatrix} \beta_4(qR) & -l(l+1)\beta_1(kR) \\ -\beta_1(qR) & \beta_3(kR) \end{pmatrix} \cdot\ \beta_1(kR) = 0, \tag{3.26}$$

giving rise to two families of normal modes which we shall term *spheroidal* and *toroidal* modes, and will describe in the following subsections.

3.3.2 Spheroidal modes

We will term *spheroidal*[2] those modes satisfying condition (3.26) in the form

$$\det\begin{pmatrix} \beta_4(qR) & -l(l+1)\beta_1(kR) \\ -\beta_1(qR) & \beta_3(kR) \end{pmatrix} = 0. \tag{3.27}$$

[2]This denomination is used in the classical book of A.E.H. Love [80] for modes satisfying (3.27) with $l = 2$. Its use to encompass all values of l has been recently introduced in modern literature [91, 76].

We shall label the solutions to the above equation k_{nl}^P, with the superindex P denoting the spheroidal family, n running from 1 to infinity and indicating *which* solution of equation (3.27), for a fixed l, we are considering. The fact that equation (3.27) does *not* depend on the index m implies that the spectrum is degenerate. Due to the fact that m runs from $-l$ to l, there will correspond, to each eigenvalue k_{nl}^P, $(2l+1)$ normal modes which will be denoted $\mathbf{s}_{nlm}^P$.

Provided equation (3.27) is satisfied, the system (3.24) is compatible, and its solutions can be written

$$C_t = C(n,l)\frac{q}{k}\beta_1(qR_{nl}^P), \qquad C_l = C(n,l)\beta_3(kR_{nl}^P), \qquad C_{t'} = 0, \tag{3.28}$$

with $C(n,l)$ an arbitrary normalization constant with dimensions of length. Introducing these values into the general solution (3.13) and using the expressions (3.17) and (3.18) for $\mathbf{s}_l$ and $\mathbf{s}_t$, we can write down the final form for spheroidal normal modes of vibration as:

$$\mathbf{s}_{nlm}^P(r,\theta,\phi) = A_{nl}(r)Y_{lm}(\theta,\phi)\mathbf{n} - B_{nl}(r)\, i\, \mathbf{n}\times\mathbf{L}Y_{lm}\,(\theta,\phi), \tag{3.29}$$

where the radial functions $A_{nl}(r)$ and $B_{nl}(r)$ have the form

$$A_{nl}(r) = C(n,l)\left[\beta_3(k_{nl}^P R)\frac{d\, j_l(q_{nl}^P r)}{d\,(q_{nl}^P r)} - l(l+1)\sqrt{\frac{\mu}{\lambda+2\mu}}\beta_1(q_{nl}^P R)\frac{j_l(k_{nl}^P r)}{k_{nl}^P r}\right] \tag{3.30}$$

$$B_{nl}(r) = C(n,l)\left[\beta_3(k_{nl}^P R)\frac{j_l(q_{nl}^P r)}{q_{nl}^P r} - \sqrt{\frac{\mu}{\lambda+2\mu}}\frac{\beta_1(q_{nl}^P R)}{k_{nl}^P r}\frac{d}{dr}\{r\, j_l(k_{nl}^P r)\}\right]. \tag{3.31}$$

As mentioned earlier, the spheroidal eigenvalues do depend on the elastic properties of the material. In fact, our derivation shows that they are only function of the quotient λ/μ. When characterizing an elastic body, it is usual to give the material's Poisson ratio [3], σ, instead of this quotient, the relation between them being

$$\frac{\lambda}{\mu} = \frac{2\,\sigma}{1-2\,\sigma}. \tag{3.32}$$

Most materials have a Poisson ratio close to 1/3, corresponding to $\lambda/\mu = k/q \approx 2$, and we shall use these values unless stated otherwise.

Before proceeding to the description of the solutions of the eigenvalue equation (3.27), it must be noted that neither this equation, nor equation (3.29), are valid for the monopolar modes. This is due to the fact that, when $l = 0$, the transverse solution $\mathbf{s}_t$ vanishes

[3] As is well known (see, e.g., [80]), σ has a direct physical meaning, for it gives the ratio between the longitudinal and transverse strains undergone by the material when subject to purely longitudinal stress.

identically, for $Y_{00}(\theta,\phi) = \text{const.}$ and, therefore, $\mathbf{L}\varphi_{00} = 0$. Thus, monopolar modes in the spheroidal family are purely radial, and their spatial part is directly given by the normal component of $\mathbf{s}_l$ (cf. (3.17)):

$$\mathbf{s}^P_{n0}(r,\theta,\phi) = A_{n0}(r)\ \mathbf{n}, \qquad A_{n0}(r) = C(n,0)\frac{dj_0(q^P_{n0}r)}{d\,(q^P_{n0}r)}, \tag{3.33}$$

with $C(n,0)$ an arbitrary constant to be fixed on by normalization. The corresponding eigenvalue equation follows immediately from the expression of $\boldsymbol{b}[\mathbf{s}_l]$, yielding

$$\frac{d^2 j_0(q^P_{n0}R)}{d\,(q^P_{n0}R)^2} - \frac{\lambda}{2\mu} j_0(q^P_{n0}R) = 0. \tag{3.34}$$

Solutions to equations (3.27) and (3.34) can be found numerically [4]. In table 3.1, an ascending list of the first twenty spheroidal eigenvalues is given, together with the corresponding ratios $C_t q/C_l k$, and the frequencies of vibration for a realistic aluminium prototype (according to the data given in [28]).

The asymptotic behaviour of these roots can be investigated analytically using the approximate expression [59]

$$j_l(z) \approx \frac{1}{z}\sin\left(z - \frac{l\pi}{2}\right), \tag{3.35}$$

which is valid for large z. Under this approximation, equation (3.27) becomes simply:

$$\sin\left(kR - \frac{l\pi}{2}\right)\sin\left(qR - \frac{l\pi}{2}\right) = 0, \tag{3.36}$$

and this gives two subfamilies of solutions, namely:

$$k^{P_1}_{nl}R = \left(n + \frac{l}{2}\right)\pi, \qquad k^{P_2}_{nl}R = \sqrt{\frac{2-2\sigma}{1-2\sigma}}\left(n + \frac{l}{2}\right)\pi. \tag{3.37}$$

When $\sigma = 1/3$ and l is even, these two subfamilies are reduced to one, for, in this case, $k^{P_1}_{(2n+l/2)l} = k^{P_2}_{nl}$. In any case, these asymptotic expansions explicitly show (in their range of application) the property of the spectrum of being real, infinite and numerable. Equations (3.37) also show that the first asymptotic subfamily $k^{P_1}_{nl}$ does not depend on the Poisson's ratio. This family is absent in monopolar modes, $k^{P_2}_{n0}$ being the only solutions to the asymptotic expansion of equation (3.34).

[4] We have developed a set of routines in the C programming language which perform the numerical work in this and the following chapters. They can be found in appendix C, together with technical notes on their implementation.

	$(l,\, n)$	$k_{nl}^P R$	$C_t q / C_l k$	ν (kHz)
1	(2, 1)	2.650057	0.442497	0.872547
2	(1, 1)	3.595977	0.987960	1.183997
3	(3, 1)	3.950174	0.173835	1.300619
4	(4, 1)	5.068344	0.079603	1.668783
5	(2, 2)	5.096570	0.382722	1.678076
6	(0, 1)	5.487415	0.000000	1.806764
7	(5, 1)	6.114831	0.039203	2.013345
8	(3, 2)	6.705269	0.212617	2.207750
9	(6, 1)	7.126136	0.020140	2.346323
10	(1, 2)	7.241487	-1.645431	2.384303
11	(7, 1)	8.117472	0.010638	2.672727
12	(4, 2)	8.308504	0.145170	2.735625
13	(1, 3)	8.549399	0.290161	2.814941
14	(2, 3)	8.625516	-1.088729	2.840003
15	(8, 1)	9.096253	0.005731	2.994996
16	(5, 2)	9.860896	0.112823	3.246760
17	(3, 3)	9.981210	-0.704011	3.286374
18	(9, 1)	10.066528	0.003133	3.314465
19	(1, 4)	10.729561	-4.366269	3.532773
20	(2, 4)	10.985709	0.222634	3.617111

Table 3.1. *First solutions to the spheroidal eigenvalue equation for $\sigma = 1/3$. The ratio between the maximum amplitudes of the transverse and longitudinal waves superposed in the corresponding normal mode is also displayed. In the last column, we list the frequency $\nu = \omega/2\pi$ of each mode for typical planned aluminium spheres ($R = 1.50\, m$, $v_t = 3160\, ms^{-1}$).*

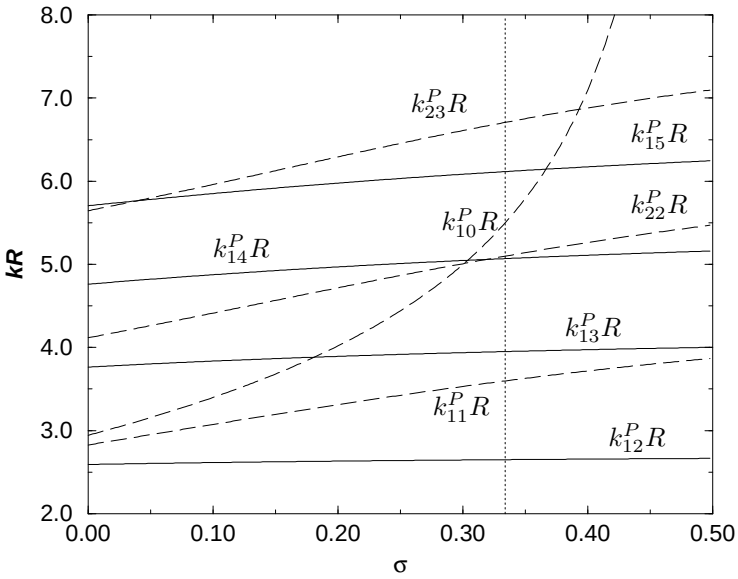

Figure 3.1. *Dependence of the first spheroidal eigenvalues $k_{nl}^P R$ on the Poisson's ratio σ. They already show, in an approximate way, the splitting into two subfamilies appearing in the asymptotical regime. The first subfamily (roots represented by continuous lines) is nearly independent of σ, while the second one (dashed lines) shows a marked dependence on Poisson's ratio. The vertical dotted line marks the usual value $\sigma = 1/3$.*

In figure 3.1, the dependence on σ of the first spheroidal eigenvalues is displayed. Remarkably, these roots can already be grouped into two subfamilies, one of them consisting of eigenvalues that vary only slightly with σ, and the other one of roots showing a more strongly marked dependence on this parameter. The relative weight that the longitudinal and transverse solutions have in each normal mode, which is given by the ratio $C_t q / C_l k$, will be also a function of σ. Figure 3.2 displays this dependence for the same set of roots, showing that increasing l implies a smaller contribution of $\mathbf{s}_t$ in the superposition conforming the normal mode.

Let us turn our attention to the spatial field of displacements associated which each

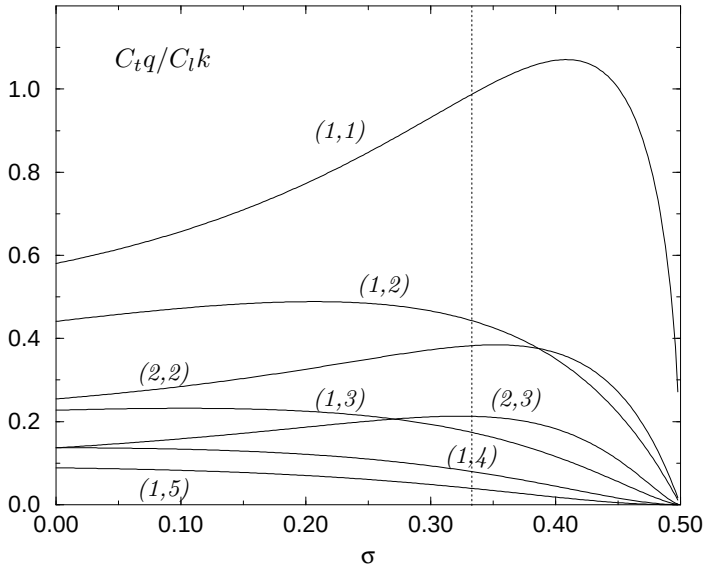

Figure 3.2. *Relative weights of the transversal ($\mathbf{s}_t$) and longitudinal ($\mathbf{s}_l$) solutions superposed in the first spheroidal normal modes, as a function of Poisson's ratio σ. The labels indicate the pair (n, l), and the dotted vertical line the usual value $\sigma = 1/3$. We observe that the longitudinal component predominates for increasing l.*

normal mode and given by equation (3.29). This equation gives a set of complex solutions, and we can make any linear combination of these modes for a fixed l, the result being again a normal mode of vibration, due to the degeneracy of eigenfrequencies. In order to cope with real displacements, instead of the usual, complex–valued spherical harmonics, we may work with the so–called *real* spherical harmonics $(Y^C_{lm}(\theta,\phi), Y^S_{lm}(\theta,\phi))$, which, for a fixed l, are given by

$$Y^C_{lm} \equiv \frac{i}{\sqrt{2}}\left(Y_{lm} + Y_{l\,-m}\right), \qquad Y^S_{lm} \equiv \frac{1}{\sqrt{2}}\left(Y_{lm} - Y_{l\,-m}\right) \qquad (m = 0 \ldots l). \tag{3.38}$$

As $Y^C_{l0} = 0$, we also have $(2l+1)$ real spherical harmonics, which are orthormal functions too. Thus, all the complex expressions obtained so far in terms of scalar and vector

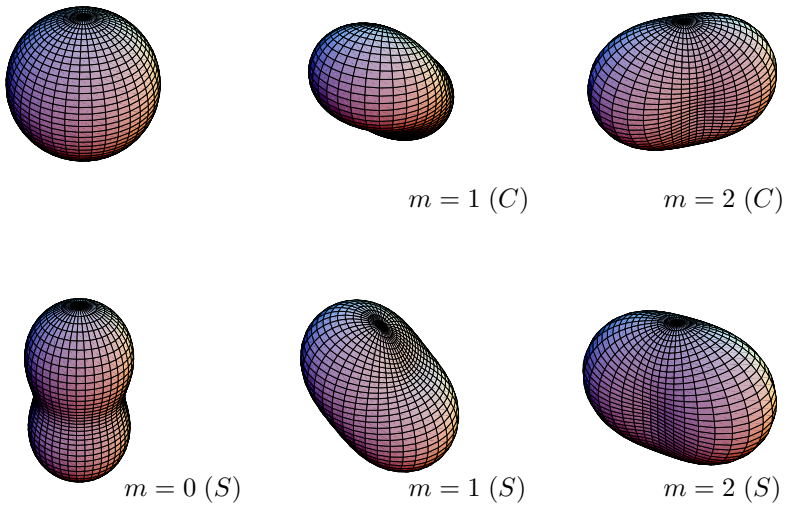

Figure 3.3. *Shape deformation induced by the quadrupolar ($l = 2$) real modes. The first row shows the undeformed sphere and modes $m = 1$ and $m = 2$ of the C-type (i.e., those induced by the normal field of displacements $Y^C_{2m}\mathbf{n}$), while in the second row the three modes of type S (corresponding to $Y^S_{2m}\mathbf{n}$) are displayed.*

spherical harmonics can be transformed to their real counterparts by simply substituting the set of functions $\{Y_{lm}\}_{m=-l\ldots l}$ by the real set $\{Y^C_{lm}, Y^S_{lm}\}_{m=0\ldots l}$.

When vibrating in a normal mode, the shape of a spherical solid will be distorted as a result of the radial displacements that its surface undergoes. This radial displacements shall be described (cf. (3.29)) by the real vector fields $A_{nl}(r)Y^{C,S}_{lm}(\theta,\phi)\mathbf{n}$, calculated at the sphere's surface. Figure (3.3) displays an overemphasized plot of the shape deformations induced by the quadrupolar normal modes of vibration, which, together with the monopolar ones (which, being isotropic, preserve the spherical shape, cf. (3.33)), will play a crucial role in the detection of gravitational radiation.

Tangential displacements also appear in spheroidal modes of vibration, due to their component along $i\,\mathbf{n}\times\mathbf{L}Y_{lm}$. In spherical coordinates, this vector has the following form:

$$-\,i\,\mathbf{n}\times\mathbf{L}Y_{lm} \;=\; \frac{\partial Y_{lm}}{\partial\,\theta}\,\boldsymbol{\theta} \;+\; \frac{1}{\sin\theta}\,\frac{\partial Y_{lm}}{\partial\,\phi}\,\boldsymbol{\phi}, \tag{3.39}$$

where $(\mathbf{n},\boldsymbol{\theta},\boldsymbol{\phi})$ is the natural orthonormal basis in spherical coordinates. Thus, the particles of the elastic solid are subject to azimuthal, as well as polar, tangential shifts.

These displacements, induced by the components of $i\,\mathbf{n}\times\mathbf{L}Y_{lm}$ along $\boldsymbol{\phi}$ and $\boldsymbol{\theta}$, are displayed, for the quadrupolar case, in figure 3.4. We have plotted in this figure only the real modes of type S, as C-modes are obtained from these by specular reflection with respect to the appropiate plane (equatorial for polar shifts and meridional for azimuthal ones). As regards the azimuthal shifts (which are null for $m=0$ due to the fact that $\partial_\phi Y_{l0}=0$), it is seen that a twist of the great circles $\theta=$const. is induced by the $m=1$ mode, while the mode $m=2$ causes a grouping of these lines. Polar displacements appear for all values of m, the case $m=0$ always preserving axial symmetry. For the sake of clarity, we have represented polar an azimuthal deformations in separate figures. The total tangential displacement caused by normal modes is obtained by vector addition of the two orthogonal shifts represented in each row of figure 3.4.

Both the radial and the tangential deformations described above repeat inside the sphere for each value of r, although weighted by the radial functions $A_{nl}(r)$ and $B_{nl}(r)$, which give the relative amplitudes of the r–independent fields $Y_{lm}\,\mathbf{n}\,,\ i\,\mathbf{n}\times\mathbf{L}Y_{lm}\,$. These functions are represented in the next section (figures 3.12 and 3.13) for the first monopolar and quadrupolar modes, together with the corresponding functions for the case of a hollow sphere.

3.3.3 Toroidal modes

The second possibility when solving equation (3.26) is to look for solutions satisfying

$$\beta_1(kR)=0 \quad\Rightarrow\quad \frac{dj_l(kR)}{d\,(kR)}=\frac{j_l(kR)}{kR}. \tag{3.40}$$

The eigenvalues obtained when solving the above equation are termed *toroidal*, and, again, they present a $(2l+1)$–fold degeneracy, as (3.40) does not depend on m. Thus, we shall label these eigenvalues k^T_{nl}, and the corresponding normal modes $\mathbf{s}^T_{nlm}$, with n and l positive integers (there are no monopolar tangential vibrations), and m (the degeneracy index) running from $-l$ to l. It should be noted that toroidal eigenvalues, unlike the case of the spheroidal family, do not depend on the material's elastic properties. Numerical evaluation of equation (3.40) yields the toroidal spectrum, whose first eigenvalues are listed in Table 3.2, together with the corresponding frequencies for the same planned detector considered in the case of spheroidal roots. The first toroidal eigenvalue happens to be the absolute minimum of the sphere's spectrum, being 5% smaller than the first spheroidal one, which is also quadrupolar.

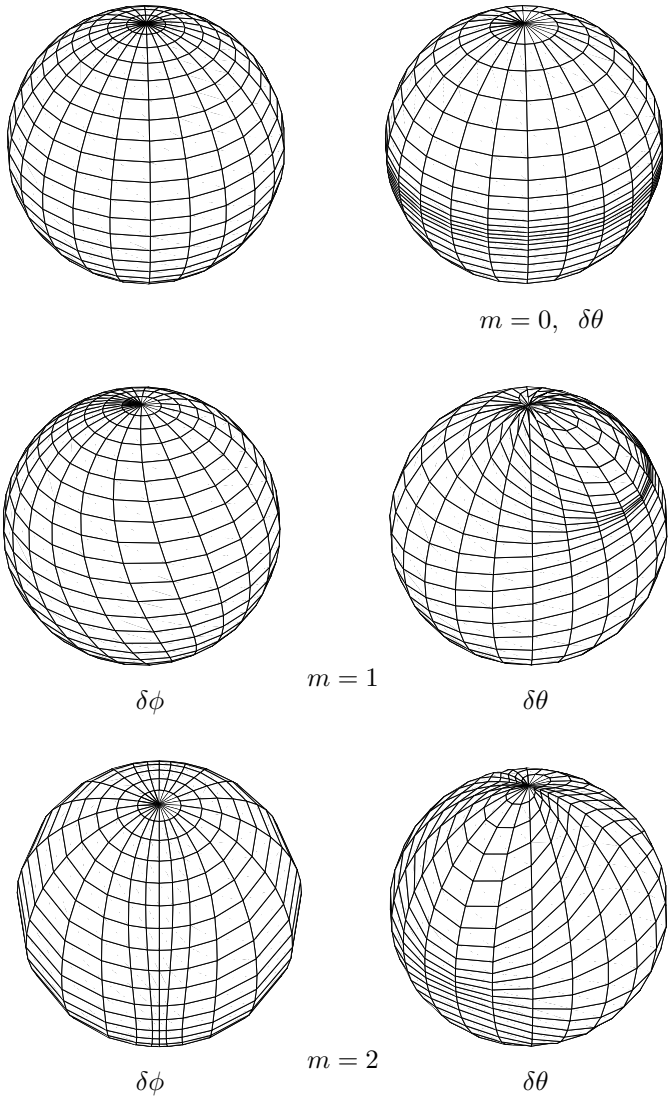

Figure 3.4. *Tangential displacements of the sphere's surface for spheroidal, quadrupolar normal modes. The first figure shows the undisturbed surface. On the left column, the azimuthal shifts appear, induced by the vector field* $(\sin\theta)^{-2}(\partial_\phi Y^S_{2m})\partial_\phi$*, which are null for* $m = 0$*. The right column displays the polar displacements, induced by the vector field* $(\partial_\theta Y^S_{2m})\partial_\theta$*.*

	(l,n)	$k_{nl}^T R$	$\nu\,(kHz)$
1	(2, 1)	2.501133	0.823513
2	(3, 1)	3.864700	1.272476
3	(4, 1)	5.094616	1.677433
4	(1, 1)	5.763459	1.897654
5	(5, 1)	6.265768	2.063042
6	(2, 2)	7.136009	2.349574
7	(6, 1)	7.403597	2.437679
8	(3, 2)	8.444922	2.780542
9	(7, 1)	8.519868	2.805218
10	(1, 1)	9.095011	2.994587

	(l,n)	$k_{nl}^T R$	$\nu\,(kHz)$
11	(8, 1)	9.620999	3.167772
12	(4, 2)	9.712504	3.197901
13	(2, 3)	10.514601	3.461996
14	(9, 1)	10.710880	3.526622
15	(5, 2)	10.950611	3.605555
16	(10, 1)	11.792051	3.882604
17	(3, 3)	11.881747	3.912137
18	(6, 2)	12.166403	4.005862
19	(1, 2)	12.322941	4.057403
20	(11, 1)	12.866264	4.236295

Table 3.2. *First toroidal eigenvalues, with the frequencies for a spherical detector with* $R = 1.5\ m$ *and* $v_t = 3160\ ms^{-1}$.

The asymptotic expression for the roots of equation (3.40) is easily computed from relation (3.35), which gives $z\,\beta_1(z) \approx -\cos(z - l\pi/2)$, and, hence,

$$k_{nl}^T R \approx \left(n + \frac{l+1}{2}\right)\pi \qquad \text{(for large kR)}. \tag{3.41}$$

In this family, the linear system for the coefficients $(C_l, C_t, C_{t'})$ has the solution

$$C_l = C_t = 0 \qquad\qquad C_{t'} = C'(n,l), \tag{3.42}$$

with $C'(n,l)$ an arbitrary constant, to be fixed by a suitable normalization condition. Thus, the spatial part of toroidal modes can be cast as

$$\mathbf{s}_{nlm}^T(r,\theta,\phi) = T_{nl}(r)\ i\,\mathbf{L}Y_{lm}\,(\theta,\phi), \tag{3.43}$$

where

$$T_{nl}(r) = C'(n,l)\,j_l(k_{nl}^T r). \tag{3.44}$$

As $i\,\mathbf{L}Y_{lm}$ is a purely tangential vector, whose components in spherical coordinates are

$$i\,\mathbf{L}Y_{lm} = \frac{1}{\sin\theta}\frac{\partial\,Y_{lm}}{\partial\,\phi}\boldsymbol{\theta} - \frac{\partial\,Y_{lm}}{\partial\,\theta}\boldsymbol{\phi}, \tag{3.45}$$

these modes give rise to purely tangential displacements of the solid's constituents. In figure 3.5 we give a pictorial representation of such displacements for the quadrupolar,

real modes of type S. As in the preceeding figure, we plot separately polar and azimuthal shifts. The total tangential deformation undergone by the surface of the sphere in each mode is obtained by the vector addition of these two orthogonal contributions.

In the next section (cf. figure 3.14), the radial function $T_{nl}(r)$ is compared with their counterparts of the hollow sphere problem.

3.4 Hollow sphere

3.4.1 Form of the solutions and boundary conditions

In this section, we shall consider the case of a hollow sphere with constant density ρ, and inner and outer radius a and R respectively. This problem preserves spherical symmetry, and has the particularity of removing the point $r = 0$ from the domain considered, and introducing a second surface ($r = a$) where boundary conditions must also be imposed. In order to find the normal modes of vibration of such a solid, we can follow the method described in section 3.2. Thus, we must solve equations (3.9) when the point $r = 0$ is removed from the domain of the functions ϕ and φ. This fact forces the introduction of the spherical Bessel functions of the second kind [2],

$$y_l(z) = (-)^{l+1} z^l \left(\frac{1}{z}\frac{d}{dz}\right)^l \frac{\cos z}{z}, \tag{3.46}$$

when constructing solutions to the radial part of (3.9), regardless the fact that $y_l(z)$ diverges at $z = 0$, which prevented its use in the case of the solid sphere. Hence, these solutions can the be cast, in spherical coordinates, as

$$\begin{aligned} \phi_{lm}(r,\theta,\phi) &= (j_l(qr) + E\, y_l(qr))\, Y_{lm}(\theta,\phi) \\ \varphi_{lm}(r,\theta,\phi) &= (j_l(kr) + F\, y_l(kr))\, Y_{lm}(\theta,\phi) \end{aligned} \tag{3.47}$$

with E and F constants[5]. The meaning and ranges of the indices l and m are the same as before.

Taking into account that the new functions ϕ, φ given in (3.47) share with their counterparts of the solid sphere case (3.15) all the properties employed in the calculations of

[5] In fact, the general solution to equations (3.9) is an arbitrary superposition of the form $\sum_{lm}(\alpha_{lm} j_l\, Y_{lm} + \beta_{lm} y_l\, Y_{lm})$, on which boundary conditions must be imposed in order to fix the set of constants $\{\alpha_{lm},\ \beta_{lm}\}$. We choose solutions with $\alpha_{l'm'} = \delta_{ll'}\delta_{mm'}$ and $\beta_{l'm'} = E\alpha_{l'm'}$, anticipating the fact that it will be enough to satisfy the requisite boundary conditions.

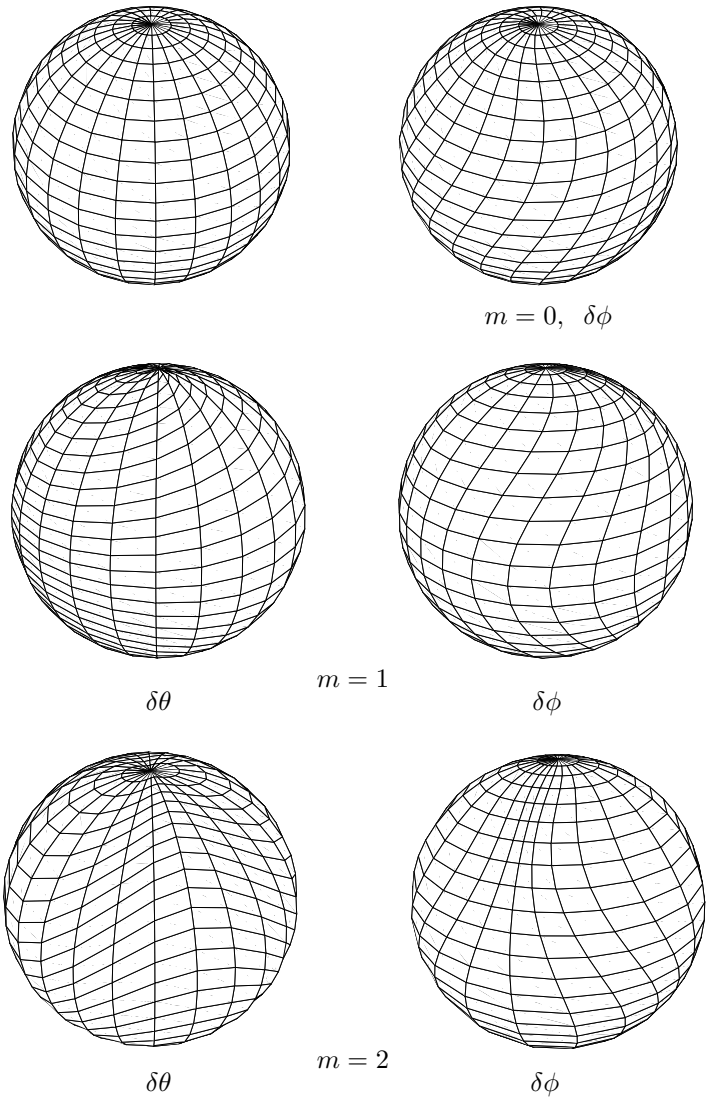

Figure 3.5. *Tangential displacements induced on the sphere's surface by toroidal modes with $l = 2$. The left column displays the polar shifts, which are induced by the vector field $(\sin\theta)^{-2}(\partial_\phi Y^s_{2m})\partial_\theta$, and cancel for $m = 0$. On the right hand column the corresponding azimuthal displacements, due to the field $(\partial_\theta Y^S_{2m})\partial_\phi$, are shown.*

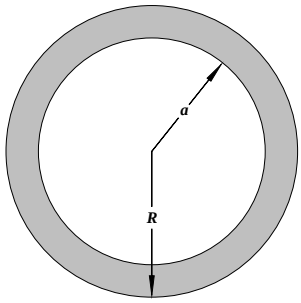

Figure 3.6. *The hollow sphere.*

the previous section, equations (3.17), (3.19) and (3.18) for the longitudinal and transverse parts of the solution in that case give us, by direct substitution, the corresponding expressions for the hollow sphere:

$$\begin{aligned}
\mathbf{s}_l(r,\theta,\phi) &= \frac{dh_l(qr,E)}{d\,r}\,Y_{lm}\,\mathbf{n} - \frac{h_l(qr,E)}{r}\,i\,\mathbf{n}\times\mathbf{L}Y_{lm}\,,\\
\mathbf{s}_t(r,\theta,\phi) &= -l(l+1)\frac{h_l(kr,F)}{r}\,Y_{lm}\,\mathbf{n} + \left(\frac{h_l(kr,F)}{r} + \frac{dh_l(kr,F)}{d\,r}\right)\,i\,\mathbf{n}\times\mathbf{L}Y_{lm}\,,\\
\mathbf{s}_{t'}(r,\theta,\phi) &= h_l(kr,F)\,i\,\mathbf{L}Y_{lm}\,,
\end{aligned} \tag{3.48}$$

where we have introduced the shorthand:

$$h_l(z,A) \equiv j_l(z) + A\,y_l(z). \tag{3.49}$$

Now, to determine completely the expression for the normal modes of vibration of a hollow sphere, we must find the relations fulfilled by the set of constants C_l, C_t, $C_{t'}$, E, F, and k appearing in our formulæ . As before, these relations are given by the boundary conditions, which for the problem in hand are

$$\frac{C_l}{q}\boldsymbol{b}[\mathbf{s}_l] + \frac{C_t}{k}\boldsymbol{b}[\mathbf{s}_t] + C_{t'}\boldsymbol{b}[\mathbf{s}_{t'}] = 0 \qquad \text{at } r = R \text{ and } r = a, \tag{3.50}$$

where the action of $\boldsymbol{b}$ on $\mathbf{s}_l$, $\mathbf{s}_t$ and $\mathbf{s}_{t'}$ can be directly obtained from the corresponding expressions for the solid sphere (3.23) by the substitutions $j_l(qr) \to h_l(qr,E)$ and $j_l(kr) \to h_l(kr,F)$. Introducing the equations thus obtained into conditions (3.50), and

defining the new set of constants

$$D_l \equiv C_l\, E \qquad D_t \equiv C_t\, F \qquad D_{t'} \equiv C_{t'}\, F, \tag{3.51}$$

the boundary conditions to be met by normal modes of vibration are translated into the following linear system of equations

$$\begin{pmatrix} \mathbb{A}_P & 0 \\ 0 & \mathbb{A}_T \end{pmatrix} \begin{pmatrix} \boldsymbol{C}_P \\ \boldsymbol{C}_T \end{pmatrix} = 0, \tag{3.52}$$

with

$$\boldsymbol{C}_P \equiv (C_l, C_t, D_l, D_t)^t, \qquad \boldsymbol{C}_T \equiv (C_{t'}, D_{t'})^t, \tag{3.53}$$

where the superscript t denotes transposition, and the corresponding matrices are:

$$\mathbb{A}_P = \begin{pmatrix} \beta_4(qR) & -l(l+1)\frac{k}{q}\beta_1(kR) & \tilde{\beta}_4(qR) & -l(l+1)\frac{k}{q}\tilde{\beta}_1(kR) \\ -\beta_1(qR) & \frac{k}{q}\beta_3(kR) & -\tilde{\beta}_1(qR) & \frac{k}{q}\tilde{\beta}_3(kR) \\ \beta_4(qa) & -l(l+1)\frac{k}{q}\beta_1(ka) & \tilde{\beta}_4(qa) & -l(l+1)\frac{k}{q}\tilde{\beta}_1(ka) \\ -\beta_1(qa) & \frac{k}{q}\beta_3(ka) & -\tilde{\beta}_1(qa) & \frac{k}{q}\tilde{\beta}_3(ka) \end{pmatrix} \tag{3.54}$$

and

$$\mathbb{A}_T = \begin{pmatrix} \beta_1(kR) & \tilde{\beta}_1(kR) \\ \beta_1(ka) & \tilde{\beta}_1(ka) \end{pmatrix} \tag{3.55}$$

Here, we have introduced the y_l–counterpart of the β-functions:

$$\begin{aligned} \tilde{\beta}_1(z) &\equiv \frac{d}{dz}\left(\frac{y_l(z)}{z}\right) \\ \tilde{\beta}_2(z) &\equiv \frac{d^2 y_l(z)}{d\, z^2} \\ \tilde{\beta}_3(z) &\equiv \frac{1}{2}\left[\tilde{\beta}_2(z) + (l+2)(l-1)\,\frac{y_l(z)}{z^2}\right] \\ \tilde{\beta}_4(z) &\equiv \tilde{\beta}_2(z) - \frac{\lambda}{2\mu} y_l(z). \end{aligned} \tag{3.56}$$

Again, in order to have solutions to the homogeneous system (3.52) other than the trivial one $\boldsymbol{C}_P = \boldsymbol{C}_T = 0$, we must impose the compatibility condition[6]

$$(\det \mathbb{A}_P) \cdot (\det \mathbb{A}_T) = 0, \tag{3.57}$$

[6]Strictly speaking, the boundary conditions are not a linear system in the set of constants $(C_l, C_t, D_l, C_t, C_{t'}, D_{t'})$, because, by virtue of (3.51), equation (3.52) must be suplemented by the condition $D_{t'}C_t = D_{t'}C_t$. Nevertheless, the natural splitting of the system of equations (3.52) into a 4×4 system and a 2×2 one allows us working either with four independent constants ($C_{t'}$, and thus $D_{t'}$ being zero) or with two independent constants ($\boldsymbol{C}_P = 0$), the aforementioned suplementary condition being trivially satisfied in both cases.

giving rise again to two families of normal modes to which we shall extend the solid sphere's terminology, calling them *spheroidal* and *toroidal* modes as well. The left hand side of the above equation is a function of the dimensionless parameters kR, σ and $\eta \equiv a/R$. Thus, the eigenvalues will be in general functions of the sphere's elastic properties, as described by σ, and the sphere's geometry, as described by η.

3.4.2 Spheroidal modes

This family of solutions is characterized by the eigenvalue equation

$$\det \mathbb{A}_P = 0, \tag{3.58}$$

allowing solutions satisfying

$$\mathbb{A}_P \cdot \boldsymbol{C}_P = 0, \qquad \boldsymbol{C}_T = 0. \tag{3.59}$$

We shall label the solutions to (3.58) k^P_{nl}, for, once again, the eigenvalue equation is independent of m, giving rise to a degenerate frequency spectrum. The above equations are rather cumbersome, as they involve rank four matrices. The simpler case is $l = 0$, which, as we know, is purely radial, and has the following eigenvalue equation:

$$\beta_4(qR)\tilde{\beta}_4(qa) - \beta_4(qa)\tilde{\beta}_4(qR) = 0, \tag{3.60}$$

with C_l and D_l solutions of the linear homogeneous system

$$\begin{pmatrix} \beta_4(qR) & \tilde{\beta}_4(qR) \\ \beta_4(qa) & \tilde{\beta}_4(qa) \end{pmatrix} \begin{pmatrix} C_l \\ D_l \end{pmatrix} = 0. \tag{3.61}$$

Spheroidal eigenvalues do depend both on σ and η. In Table 3.3 we list the first spheroidal eigenvalues (and the corresponding frequencies for an aluminium sample with $R = 1.5\,m$) for $\sigma = 1/3$ and $\eta = 0.25,\ 0.50$ and 0.75. Although the order of the different roots varies with η, the first quadrupolar frequency is always the lowest one in the spheroidal family. Numerical solution of the eigenvalue equation shows that k^P_{nl} has a dependence on η which, qualitatively, is given by n. In fact, the first root for modes with $l \geq 2$ is always a decreasing function of η (cf. figure 3.7), this property being also shared by the first monopolar mode; when $n = 2$ (and for $n = 1$ when $l = 1$) the root oscillates slightly in a pattern shown in figure 3.8; and, finally, for $n \geq 3$, k^P_{nl} diverges when $\eta \to 1$ (thin shell limit), this divergence appearing also in monopolar and dipolar modes for $n > 1$ (figure 3.9). Thus, a thin shell has, at most, *two* eigenfrequencies for each l, and

	(l, n)	$k_{nl}^{P} R$	$(C_{tl},\ D_{ll},\ D_{tl})$	ν (kHz)
		$\eta = 0.25$		
1	(2, 1)	2.491216	(0.303268, 0.003210, -0.012471)	0.820248
2	(1, 1)	3.700662	(1.056228, -0.027622, 0.097136)	1.218465
3	(3, 1)	3.894918	(0.159434, 0.000441, -0.002232)	1.282425
4	(2, 2)	4.912235	(0.323602, 0.019483, -0.069335)	1.617383
5	(0, 1)	5.048421	(0.000000, -0.179998, 0.000000)	1.662223
6	(4, 1)	5.056670	(0.078462, 0.000027, -0.000203)	1.664939
7	(5, 1)	6.112869	(0.039120, 0.000001, -0.000015)	2.012699
8	(3, 2)	6.586822	(0.194668, 0.007004, -0.032137)	2.168751
9	(6, 1)	7.125845	(0.020134, 0.000000, -0.000001)	2.346227
		$\eta = 0.50$		
1	(2, 1)	1.943404	(0.150106, 0.003041, -0.011338)	0.639877
2	(3, 1)	3.168814	(0.072334, 0.001346, -0.006256)	1.043351
3	(0, 1)	3.969140	(0.000000, -0.631168, 0.000000)	1.306863
4	(1, 1)	3.998811	(1.183588, -0.253215, 0.540663)	1.316633
5	(4, 1)	4.445421	(0.042265, 0.000520, -0.003362)	1.463682
6	(2, 2)	5.064527	(0.372629, 0.005133, -0.014444)	1.667526
7	(5, 1)	5.697438	(0.026191, 0.000160, -0.001540)	1.875916
8	(3, 2)	6.517863	(0.180908, 0.021559, -0.058763)	2.146046
9	(6, 1)	6.880729	(0.016035, 0.000038, -0.000570)	2.265521
		$\eta = 0.75$		
1	(2, 1)	1.449650	(0.112520, 0.001376, -0.005086)	0.477306
2	(3, 1)	2.068307	(0.041973, 0.000208, -0.000980)	0.681002
3	(4, 1)	2.828082	(0.018489, 0.000046, -0.000309)	0.931163
4	(0, 1)	3.265239	(0.000000, -0.901291, 0.000000)	1.075100
5	(5, 1)	3.742582	(0.008995, 0.000015, -0.000149)	1.232268
6	(1, 1)	3.877391	(1.148976, -0.676016, 0.804162)	1.276654
7	(6, 1)	4.758597	(0.004698, 0.000006, -0.000090)	1.566797
8	(2, 2)	5.215992	(0.455499, -0.197532, 0.204720)	1.717397
9	(7, 1)	5.835086	(0.002588, 0.000003, -0.000059)	1.921237

Table 3.3. *Roots and relative weights of the transverse and longitudinal solutions superposed in spheroidal normal modes for different values of η and $\sigma = 1/3$.*

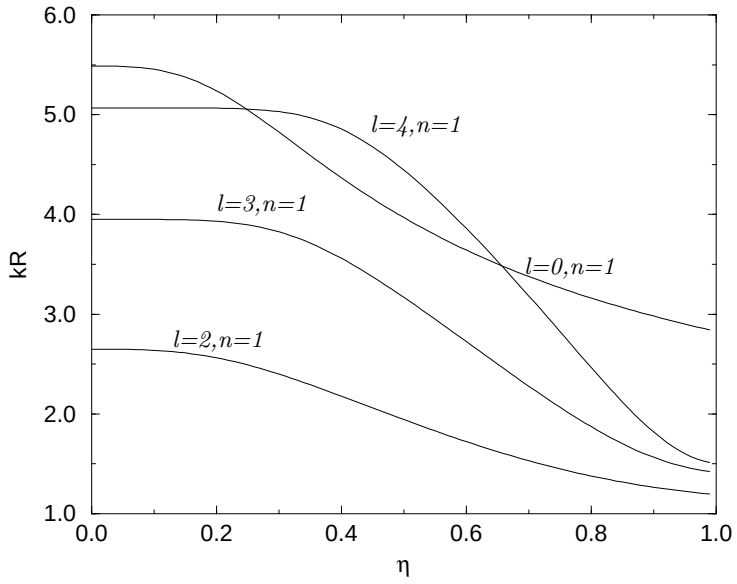

Figure 3.7. *Spheroidal eigenvalues with finite limit for $\eta = 1$. The graphic shows the decreasing profile shared by the first monopolar mode and modes with $n = 1$ and $l \geq 2$.*

just *one* monopolar and dipolar modes of vibration. This cut–off in the spectrum can be seen analytically when $l = 0$. In this case, the eigenvalue equation (3.60), becomes, for η close to 1,

$$0 = \beta_4(qR)\frac{d\tilde{\beta}_4(qR)}{d\,(qR)} - \frac{d\beta_4(qR)}{d\,(qR)}\tilde{\beta}_4(qR) = \left(\frac{\lambda}{2\mu}+1\right)^2 \frac{1}{(qR)^2} - \left(\frac{3\lambda}{\mu}+2\right)\frac{1}{(qR)^4},$$

having thus just one eigenvalue, namely

$$k_{10}^P R = 2\sqrt{(1+\sigma)/(1-\sigma)} \qquad\qquad (\eta = 1). \tag{3.62}$$

The asymptotic behaviour of spheroidal roots is obtained from the asymptotic expansions of spherical Bessel functions [59]

$$j_l(z) \approx \frac{\sin(z - l\phi/2)}{z}, \qquad y_l(z) \approx (-)^{l+1}\frac{\cos(z + l\pi/2)}{z}, \tag{3.63}$$

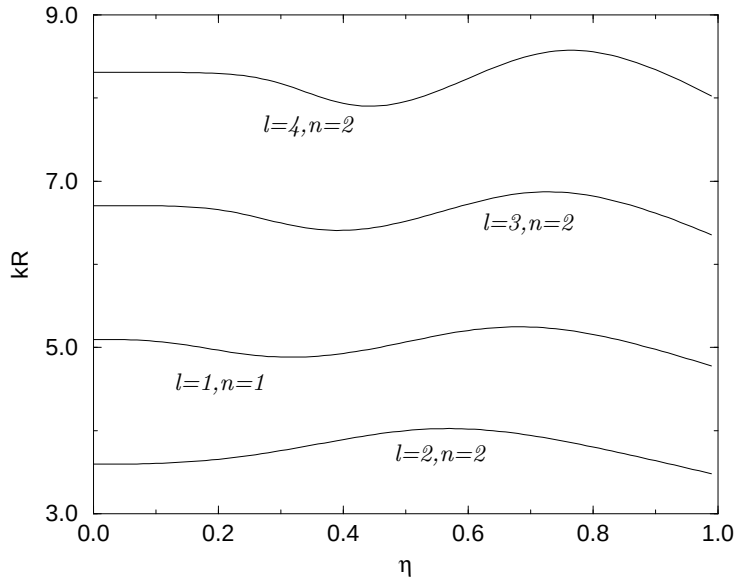

Figure 3.8. *Spheroidal eigenvalues with finite limit for $\eta = 1$. This figure displays the oscillatory behaviour of roots such that $n = 2$ and $l \geq 2$, which also appears in the first dipolar mode.*

which are valid for large z. Using the above approximations, we can easily obtain

$$\det \mathbb{A}_p = \left(1 + \frac{\lambda}{2\mu}\right)^2 \frac{q^2}{4k^2\eta^2} \frac{1}{(kR)^4} \sin[kR(1-\eta)] \, \sin[qR(1-\eta)] + O\left(\frac{1}{(kR)^6\eta^3}\right). \quad (3.64)$$

This equation gives us two subfamilies of spheroidal eigenvalues in the asymptotic regime of large kR *and* $kR\eta$, namely

$$k_{nl}^{P_1} R = \frac{n\pi}{1-\eta} \qquad k_{nl}^{P_2} R = \sqrt{\frac{2-2\sigma}{1-2\sigma}} \frac{n\pi}{1-\eta}, \quad (3.65)$$

which have the remarkable property of being independent of l. The divergence of the roots as $\eta \to 1$ also appears explicitly. Both properties are already present in figure 3.9, where we observe some diverging roots with $n = 3$ (or $n = 2$ for $l = 1$) becoming closer as their values increase, and approaching the curve $kR = \pi/(1-\eta)$ (we take $n = 1$ for

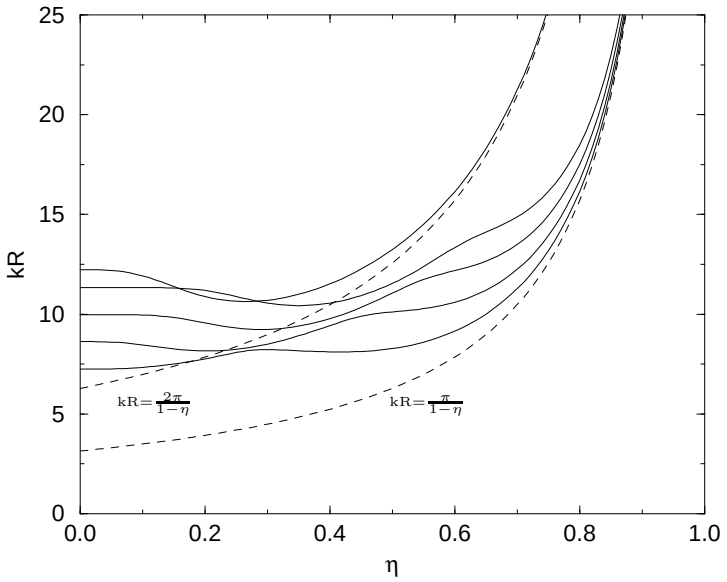

Figure 3.9. *Spheroidal eigenvalues diverging as $\eta \to 1$. This behaviour appears for the second and higher monopolar and dipolar eigenvalues, and for $n \geq 3$ when $l \geq 2$. Dotted lines display the asymptotic values to which the roots approach for large values of kR. In ascending order, the eigenvalues represented are k_{21}, k_{32}, k_{33}, k_{34} (this group approaching the first asymptotic curve) and k_{20}.*

$k_{nl}^{P_1}$ as the roots considered are the first divergent ones for each l). In this figure appears also the first monopole eigenvalue, whose asymptotic expression must be obtained from equations (3.60), yielding

$$k_{0n}^{P} R = \sqrt{\frac{2-2\sigma}{1-2\sigma}}\, n\,\pi, \tag{3.66}$$

which becomes $k_{0n}^{P} R = 2n\pi$ for $\sigma = 1/3$. Thus, the first divergent eigenvalue of $l = 0$ approaches the curve $kR = 2\pi/(1-\eta)$, as shown in the figure.

Provided (3.58) holds, the first of equations (3.59) can be solved for the quotients

$$C_{tl} \equiv \frac{C_t q}{C_l k}, \qquad D_{ll} \equiv \frac{D_l q}{C_l k}, \qquad D_{tl} \equiv \frac{D_t q}{C_l k}, \tag{3.67}$$

which have rather cumbersome explicit expressions and depend not only on k_{nl}^{P} but also

on σ and η. With these definitions, the final form of the spheroidal normal modes of vibration for the hollow sphere is given by

$$\mathbf{s}^P_{nlm}(r,\theta,\phi) = A_{nl}(r)Y_{lm}(\theta,\phi)\mathbf{n} - iB_{nl}(r)\mathbf{n}\times\mathbf{L}Y_{lm}(\theta,\phi), \tag{3.68}$$

with radial functions

$$\begin{aligned} A_{nl}(r) = C(n,l) \quad & \left[\frac{dj_l(q^P_{nl}r)}{d\,(q^P_{nl}r)} - C_{tl}\,l(l+1)\,\frac{j_l(k^P_{nl}r)}{k^P_{nl}r} + \right. \\ & \left. D_{ll}\frac{dy_l(q^P_{nl}r)}{d\,(q^P_{nl}r)} - D_{tl}\,l(l+1)\,\frac{y_l(k^P_{nl}r)}{k^P_{nl}r}\right], \end{aligned} \tag{3.69}$$

$$\begin{aligned} B_{nl}(r) = C(n,l) \quad & \left[\frac{j_l(q^P_{nl}r)}{q^P_{nl}r} - C_{tl}\frac{1}{k^P_{nl}r}\frac{d}{dr}\{r\,j_l(k^P_{nl}r)\} + \right. \\ & \left. D_{ll}\frac{y_l(q^P_{nl}r)}{q^P_{nl}r} - D_{tl}\frac{1}{k^P_{nl}r}\frac{d}{dr}\{r\,y_l(k^P_{nl}r)\}\right], \end{aligned} \tag{3.70}$$

where $C(n,l)$ is, again, free up to normalization.

Monopolar modes have simpler expressions, due to the fact that they are purely normal. They can be written as

$$\mathbf{s}^P_{n00}(r,\theta,\phi) = A_{n0}(r)\,\mathbf{n}, \tag{3.71}$$

with

$$A_{n0}(r) = C(n,0)\left[\tilde{\beta}_4(k^P_{n0}R)\frac{dj_0(q^P_{n0}r)}{d(q^P_{n0}r)} - \beta_4(k^P_{n0}R)\frac{dy_0(q^P_{n0}r)}{d(q^P_{n0}r)}\right]. \tag{3.72}$$

The shape deformations induced by normal modes of vibration in a hollow sphere are identical to those appearing in the solid sphere (see figure 3.4 in the preceeding section), the only difference between the two cases being the form of the radial functions $A_{nl}(r)$ and $B_{nl}(r)$.

The coefficients C_{tl}, D_{ll} and D_{tl} measure the relative weights of the j_l and y_l contributions of transverse and longitudinal solutions to the normal modes of vibration. In Table 3.3 we give their values for some values of η and (l,n). Their dependence on the Poisson's ratio is found to be qualitatively the same as that of the coefficients C_tq/C_lk of the solid sphere (cf. figure 3.2; the eigenvalues also show a profile similar to that of figure 3.1, which corresponds to the solid sphere, for any η). As regards the dependence of these weights on the parameter η, it is displayed (for $\sigma = 1/3$ and the first few roots) in figure 3.10 for the j_l contribution of $\mathbf{s}_t$, and in figure 3.11 for the y_l transverse and longitudinal parts. As expected, D_{tl} and D_{ll} both vanish for $\eta = 0$.

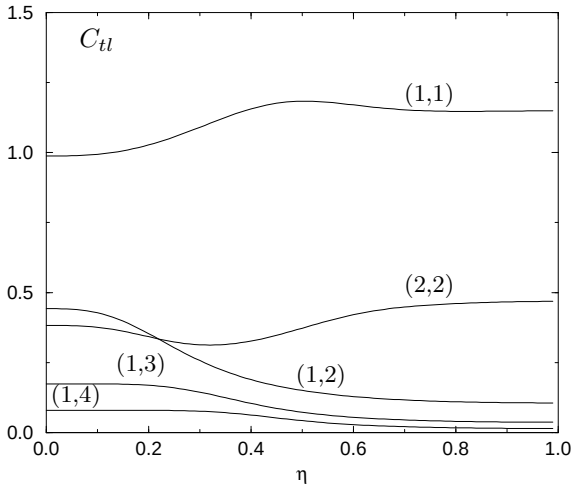

Figure 3.10. *Relative weights of the j_l transverse part of spheroidal normal modes, as a function of η. Labels denote the indices (n, l).*

Let us now turn our attention to the radial functions $A_{nl}(r)$ and $B_{nl}(r)$. We shall fix the normalization constant appearing in those functions as follows

$$\int_V \rho\,(\mathbf{s}^P_{nlm}) \cdot (\mathbf{s}^P_{n'l'm'})^*\, dV = M\,\delta_{nn'}\delta_{ll'}\delta_{mm'}, \tag{3.73}$$

where M denotes the total mass of the solid, i.e., when ρ =const.,

$$M = \frac{4\pi}{3}\rho\, R^3(1-\eta^3).$$

In this case, the angular dependence can be immediately integrated using the orthogonality relations of vector spherical harmonics (3.20), so that the normalization condition becomes

$$\int_{R\eta}^{R} r^2\, dr\, \left(A^2_{nl}(r) + l(l+1)\, B^2_{nl}(r)\right) = \frac{4\pi}{3} R^3(1-\eta^3). \tag{3.74}$$

Figures 3.12 and 3.13 show $A_{nl}(r)$ and $B_{nl}(r)$, with the above normalization, for the first two monopolar and quadrupolar eigenvalues and the values 0, 0.375 and 0.750

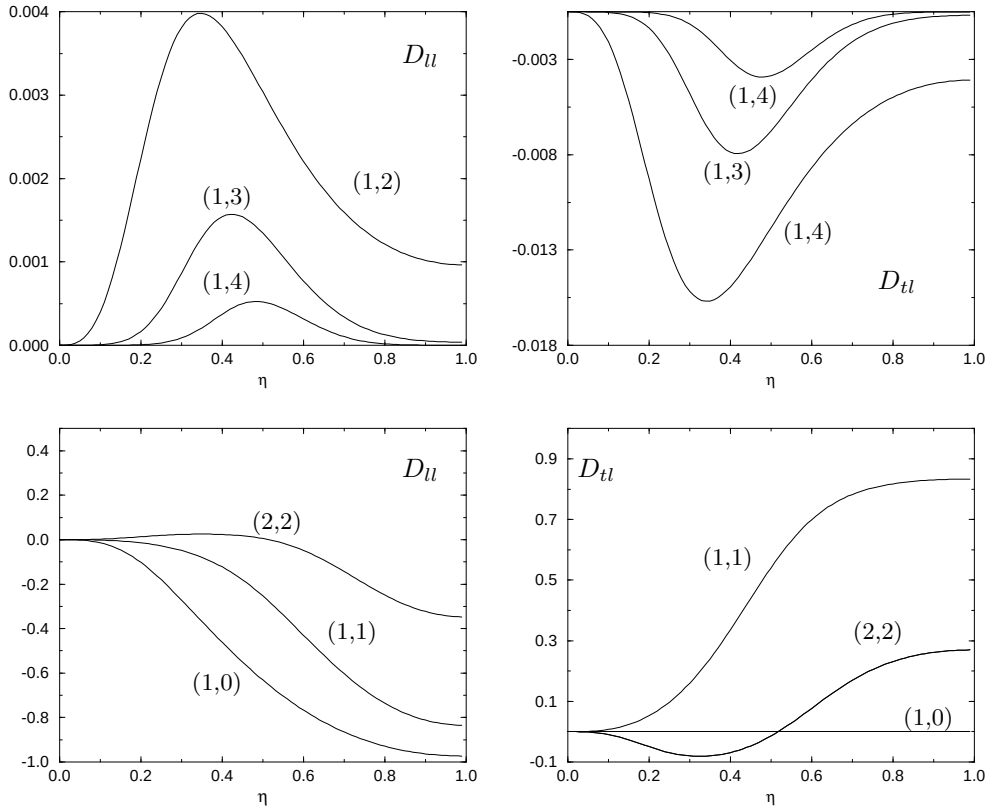

Figure 3.11. *Relative weights, as a function of η, for the y_l longitudinal (D_{ll}) and transverse (D_{tl}) contributions to a spheroidal normal mode. Labels indicate the indices (n, l).*

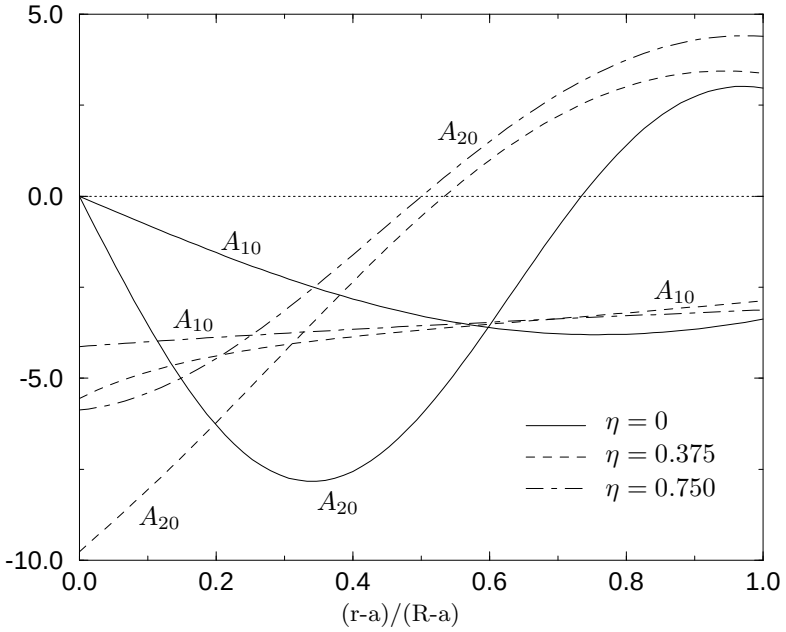

Figure 3.12. *Radial functions for the first two monopolar eigenvalues in the spheroidal family, calculated at different values of the parameter η.*

for the parameter η. For observational purposes, the value that these functions take at the sphere's outer surface is of the utmost importance, because measurements of the deformations will be performed there. For instance, detection of the second quadrupolar mode by measurement of normal displacements on the surface of a solid sphere is severely hadicapped by the small value of $A_{22}(R)$ when $\eta = 0$ (cf. figure 3.13). As can be observed in the figures, the normal and tangential amplitudes on the surface show little dependence on η, with the exception of $A_{22}(R)$, which shows a significant relative improvement with increasing η.

3.4.3 Toroidal modes

Toroidal eigenvalues are solutions to equation (3.57) satisfying

$$\det \mathbb{A}_T = \beta_1(kR)\tilde{\beta}_1(ka) - \beta(ka)\tilde{\beta}_1(kR) = 0, \tag{3.75}$$

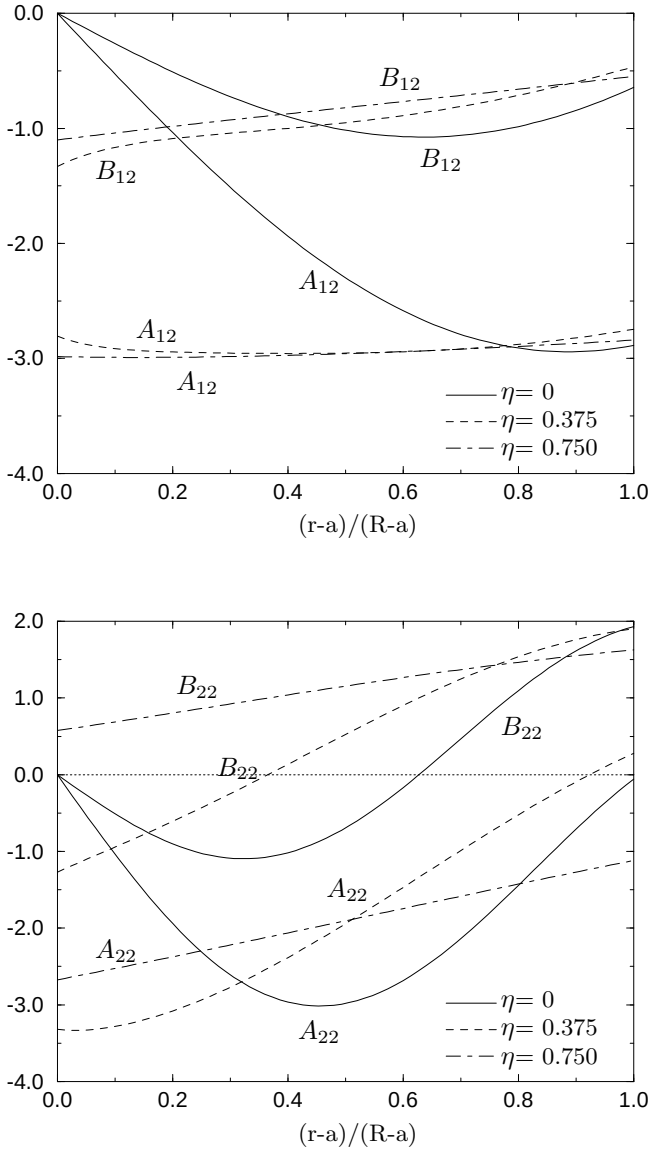

Figure 3.13. *Radial functions for the first two quadrupolar eigenvalues in the spheroidal family, calculated at different values of the parameter η.*

and giving rise to purely tangential solutions with

$$\mathbb{A}_T \cdot \boldsymbol{C}_T = 0 \qquad \boldsymbol{C}_P = 0. \tag{3.76}$$

Again, we are left with a degenerate spectrum k_{nl}^T which is not dependent on the material's Poisson's ratio. In Table 3.4 we give a list of the first solutions to equation (3.75) for some values of the parameter η, as well as the corresponding frequencies for the usual aluminium sample. As in the case of the solid sphere, the first quadrupolar mode of the toroidal family happens to be the absolute minimum in the hollow sphere's spectrum.

In the thin shell limit ($\eta \to 1$), the eigenvalue equation has the form

$$\beta_1(kR)\frac{d\tilde{\beta}_1(kR)}{d\,(kR)} - \tilde{\beta}_1(kR)\frac{d\beta_1(kR)}{d\,(kR)} = 0.$$

Using standard properties of spherical Bessel functions, the following useful relation is easily proved[7]

$$\beta_1(z)\frac{d\tilde{\beta}_1(z)}{d\,z} - \tilde{\beta}_1(z)\frac{d\beta_1(z)}{d\,z} = z^{-6}\left[z^2 + 2 - l(l+1)\right],$$

whence toroidal modes in the thin shell limit have the explicit value

$$k_{1l}^T R = \sqrt{l(l+1) - 2} \qquad (\eta = 1,\ l > 1). \tag{3.77}$$

When plotting k_{nl}^T as a function of η, this property appears as a divergence of the first monopolar mode and all modes with $n \geq 2$ when $\eta \to 1$ (cf. figures 3.15 and 3.16). On the other hand, asymptotic expansion yields

$$\det \mathbb{A}_T = (-)^{l+1}\frac{1}{\eta^2 (kR)^4}\sin[kR\,(1-\eta)] + O\left(\frac{1}{(kR)^6\eta^3}\right), \tag{3.78}$$

so that, for large values of kR and ka, the eigenvalues adopt the approximate form

$$k_{nl}^T R \approx \frac{(n-1)\pi}{1-\eta}, \tag{3.79}$$

[7] The recurrence relationship $j_l'(z) = j_{l-1}(z) - (l+1)z^{-1}j_l(z)$, where prime denotes derivative, yields

$$z\beta_1(z) = j_{l-1}(z) - (l+2)z^{-1}j_l(z), \qquad z^3{\beta'}_1(z) = [(l+2)(l+3) - z^2]j_l(z) - 4zj_{l-1}(z),$$

with analogous expressions for $\tilde{\beta}_1$ and $\tilde{\beta}_1'$. Using these equations and the identity

$$j_l(z)y_{l-1}(z) - j_{l-1}(z)y_l(z) = z^{-2},$$

the given relationship follows.

	(l,n)	$k_{nl}^T R$	ν (kHz)
	$\eta = 0.25$		
1	(2, 1)	2.498049	0.822498
2	(3, 1)	3.864003	1.272246
3	(4, 1)	5.094490	1.677392
4	(1, 1)	5.857718	1.928689
5	(5, 1)	6.265748	2.063035
6	(2, 2)	7.102061	2.338397
7	(6, 1)	7.403594	2.437678
8	(3, 2)	8.421440	2.772810
9	(7, 1)	8.519868	2.805218
10	(1, 2)	9.570403	3.151113
	$\eta = 0.50$		
1	(2, 1)	2.435374	0.801861
2	(3, 1)	3.813204	1.255520
3	(4, 1)	5.061620	1.666569
4	(5, 1)	6.246701	2.056764
5	(1, 1)	7.111576	2.341529
6	(6, 1)	7.393275	2.434281
7	(2, 2)	7.742637	2.549310
8	(7, 1)	8.514524	2.803458
9	(3, 2)	8.605614	2.833451
10	(8, 1)	9.618318	3.166889

	(l,n)	$k_{nl}^T R$	ν (kHz)
	$\eta = 0.75$		
1	(2, 1)	2.247062	0.739859
2	(3, 1)	3.550788	1.169118
3	(4, 1)	4.760115	1.567297
4	(5, 1)	5.931117	1.952856
5	(6, 1)	7.080886	2.331424
6	(7, 1)	8.216433	2.705310
7	(8, 1)	9.341120	3.075620
8	(9, 1)	10.456733	3.442942
9	(10, 1)	11.564321	3.807623
10	(11, 1)	12.664570	4.169886
	$\eta = 1$		
1	(2, 1)	2.000000	0.658512
2	(3, 1)	3.162278	1.041199
3	(4, 1)	4.242641	1.396915
4	(5, 1)	5.291503	1.742259
5	(6, 1)	6.324555	2.082398
6	(7, 1)	7.348469	2.419528
7	(8, 1)	8.366600	2.754754
8	(9, 1)	9.380832	3.088695
9	(10, 1)	10.392305	3.421729
10	(11, 1)	11.401754	3.754096

Table 3.4. *First toroidal eigenvalues for different values of the parameter η. The limit case of the thin shell, which presents just one root for each multipole, can be calculated analytically. The frequencies listed are those of an aluminium prototype with $R = 1.5\,m$ and $v_t = 3160\ ms^{-1}$.*

where the factor $(n-1)$ takes into account the fact that the first root of each multipole remains finite and does not enter in the asymptotic regime (for dipolar eigenvalues, $(n-1)$ must be replaced by n, because, as has been shown, there are no roots with $l=1$ and finite limit when $\eta=1$). As in the case of spheroidal roots, $k_{nl}^T R$ becomes asymptotically independent of l, and we have a convergence of roots with the same value of n. This behaviour is effectively found in numerical calculations, as is reflected in figure 3.15.

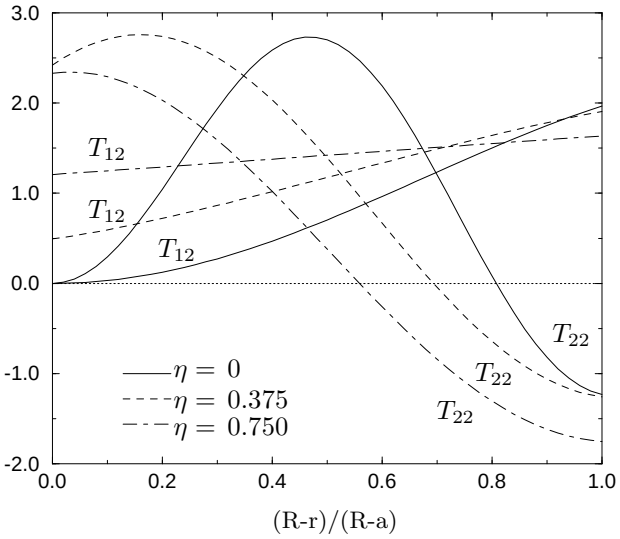

Figure 3.14. *Radial functions for the two first quadrupolar normal modes of the toroidal family.*

Finally, the spatial part of toroidal normal modes of vibration for the hollow sphere can be written

$$\mathbf{s}_{nlm}^T(r,\theta,\phi) = T_{nl}(r)\, i\, \mathbf{L} Y_{lm}\,(\theta,\phi), \tag{3.80}$$

where

$$T_{nl}(r) = C'(n,l)[\tilde{\beta}_1(k_{nl}^T R) j_l(k_{nl}^T r) - \beta_1(k_{nl}^T R) y_l(k_{nl}^T r)(k_{nl}^T r), \tag{3.81}$$

where $C'(n,l)$ is a normalization constant, which can be fixed imposing, for instance,

$$\int_V (\mathbf{s}_{nlm}^T)\cdot(\mathbf{s}_{n'l'm'}^T)^*\,\rho\, dV = M\,\delta_{nn'}\delta_{ll'}\delta_{mm'}. \tag{3.82}$$

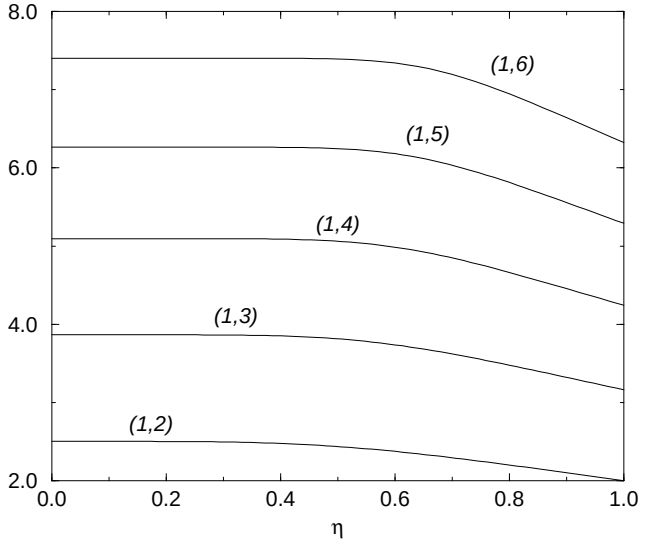

Figure 3.15. *Toroidal eigenvalues as a function of η. The above figure shows roots with finite limit as $\eta \to 1$. The dotted lines represent the asymptotic values $kR = \pi(1-\eta)^{-1}$ and $kR = 2\pi(1-\eta)^{-1}$.*

For ρ =const., the above condition becomes (cf. (3.20))

$$\int_{R\eta}^{R} T_{nl}^2 r^2 dr = \frac{4\pi}{3l(l+1)} R^3(1-\eta^3). \tag{3.83}$$

In figure 3.14 we plot, using this normalization, T_{12} and T_{22} for different values of η, including the solid sphere case. We observe again that the values of the radial functions at the sphere's outer surface do not vary significantly with η.

3.5 Deviations from spherical symmetry

To close our study of spherical elastic bodies, we address the problem of how small deviations from spherical symmetry affect the spectrum properties. Our main motivation is to take into account the deformations induced in a perfectly spheric and homogeneous sphere by its being suspended in a homogeneous gravitational field. The previous calculations have ended in a set of somewhat cumbersome equations describing the solutions to the unperturbed problem, which are little adapted to further manipulation. We begin,

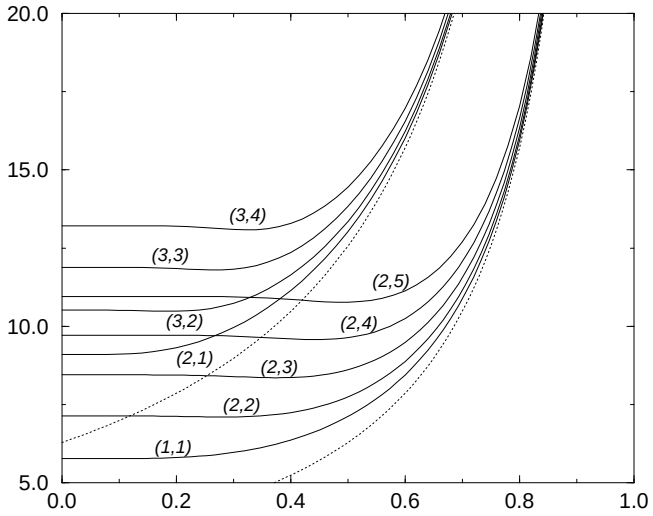

Figure 3.16. *Toroidal eigenvalues as a function of η. The above figure shows roots with finite divergent as $\eta \to 1$. The dotted lines represent the asymptotic values $kR = \pi(1-\eta)^{-1}$ and $kR = 2\pi(1-\eta)^{-1}$.*

thus, with a reformulation of the equations of motion in the language of linear differential operators in Hilbert spaces. This will allow us taking advantage of the well-known formalism of eigenfunction expansions and Green functions, which permit an elegant formulation of the perturbed problem and a quick solution, at least from a formal point of view, in subsection x3.5.2. There, we give perturbative expansions for the spectrum of a solid which is not exactly spheric and/or has small density inhomogeneities. In order to see this formalism at work, we calculate in x3.6 the actual shape deformation and density variations caused by the suspension of a solid sphere in the Earth's gravitational field, for a general surface suspension; and, finally, give a numerical example with the calculation of the threefold splitting of the first quadrupole spheroidal eigenfrequency of the solid sphere as an outcome of an axial suspension. For the sake of simplicity, we limit ourselves in the following to the solid sphere, but, as we have shown, the generalization of our expressions to the hollow sphere's case can be easily undertaken.

3.5.1 Unpertubed problem: notation

In order to take advantage of the eigenvalue expansions of Green's functions associated to partial differential equations, let us reformulate our unperturbed problem—i.e., the determination of the normal modes of vibration of an elastic solid—in a notation which makes explicit that we are dealing with an eigenvalue problem in a Hilbert space.

Let V and S denote, respectively, the three-dimensional domain occupied by the body at hand and its surface. Given two vector fields on V, say $\boldsymbol{A}(\mathbf{x})$ and $\boldsymbol{B}(\mathbf{x})$, we define their Hermitian scalar product $(\boldsymbol{A}, \boldsymbol{B})$ in the usual way:

$$(\boldsymbol{A}, \boldsymbol{B}) \equiv \int_V \boldsymbol{A}^* \cdot \boldsymbol{B}\, dV, \tag{3.84}$$

where an asterisc denotes complex conjugation. This product endows the set of square integrable vector fields over V with the structure of a Hilbert space which we shall term $\mathcal{H}$. On this space, linear differential operators are represented by 3×3 matrices whose elements are scalar differential operators. In particular, we shall introduce the linear operators $\mathbb{L}$ and $\mathbb{T}$ given by

$$(\mathbb{L})_{ij} \equiv (1+h)\partial_i\partial_j + \delta_{ij}\partial_k\partial_k, \tag{3.85}$$

$$(\mathbb{T})_{ij} \equiv h n_i \partial_j + 2\delta_{ij} n_k \partial_k + \epsilon_{ikl}\epsilon_{lmj} n_k \partial_m, \tag{3.86}$$

where h is the real quotient λ/μ, $\mathbf{n}$ denotes the outward normal to S and ϵ_{ijk} is Levi-Civita's totally antisymmetric tensor. The following relation between these operators is easily seen to hold for arbitrary vector fields $\boldsymbol{A}$ and $\boldsymbol{B}$:

$$(\boldsymbol{A}, \mathbb{L}\boldsymbol{B}) = (\mathbb{L}\boldsymbol{A}, \boldsymbol{B}) + \int_S (\boldsymbol{A}^* \cdot \mathbb{T}\boldsymbol{B} - \boldsymbol{B} \cdot \mathbb{T}\boldsymbol{A}^*)\, dS, \tag{3.87}$$

so that $\mathbb{L}$ is a self–adjoint operator when acting on the subspace $\mathcal{H}_h$ of vector fields satisfying homogeneous boundary conditions, i.e.,

$$\mathcal{H}_h \equiv \{\boldsymbol{A} \in \mathcal{H} \mid \ \mathbb{T}\boldsymbol{A}|_S = 0\}. \tag{3.88}$$

Within this formalism, the problem of determining the normal modes of vibration of the given solid translates into the the eigenvalue problem

$$\mathbb{L}\mathbf{s}_N(\mathbf{x}) = -\frac{\rho}{\mu}\omega_N^2 \mathbf{s}_N(\mathbf{x}), \qquad \mathbf{s}_N \in \mathcal{H}_h. \tag{3.89}$$

$\mathbb{L}$ being a self–adjoint operator, the above equations admit a denumerably infinite set of solutions (labelled here with a generic index N), with real spectrum. Moreover, these

solutions form a complete set over $\mathcal{H}_h$ and, thus, the following closure relation holds:

$$\sum_N \mathbf{s}_N^*(\mathbf{x}') \otimes \mathbf{s}_N(\mathbf{x}) = \frac{M}{\rho}\,\mathbb{I}\,\delta^{(3)}(\mathbf{x}-\mathbf{x}'), \tag{3.90}$$

where $\otimes$ denotes the tensor product, $\mathbb{I}$ is the unit matrix, $\delta^{(3)}(\mathbf{x}-\mathbf{x}')$ stands for the three–dimensional Dirac's function, and the eigenvectors have been normalized so that

$$(\rho\,\mathbf{s}_N, \mathbf{s}_L) = \delta_{LN} M. \tag{3.91}$$

The previous sections have been devoted to a detailed analysis of the eigenvectors of $\mathbb{L}$ when V is a spherically symmetric domain.

When dealing with small perturbations of equations (3.89) we shall make use of their associated Green's operator $\mathbb{G}(\mathbf{x}, \mathbf{x}', \omega)$, which is defined[95] to be the solution to

$$\mathbb{L}\mathbb{G} + \frac{\rho\omega^2}{\mu}\mathbb{G} = -\mathbb{I}\frac{1}{\rho}\delta^{(3)}(\mathbf{x}-\mathbf{x}'), \tag{3.92}$$

satisfying homogeneous boundary conditions on S:

$$\mathbb{T}\mathbb{G}|_S = 0. \tag{3.93}$$

From the closure relationship (3.90) the following expansion of $\mathbb{G}$ in terms of eigenfunctions is readily obtained

$$\mathbb{G}(\mathbf{x}, \mathbf{x}', \omega) = \sum_N \frac{\mu}{\rho M}\frac{\mathbf{s}_N^*(\mathbf{x}') \otimes \mathbf{s}_N(\mathbf{x})}{\omega_N^2 - \omega^2}. \tag{3.94}$$

3.5.2 Peturbed problem: formal solution

As previously discussed, two types of perturbation will be considered:

Density variation. The deformation changes the uniform density to a function of the point:

$$\rho \to \rho\,(1 - \zeta g(\mathbf{x})) \tag{3.95}$$

We denote by ζ a small, dimensionless perturbative parameter, and we will consider quantities up to first order in it. On the other hand, $g(\mathbf{x})$ is an arbitrary, dimensionless function describing the inhomogenities of the body. The above density variation will induce a modification in the differential equations (3.89) given by

$$\mathbb{L} \to [1 - \zeta g(\mathbf{x})]^{-1}\,\mathbb{L} = [1 + \zeta g(\mathbf{x})]\,\mathbb{L} + O(\zeta^2)$$

Boundary variation. The surface S' on which we shall impose boundary conditions will slightly depart from the perfectly spherical shape, and will be given by an equation of the form

$$S': \qquad r = R(1 + \zeta\, f(\theta, \phi)) \qquad\qquad (f < 0 \Rightarrow V' \subset V), \tag{3.96}$$

where V' denotes the volume enclosed by S', and R is the radius of a reference sphere enclosing this perturbed, non–spherical volume.

The problem to solve as a perturbation of (3.89) can thus be written as:

$$(1 + \zeta\, g)\mathbb{L}\mathbf{s}(\mathbf{x}) = -k^2\mathbf{s}(\mathbf{x})\ , \qquad\qquad \mathbb{T}\mathbf{s}|_{S'} = 0, \tag{3.97}$$

where $k^2 = \rho\omega^2/\mu$ is the new, perturbed eigenvalue. Multiplying the first of the above equation by the previously introduced Green operator $\mathbb{G}(\mathbf{x}, \mathbf{x}', \omega)$, and substracting it from $\mathbf{s}$ times equation (3.92), we obtain

$$(\mathbb{G}\mathbb{L} - \mathbb{L}\mathbb{G})\mathbf{s}(\mathbf{x}) + \zeta\, g(\mathbf{x})\, \mathbb{G}\mathbb{L}\mathbf{s}(\mathbf{x}) = \frac{1}{\rho}\delta^{(3)}(\mathbf{x} - \mathbf{x}')\, \mathbf{s}(\mathbf{x})$$

We can now integrate over $\mathbf{x}'$ in the perturbed body, and use the property (3.87)—which is valid for an arbitrary volume and its corresponding boundary—and the boundary conditions satisfied by $\mathbf{s}$, to obtain the integral form of equations (3.97):

$$\mathbf{s}(\mathbf{x}) = -\rho \int_{S'} \mathbb{T}\mathbb{G}(\mathbf{x}, S', \omega)\mathbf{s}(S')\, dS' + \rho\zeta \int_{V'} g(\mathbf{x}')\mathbb{G}(\mathbf{x}, \mathbf{x}', \omega)\mathbb{L}\mathbf{s}(\mathbf{x}')\, dV' \tag{3.98}$$

Introducing in the above integral equation the series (3.94) for the Green function, we can recast it as

$$\mathbf{s}(\mathbf{x}) = \frac{\rho}{M} \sum_N \left(D^N[\mathbf{s}] + B^N[\mathbf{s}]\right) \left(k^2 - {k^2}_N\right)^{-1} \mathbf{s}_N(\mathbf{x}) \tag{3.99}$$

where the scalar operators $D^N[.]$ and $B^N[.]$ are defined, up to first order in ζ as

$$D^N[\boldsymbol{A}] \equiv -\frac{\rho}{M}\zeta\, (s_N, \mathbb{L}\boldsymbol{A}), \qquad\qquad B^N[\boldsymbol{A}] \equiv \frac{\rho}{M} \int_{S'} \boldsymbol{A} \cdot \mathbb{T}\mathbf{s}_N^*\, dS'. \tag{3.100}$$

where $(,)$ is the scalar product over V defined in the previous section.

If we let $\zeta \to 0$ and, simultaneously, $k^2 \to k_{nl}^2$, for a fixed N—i.e., if we are looking for the small perturbations of the eigenvalue k_{nl}^2—we must have $\mathbf{s} \to \sum_m C_m\, \mathbf{s}_m$, with requisite constants C_m, where m is the degeneracy index of k_{nl}^2. Introducing these limits into (3.99) and taking into account the orthogonality of the basis, we get

$$\lim_{k^2 \to k_{nl}^2} (k^2 - k_{nl}^2)\, C_m = \lim_{\zeta \to 0} \sum_{m'} (B^m + D^m)[\mathbf{s}_{m'}]\, C_{m'} \tag{3.101}$$

Thus,

the vectors $\{C_m\}$ *diagonalize the matrix*

$$B_{mm'} + D_{mm'} \equiv (B^m + D^m)[\mathbf{s}_{m'}],$$

its proper values being the first order corrections to the eigenvalue k_{nl}^2.

Thus, the problem of determining the effect on the solid's spectrum of small shape and density pertubations is reduced to an analysis of the matrix $D + B$. So far, the formalism introduced is general enough to tackle arbitrary shapes of the unperturbed solid. Choosing a particular geometry and solving its corresponding eigenvalue equations, we will be able to compute the aformentioned matrices. In the following subsections, we address this problem for the case of a solid sphere.

3.5.3 Solid sphere pertubations

Let us compute more explicit expressions for the matrices introduced above when V is an spherical domain, and the unperturbed eigenvalue k_{nl}^2 belongs into the spheroidal family. We shall also limit ourselves to the case of axisymmetric perturbations, i.e., to the case that the functions g and f describing the perturbation can be expressed by the linear expansions

$$g(\mathbf{x}) = g(r,\theta) = \sum_l g_l(r)\, Y_{l0}(\theta), \qquad f(\theta) = \sum_l f_l Y_{l0}(\theta). \tag{3.102}$$

Using the definition (3.100) of D, and the fact that $\mathbf{s}_m$ is an eigenvector of $\mathbb{L}$, we get

$$D_{mm'} = \zeta \frac{\rho}{M} k_{nl}^2\, (\mathbf{s}_m, g\, s_{m'}). \tag{3.103}$$

The descomposition (3.102) of the function $g(\mathbf{x})$ allows to write the integrand in the expression for D as a linear combination of products three spherical harmonics. The angular integration can then be performed with the aid of the equation

$$\int Y^*{}_{l\,m}\, Y_{l\,m'}\, Y_{l'0}\, d\Omega = [(2l'+1)/4\pi]^{1/2} C_0^{l'} C_{m'}^{l'} \delta_{m,m'}.$$

with $C_{m'}^{l'} \equiv C(L\, l\, l; m - m', m', m - m')$, where $C(l_1\, l_2\, l_3; m_1\, m_2\, m_3)$ is the Clebsch–Gordan symbol with the Condon-Shortley sign convention [43]. Some rather lengthy algebra, involving the above expressions and the explicit form of the eigenvectors $\mathbf{s}_m$, yields the following equation for $D_{mm'}$,

$$D_{mm'} = \delta_{mm'} \zeta \sum_{l'=0}^{l} \left\{ \mathcal{N}_{2l'}\, C_{m'}^{2l'} + \mathcal{E}_{2l'} \left(a_+^m\, C_{m'+1}^{2l'} + a_-^m\, C_{m'-1}^{2l'} + m^2 C_{m'}^{2l'} \right) \right\} \tag{3.104}$$

where $a^m_\pm \equiv (l \mp m)(l \pm m + 1)/2$, and

$$\mathcal{N}_{l'} \equiv \frac{k^2_{nl}}{M}\sqrt{\frac{2l'+1}{4\pi}}C_0^{l'} \int_0^R A^2_{nl}(r) g_{l'}(r)\, r^2\, \rho\, dr \tag{3.105}$$

$$\mathcal{E}_{l'} \equiv \frac{k^2_{nl}}{M}\sqrt{\frac{2l'+1}{4\pi}}C_0^{l'} \int_0^R B^2_{nl}(r) g_{l'}(r)\, r^2\, dr \tag{3.106}$$

In the above equations, the pair (n, l) label the mode being perturbed, and $A_{nl}(r)$, $B_{nl}(r)$ denote its corresponding radial functions.

Analogous considerations and more lengthy algebra, allows expressing the matrix $B_{mm'}$ in terms of the components f_l of the shape deformation in the following form

$$B_{mm'} = \zeta\, \delta_{mm'} \frac{\rho\, R}{M} \sum_{l'=0}^{l} \sqrt{\frac{4l'+1}{4\pi}} C_0^{2l'}\, f_{2l'} \sum_{t=-2}^{2} Q_m^{(t)} C^{2l'}_{m'+t}, \tag{3.107}$$

where the coefficients $Q_m^{(t)}$ have the explicit form

$$\begin{aligned}
Q_m^{(\pm 2)} &= a^m_\pm\, a^{m\pm 1}_\pm\, B^2_{nl} && (3.108)\\
Q_m^{(\pm 1)} &= a^m_\pm [4m(m \pm 1) - (k^2_{nl}R)^2]\, B^2_{nl} && (3.109)\\
Q_{mm}^{(0)} &= [2a^m_+\, a^{m+1}_- + 2m^2(m^2 - 1 - (k^2_{nl}R)^2)]\, B^2_{nl} + 5(k^2_{nl}R)^2 A^2_{nl} \\
&\quad + 2h(h+2)^{-1}(2A_{nl} - l(l+1)B_{nl})^2 - 4l(l+1)A_{nl}\, B_{nl} && (3.110)
\end{aligned}$$

In the above equations, the functions A_{nl} and B_{nl} are taken at $r = R$.

As our expressions show, the matrices $B_{mm'}$ and $D_{mm'}$ have already diagonal form for axisymmetric pertubations, so that $B_{mm} + D_{mm}$ gives us directly the mth correction to k^2_{nl}. Thus, the perturbation would induce a splitting of the degenerate modes of vibration of a perfect sphere. We note also that only even components, up to $2l$, of the functions f and g are needed to compute the corrections for a mode with multipole l. For instance, it suffices to know $f_{0,2,4}$ and $g_{0,2,4}(r)$ to compute the corrections to the quadrupole frequencies induced by these deformations. It is also worth noting that this property does not depend on the peturbation being axisymmetric.

3.6 The suspended sphere

We will treat in this section the problem of the elastic deformation of a sphere when suspended, by means of an arbitrary surface traction, in a homogenous gravitational field. This deformation, described by a vector field $\mathbf{z}$ (with dimensions of length), will

give rise to density as well as shape deformations. In the notation introduced in the previous section to characterize small deviations,

$$f(\theta,\phi) = R^{-1}\mathbf{z}\cdot\mathbf{n}|_S \qquad\qquad \zeta g(\mathbf{x}) = \nabla\cdot\mathbf{z} \tag{3.111}$$

Once the vector field $\mathbf{z}$ is known we shall be able to calculate the perturbations to the spectrum, using the formalism just described.

3.6.1 General solution

The field of deformations $\mathbf{z}$ for a solid under the action of a constant force per unit volume $(-a\mathbf{k})$ (a being 9.8 ms^{-2}) and a field of tractions on its surface (force per unit area) $\mathbf{T}$, is a solution of the equations

$$\mathbb{L}\mathbf{z} = -\frac{\zeta}{R}\mathbf{k}, \qquad\qquad \mathbb{T}\mathbf{z}|_S = \frac{1}{\mu}\mathbf{T} \tag{3.112}$$

where the parameter ζ is

$$\zeta \equiv \frac{R\rho\, a}{\mu}, \tag{3.113}$$

(which shall be small for real samples), and $\mathbf{T}$ is subjected to the further conditions

$$\int_S (\mathbf{n}\times\mathbf{T})\, dS = 0 \qquad\qquad \int_S \mathbf{T}\, dS = \frac{4\pi R^3}{3}\, a\rho\,\mathbf{k} \tag{3.114}$$

so that it counteracts the total gravitational force on the sphere and produces no total torque, allowing an equilibrium configuration.

The solution to equations (3.112) is obtained by adding to a particular solution the suitable linear combination of solutions of the homogeneous equation to satisfy the boundary conditions. For the particular solution to (3.112) we can take (cf. [80], x174):

$$\begin{aligned}\mathbf{z}_p &= \frac{\zeta(\pi/3)^{1/2}}{5R(h+2)}\nabla(r^3 Y_{10}) \\ &= \zeta\frac{1}{5(2+h)}\sqrt{\frac{\pi}{3}}\frac{r^2}{R}(3Y_{10}\mathbf{n} - i\mathbf{n}\times\mathbf{L}Y_{10})\end{aligned} \tag{3.115}$$

while the solutions of the homogeneous equation are (cf. [80], x172):

$$\mathbf{z}^{(1)}_{lm} = R^{2-l}\nabla(r^l Y_{lm}) = R^{2-l}r^{l-1}(Y_{lm}\mathbf{n} - i\mathbf{n}\times\mathbf{L}Y_{lm}) \tag{3.116}$$

$$\mathbf{z}^{(2)}_{lm} = R^{1-l}i\mathbf{L}(r^l Y_{lm}) = R^{1-l}r^l i\mathbf{L}Y_{lm} \tag{3.117}$$

$$\mathbf{z}^{(3)}_{lm} = R^{-l}r^{l+1}((l+A_l)Y_{lm}\mathbf{n} - i\mathbf{n}\times\mathbf{L}Y_{lm}) \tag{3.118}$$

$$A_l = -2\frac{(h+3)l+1}{(h+1)l+3h+5} \tag{3.119}$$

which are three linearly independent vectors for each pair (l, m). The solution of (3.112) satisfying the non–homogeneous boundary conditions will have the form

$$\mathbf{z} = \mathbf{z}_p + \sum_{l=0}^{\infty} \sum_{m=-l}^{l} \sum_{i=1}^{3} C_{lm}^{(i)} \mathbf{z}_{lm}^{(i)} \tag{3.120}$$

with $C_{lm}^{(i)}$ requisite non-dimensional constants. To impose the boundary conditions, let us represent the surface traction $\mathbf{T}$ as a linear combination of vector spherical harmonics:

$$\mathbf{T} = (a\rho_0\, R) \sum_{lm} (a_{lm} Y_{lm} \mathbf{n} + b_{lm} i\mathbf{L} Y_{lm} - d_{lm} i\mathbf{n} \times \mathbf{L} Y_{lm}) \tag{3.121}$$

where a_{lm}, b_{lm}, d_{lm} are non-dimensional constants. Then, as vector spherical harmonics are orthogonal, the boundary conditions are:

$$\sum_{i=1}^{3} C_{lm}^{(i)} \boldsymbol{b}[\mathbf{z}_{lm}^{(i)}] + \delta_{l1}\delta_{m0} \boldsymbol{b}[\mathbf{z}_p] = \zeta(a_{lm} Y_{lm} \mathbf{n} + b_{lm} i\mathbf{L} Y_{lm} - d_{lm} i\mathbf{n} \times \mathbf{L} Y_{lm}) \tag{3.122}$$

where the operator $\boldsymbol{b}[.]$ is given by (3.22). Then, introducing using the explicit expressions for the vectors $\mathbf{z}_{lm}^{(i)}$ and $\mathbf{z}_p$ and equating the coefficients for each vector spherical harmonic, we obtain the following relations between the tensions applied (as described by the constants a_{lm}, b_{lm} and d_{lm}) and the resulting deformation (as described by the constans $C_{lm}^{(i)}$):

$$\textit{for } l \neq 1 \quad : \quad C_{lm}^{(1)} = \zeta \frac{D_l}{l-1} \left(\frac{2l + A_l}{2}\, a_{lm} - E_l\, d_{lm} \right) \tag{3.123}$$

$$C_{lm}^{(2)} = \zeta \frac{1}{l-1}\, b_{lm} \tag{3.124}$$

$$C_{lm}^{(3)} = \zeta\, D_l (l\, d_{lm} - a_{lm}) \tag{3.125}$$

with

$$E_l = \frac{(l+1)^2(l-2) + h(l+1)(l^2 - l - 3)}{5 + l + h(l+3)} \tag{3.126}$$

$$D_l = \frac{5 + l + h(l+3)}{(1+l)^2 - l + h(1 + (1+l)^2)} \tag{3.127}$$

and

$$\textit{for } l=1 \quad : \quad C_{1m}^{(1)} \quad \text{and} \quad C_{1m}^{(2)} \quad \text{arbitrary} \tag{3.128}$$

$$C_{1m}^{(3)} = \zeta \frac{2h+3}{3h+2} \left(-\frac{1}{2}\, a_{1m} + \delta_{m0} \sqrt{\frac{\pi}{3}} \frac{2}{5h+5} \right) \tag{3.129}$$

The arbitrariness of $C_{1m}^{(1,2)}$ should have to be expected, as these constants give rise to solid movements (displacements and rotations) of the sphere as a whole. Also, equation (3.122) for $l = 1$ imposes the following conditions on the given tensions:

$$b_{1m} = 0 \qquad\qquad a_{1m} + 2d_{1m} = 2\sqrt{\frac{\pi}{3}}\delta_{m0} \tag{3.130}$$

These are simply conditions (3.114), as is shown by using the following formulæ for the integration of vector spherical harmonics[8]:

$$\begin{aligned}
\sqrt{\frac{3}{2\pi}}\int Y_{lm}\mathbf{n}\,d\Omega &= \delta_{l1}((\delta_{m-1}-\delta_{m1})\mathbf{i} - i(\delta_{m-1}+\delta_{m1})\mathbf{j} + \sqrt{2}\delta_{m0}\mathbf{k} \\
\int i\mathbf{n}\times\mathbf{L}Y_{lm}\,d\Omega &= -2\int Y_{lm}\mathbf{n}\,d\Omega \\
\int i\mathbf{L}Y_{lm}\,d\Omega &= 0
\end{aligned}$$

which, used with expression (3.121) for $\mathbf{T}$, give

$$\begin{aligned}
\sqrt{\frac{3}{2\pi}}(R^3\rho\,a)^{-1}\int_S \mathbf{T}\,dS &= (a_{1-1} - a_{11} + 2d_{1-1} - 2d_{11})\mathbf{i} \\
&\quad -i(a_{11} + a_{1-1} + 2d_{11} + 2d_{1-1})\mathbf{j} \\
&\quad +\sqrt{2}(a_{10} + 2d_{10})\mathbf{k}
\end{aligned} \tag{3.131}$$

$$\int_{\partial E}(\mathbf{n}\times\mathbf{T})\,dS \propto (b_{1-1} - b_{11})\mathbf{i} - i(b_{11} + b_{1-1})\mathbf{j} + b_{10}\mathbf{k} \tag{3.132}$$

whence

$$\int_S \mathbf{T}\,dS = R^3\rho\frac{4\pi}{3}\mathbf{k} \iff a_{1m} + 2d_{1m} = 2\sqrt{\frac{\pi}{3}}\delta_{m0} \tag{3.133}$$

$$\int_S (\mathbf{n}\times\mathbf{T})\,dS = 0 \iff b_{1m} = 0 \tag{3.134}$$

We have thus obtained the field of elastic displacements, $\mathbf{z}$, of a sphere subjected to arbitrary surface tensions but in equilibrium in a homogenous gravitational field. We can now compute the series for the functions f and g, which will allow the calculus of the perturbations to the proper fequencies of the suspended sphere. As perturbative parameter, we shall use $\zeta = aR\rho/\mu$, which appears naturally in our expressions and gives the size of the deformations produced by the suspension.

[8]The integrations are easily done noting that

$$\sqrt{\frac{3}{2\pi}}\mathbf{n} = (Y_{1-1}^* - Y_{11}^*)\mathbf{i} - i(Y_{1-1}^* + Y_{11}^*)\mathbf{j} + \sqrt{2}Y_{10}^*\mathbf{k}$$

3.6.2 Functions f and g for the suspended sphere

Shape deformation:

Due to the deformation of the supended sphere, its surface takes the form given by the equation:

$$S' : \qquad r = R + \mathbf{z}\cdot\mathbf{n}|_{r=R} \tag{3.135}$$

whence

$$\zeta f(\theta,\phi) = \frac{1}{R}\mathbf{z}\cdot\mathbf{n}|_{r=R} = \sum_{lm}[lC_{lm}^{(1)} + (l+A_l)C_{lm}^{(3)}]Y_{lm} \tag{3.136}$$

Although the undeformed sphere of radius R does not contain the suspended one, we can take R as reference radius, for we know that we can choose it up to a constant, and our aim is to compare the free and "suspended" spectra. Thus,

$$f_{lm} = D_l\left(\frac{l(2l+A_l)}{2(l-1)} - A_l - l\right)a_{lm} + D_l\left(l(l+A_l) - \frac{lE_l}{l-1}\right)d_{lm} \tag{3.137}$$

the above expression being valid only for l even, as these are the terms appearing in the perturbative series.

Density variation:

Taking into account that $\nabla\cdot\mathbf{z}_{lm}^{(1,2)} = 0$, the variation of the density will be:

$$\zeta g(\mathbf{x}) = \nabla\cdot\mathbf{z}_p + \sum_{lm} C_{lm}^{(3)}\nabla\cdot\mathbf{z}_{lm}^{(3)} \tag{3.138}$$

The first term gives rise to a contribution to the series in (l,m) for $l=1$, and, as this term does not appear in the perturbative formulæ (3.100), we shall drop it. Thus, using the form of $C_{lm}^{(3)}$ to compute its divergence, we get

$$\zeta g_{lm}(r) = \left(\frac{r}{R}\right)^l C_{lm}^{(3)}(2l + A_l(3+l)) \qquad (\text{l even}) \tag{3.139}$$

3.6.3 Particular case: first quadrupole mode.

In this section we will compute the corrections to the frequency of the first quadrupole mode of the free sphere with Poisson ration 1/3, i.e. $h=2$. Thus, we will take $l=2$, $n=1$, for which $KR = 2.650$ is the unperturbed eigenvalue. In table 3.5 the values of the constants $R^3M^{-1}Q_m^{(t)}$ are displayed. Besides, we shall consider the case of a constant normal suspension applied on a spherical cap of width $\gamma = \cos\theta_0$ around the North pole of the sphere, i.e.,

$$\mathbf{T} = \Theta(\cos\theta - \gamma)\frac{4a\rho_0\, R}{3(1-\gamma^2)}\mathbf{n} \tag{3.140}$$

m\(t)	-2	-1	0	1	2
2	1.19293	0.19429	-15.4328	0	0
-2	0	0	-15.4328	0.19429	1.19293
1	1.78939	-2.09442	-13.9349	0.194288	0
-1	0	0.194288	-13.9349	-2.09442	1.78939
0	1.19293	-2.09442	-12.2426	-2.09442	1.19293

Table 3.5. *Constants* $R^3M^{-1}Q_m^{(t)}$ *for* $h=2$, $l=2$, $n=1$.

The coefficients a_{lm}, b_{lm} and d_{lm} for this tension are:

$$a_{lm}=\delta_{m0}\frac{4}{3(1-\gamma^2)}\sqrt{\frac{\pi}{2l+1}}(P_{l-1}(\gamma)-P_{l+1}(\gamma)) \qquad b_{lm}=d_{lm}=0 \tag{3.141}$$

where $P_l(x)$ are the Legendre polynomials. We need the values for $l=0,2,4$, which are:

$$a_{00}=\frac{4\sqrt{\pi}}{3(1+\gamma)} \quad a_{20}=\frac{2\sqrt{5\pi}}{3}\gamma \quad a_{40}=\frac{\sqrt{\pi}}{2}\gamma(7\gamma^2-3) \tag{3.142}$$

Using now equation (3.137) and the definitons for A_l and D_l we obtain:

$$\begin{aligned} f_0=\frac{-320}{121}\,a_{00} &= \frac{-1280\sqrt{\pi}}{363(1+\gamma)} \\ f_2=\frac{208}{17}\,a_{20} &= \frac{416\sqrt{5\pi}}{51}\gamma \\ f_4=\frac{26112}{529}\,a_{40} &= \frac{13056\sqrt{\pi}}{529}\gamma(7\gamma^2-3) \end{aligned}$$

For the perturbations due to density variations, numerical integration gives

$$\mathcal{N}^0=\frac{30.343\pi}{1+\gamma} \quad \mathcal{N}^2=-71.976\pi\gamma \quad \mathcal{N}^4=10.882\pi\gamma(7\gamma^2-3)$$
$$\mathcal{E}^0=\frac{3.455\pi}{1+\gamma} \quad \mathcal{E}^2=-7.049\pi\gamma \quad \mathcal{E}^4=0.957\pi\gamma(7\gamma^2-3)$$

The parameter γ will be close to 1 when the width of the suspension is small. So, we can take $\gamma=1$. Then, the original 5-degenerate eigenvalue K splits into three perturbed eigenvalues $k_i^2=K^2+\zeta\Delta_i$ which are given by the above formulæ:

$$k_0^2R^2=7.023-184.068\,\zeta \tag{3.143}$$
$$k_1^2R^2=7.023+345.834\,\zeta \tag{3.144}$$
$$k_2^2R^2=7.023-22.2745\,\zeta \tag{3.145}$$

This gives corrections of order $10^{-3} - 10^{-4}$, as $\zeta \approx 10^{-5} - 10^{-6}$.

Chapter 4

Quasi–normal modes of vibration for viscoelastic solids

4.1 Introduction

In chapter 3, we have presented a detailed analysis of the free oscillations of a spherical, perfectly elastic body satisfying a linear constitutive equation relating the stress and strain tensors (Hooke's law). It has been shown that a denumerably infinite set of solutions with periodic time dependence can be found, the so-called normal modes of vibration, which constitute a basis for constructing any free (and, as we shall show in the next chapter, driven) solution to the equations of motion. As as result of the conservative nature of Hooke's law, it is immediately shown that the total energy of the body is conserved in such vibrations, and, thus, a perfectly elastic body would oscillate with constant amplitude indefinitely, provided it is not influenced by external forces. But, from an experimental point of view, it is well known that real bodies, due to their internal structure, undergo dissipative processes which transform ordered, macroscopic motions into disordered, molecular motions (that is, heat). As a result of these processes, the periodic vibrations of a real *elastic* body are damped, the initial elastic potential energy stored in the body is eventually dissipated into termal energy, and the amplitude of its oscillations eventually vanishes after a finite period of time. This damping is usually modelled by substituting the periodic dependence in $\cos(\omega t)$ by one of the form $\exp(-\omega t/Q)\cos(\omega t)$, where Q, the *quality factor*, is a time-independent parameter (which is, however, a function of frequency). Thus, the quality factor describes the effect of internal friction, and

can be readily interpreted as the number of oscillations after which the original amplitude of vibration is reduced by a factor of e^{-1}. Experimental researchers had long devoted their efforts to the determination of the quality factor of different materials, and metals in particular (see [130] for a classical account, and [74] for materials proposed for the construction of cryogenic resonant detectors), which are characterized by a high value ($\approx 10^7$) of Q (see, e.g., [28, 14]). Regarding the frequency spectrum, it is observed [88] to be very close to that predicted by the elastic model studied in chapter 3. Thus, it is a common practice, in the literature dealing with gravitational wave detection, to introduce the internal friction *by hand* as a decreasing exponential in the time dependence of normal modes—or, what amounts to the same, an *ad hoc* term in the expressions resulting from separation of variables in the equations of motion, which gives rise to such a time dependence (see, e.g. [127, 93, 88]). Such approaches demand the introduction of experimental values of the quality factor at each frequency considered, as they provide no means to their calculation from a finite set of parameters characterizing the solid. This problem can be overcome by the introduction of a suitable theoretical model describing both the elastic behaviour of the small deformations of the solid, and the dissipation effects which it undergoes. As mentioned in chapter 2, a wide variety of such models has been proposed to describe the so–called *viscoelastic* solids, each one starting from a given constitutive relation between the stress and strain tensors. In this chapter, we solve in detail the simplest ones (i.e., the Kelvin-Voigt model, the Maxwell model and the Standard Linear Model; see chapter 2) for the solid sphere, showing to which degree of approximation the spectrum and quasi–periodic motions of a free viscoelastic body can be regarded coincident with that of an ideal elastic body [1]. Explicit expressions for the quality factor (as a function of frequency and the parameters characterizing the model at hand) are also obtained. The chapter is completed with a brief discussion of possible generalizations of the aforementioned simple models.

Each model dealt with in the following sections is characterized by a stress-strain relationship attempting to describe the internal friction appearing in real metals. When introduced into the equations of motion

$$\frac{\partial \sigma_{ij}}{\partial x^j} + f_i = \rho \frac{\partial^2 s_i}{\partial t^2}, \tag{4.1}$$

the constitutive relation gives us a differential equation in the field of displacements

[1] Using a nomenclature introduced by the researchers on neutron stars, which also behave as a viscoelastic body under certain circumstances [75], we call these quasi–periodic motions *quasi–normal modes of vibration*.

$\mathbf{s}(\mathbf{x},t)$. We shall look for free ($\boldsymbol{f}=0$) solutions to this equation which are separable:

$$\mathbf{s}(\mathbf{x},t) = T(t)\,\mathbf{s}(\mathbf{x}), \tag{4.2}$$

and will find that purely periodic time dependence ($T(t)=e^{i\omega t}$, with real ω) is no longer allowed. A complex exponential appears instead, with a complex parameter whose values are given by the usual, homogeneous boundary conditions:

$$\sigma_{ij}n_j = 0 \qquad\qquad \text{at } r=R. \tag{4.3}$$

4.2 Kelvin–Voigt model

4.2.1 Constitutive relation and construction of solutions

As discussed in chapter 2, the one–dimensional version of this model describes the viscoelastic solid as an elastic spring and a dashpot in parallel, which furnishes the desired dissipation effects (see also [16, 60]). For the case of a three–dimensional solid, the constitutive equation relating strain and stress can be written as

$$\sigma_{ij} = (\lambda + \lambda'\partial_t)\, s_{kk}\delta_{ij} + 2\,(\mu + \mu'\partial_t)\, s_{ij}, \tag{4.4}$$

where isotropy and homogeneity are assumed. The constants λ and μ are the usual Lamé coefficients describing the purely elastic behaviour of the body, while the positive coefficients λ' and μ' parametrize its viscous properties [2], which is proportional to the rate of strain tensor, $\partial_t s_{ij}$. Introducing the splitting (4.2) and the constitutive equation (4.4) into the equations of motion (4.1), we obtain the following relationship:

$$\rho\ddot{T}(t)\mathbf{s}(\mathbf{x}) = \Big[(\lambda+\mu)T(t) + (\lambda'+\mu')\dot{T}(t)\Big]\,\nabla\left(\nabla\cdot\mathbf{s}(\mathbf{x})\right) + \Big[\mu\,T(t) + \mu'\,\dot{T}(t)\Big]\,\nabla^2\mathbf{s}(\mathbf{x}), \tag{4.5}$$

where a dot denotes differentation with respect of time. As was done in the case of the elasticity equations of motion, we can now split the spatial part $\mathbf{s}(\mathbf{x})$ of the field of displacements into its longitudinal and transverse components:

$$\mathbf{s} = \mathbf{s}_t + \mathbf{s}_l \qquad\qquad \nabla\cdot\mathbf{s}_t = \nabla\times\mathbf{s}_l = 0,$$

so that equation (4.5) can be written as

$$\rho\ddot{T}(t)(\mathbf{s}_t+\mathbf{s}_l) = \Big[(\lambda+\mu)T(t) + (\lambda'+\mu')\dot{T}(t)\Big]\,\nabla\left(\nabla\cdot\mathbf{s}_l\right) + \Big[\mu\,T(t) + \mu'\,\dot{T}(t)\Big]\,\nabla^2(\mathbf{s}_t+\mathbf{s}_l),$$

[2] In fact, these coefficients are analogous to those appearing in hydrodynamics to describe the viscosity of fluids: shear viscosity (μ') and bulk viscosity ($2\mu'+3\lambda'$).

whence, taking the rotational,

$$\nabla \times \left[\rho \ddot{T}\, \mathbf{s}_t - (\mu\, T + \mu'\, \dot{T}) \nabla^2 \mathbf{s}_t\right] = 0.$$

The vector between square brackets is thus divergence–free and irrotational, so that it must vanish. We have therefore:

$$\nabla^2 \mathbf{s}_t = \left\{ \frac{\rho\, \ddot{T}}{\mu\, T + \mu'\, \dot{T}} \right\} \mathbf{s}_t.$$

As the left hand side of the above equation does not depend on time, the term between braces in the right hand side must equal a (complex) constant, say $-\mathcal{K}^2$, and thus,

$$\nabla^2 \mathbf{s}_t + \mathcal{K}^2\, \mathbf{s}_t = 0 \tag{4.6}$$

$$\mu\, T + \mu'\, \dot{T} + \mathcal{K}^{-2} \ddot{T} = 0 \quad . \tag{4.7}$$

An analogous procedure, after taking the divergence of the equations of motion (cf. x3.2), gives us the corresponding formulæ for the longitudinal part:

$$\nabla^2 \mathbf{s}_l + \mathcal{Q}^2\, \mathbf{s}_l = 0 \tag{4.8}$$

$$(\lambda + 2\mu)\, T + (\lambda' + 2\mu')\, \dot{T} + \mathcal{Q}^{-2} \ddot{T} = 0 \quad , \tag{4.9}$$

where $\mathcal{Q}^2$ stands for a complex separation constant. Due to the fact that $T(t)$ must fulfil both equation (4.7) and equation (4.9), the two constants $\mathcal{K}$ and $\mathcal{Q}$ are not independent. Writing the solution to these equations as

$$T(t) = e^{\gamma\, t}, \tag{4.10}$$

with γ also a complex constant, we obtain immediately the values of $\mathcal{Q}$ and $\mathcal{K}$ as functions of this unique parameter:

$$\begin{aligned} \mathcal{Q}^2 &= -\rho\gamma^2 \left[\lambda + 2\mu + \gamma\, (\lambda' + 2\mu')\right]^{-1} \\ \mathcal{K}^2 &= -\rho\gamma^2 \left[\mu + \gamma\, \mu'\right]^{-1}. \end{aligned} \tag{4.11}$$

The boundary conditions (4.3) will fix the allowed values for the parameter γ. We have obtained a set of equations which is analogous to that for the elastic case: two Helmholtz equations for the longitudinal and transverse parts of the displacement, with the parameters $\mathcal{Q}$ and $\mathcal{K}$ playing the part of q and k, and the real frequency ω being substituted by the complex quantity $i\gamma$. Thus, as regards the solution of equations (4.8)

and (4.6), we can simply take the expressions derived in x3.2 and substitute the couple of constants $(q,\ k)$ by their counterparts $(\mathcal{K},\ \mathcal{Q})$, obtaining (cf. (3.13)):

$$\begin{aligned}\mathbf{s}(\mathbf{x}) &= \frac{C_l}{\mathcal{Q}}\mathbf{s}_l(\mathbf{x}) + \frac{C_t}{\mathcal{K}}\mathbf{s}_t(\mathbf{x}) + C_{t'}\mathbf{s}_{t'},\\ &= \frac{C_l}{\mathcal{Q}}\nabla\phi(\mathbf{x};\mathcal{Q}) + i\frac{C_t}{\mathcal{K}}\nabla\times\mathbf{L}\varphi(\mathbf{x};\mathcal{K}) + iC_{t'}\mathbf{L}\varphi(\mathbf{x};\mathcal{K}),\end{aligned} \tag{4.12}$$

where the scalar functions ϕ and φ satisfy corresponding Helmholtz equations:

$$\nabla^2\phi(\mathbf{x};\mathcal{Q}) + \mathcal{Q}^2\phi(\mathbf{x};\mathcal{Q}) = 0 \qquad \nabla^2\varphi(\mathbf{x};\mathcal{K}) + \mathcal{K}^2\varphi(\mathbf{x};\mathcal{K}) = 0, \tag{4.13}$$

4.2.2 Form of solutions and boundary conditions for the sphere

The explicit expressions for $\mathbf{s}_l$, $\mathbf{s}_t$ and $\mathbf{s}_{t'}$ when spherical symmetry is assumed are obtained by following exactly the same steps which were described in x3.3.1 and appendix A.1.1. Therefore, we end up with explicit expressions analogous to equations (3.17), (3.18) and (3.19), that is

$$\mathbf{s}_l(r,\theta,\phi) = \frac{dj_l(\mathcal{Q}r)}{d\,r}\,Y_{lm}\,\mathbf{n} - \frac{j_l(\mathcal{Q}r)}{r}\,i\,\mathbf{n}\times\mathbf{L}Y_{lm}\,. \tag{4.14}$$

$$\mathbf{s}_t(r,\theta,\phi) = -l(l+1)\frac{j_l(\mathcal{K}r)}{r}\,Y_{lm}\,\mathbf{n} + \left(\frac{j_l(\mathcal{K}r)}{r} + \frac{dj_l(\mathcal{K}r)}{d\,r}\right)\,i\,\mathbf{n}\times\mathbf{L}Y_{lm}\,. \tag{4.15}$$

$$\mathbf{s}_{t'}(r,\theta,\phi) = j_l(\mathcal{K}r)\,i\,\mathbf{L}Y_{lm}\,. \tag{4.16}$$

The explicit form of the boundary conditions can also be obtained taking the corresponding expressions for the elastic case (equations (3.23)), where, besides the substitution of k and q, the constants $\lambda,\ \mu$ must be replaced, respectively, by $\lambda+\gamma\lambda'$ and $\mu+\gamma\mu'$. Thus, the vector form of equation (4.3) is, for this model (cf. (3.14)),

$$(\lambda+\gamma\lambda')\,(\nabla\cdot\mathbf{s}(\mathbf{x}))\,\mathbf{n} + 2(\mu+\gamma\mu')\,\mathbf{n}\cdot\nabla\mathbf{s}(\mathbf{x}) + 2(\mu+\gamma\mu')\,\mathbf{n}\times(\nabla\times\mathbf{s}(\mathbf{x})) = 0 \tag{4.17}$$

and the homogeneous linear system to be satisfied by the constants $C_l,\ C_t,\ C_{t'}$ appearing in (4.12) is now

$$\begin{pmatrix} \beta_4\left(\mathcal{Q}R, \frac{\lambda+\gamma\lambda'}{\mu+\gamma\mu'}\right) & -l(l+1)\frac{\mathcal{K}}{\mathcal{Q}}\beta_1(\mathcal{K}R) & 0\\ -\beta_1(\mathcal{Q}R) & \frac{\mathcal{K}}{\mathcal{Q}}\beta_3(\mathcal{K}R) & 0\\ 0 & 0 & -\frac{\mathcal{K}}{\mathcal{Q}}\,\mathcal{K}R\,\beta_1(\mathcal{K}R)\end{pmatrix}\begin{pmatrix} C_l\\ C_t\\ C_{t'}\end{pmatrix} = 0, \tag{4.18}$$

where the definition of the functions β_i is that given in (3.25) for $i=1,2,3$, and we have redefined β_4 introducing a second argument:

$$\beta_4(z,A) \equiv \beta_2(z) - \frac{A}{2}j_l(z), \tag{4.19}$$

so that $\beta_4(z) = \beta_4(z, \lambda/\mu)$. Again, imposing compatibility of the above linear system gives us two families of quasi-normal modes, which we shall term in the same fashion as in the elastic case: toroidal and spheroidal quasi–normal modes of vibration.

4.2.3 Toroidal modes

These modes are obtained by solving the system (4.18) imposing

$$\beta_1(\mathcal{K}R) = 0 \tag{4.20}$$

as the compatibility condition, so that $C_l = C_t = 0$. This is exactly the same equation as the one satisfied by $k^T_{nl}R$, the toroidal eigenvalues for the elastic solid, so that we already have the toroidal spectrum of the Kelvin-Voigt solid, which we shall also label with three indices:

$$\mathcal{K}^T_{nl} = k^T_{nl} = \sqrt{\frac{\rho}{\mu}}\omega^T_{nl}, \tag{4.21}$$

where ω^T_{nl} denotes the angular eigenfrequency of the elastic mode. The above equation, combined with the second (4.11), gives us the allowed values for the parameter γ appearing in the time–dependence of toroidal quasi–normal modes:

$$\gamma^T_{nl} = -(\omega^T_{nl})^2\frac{\mu'}{2\mu} + i\omega^T_{nl}\sqrt{1 - \left(\frac{\omega^T_{nl}\mu'}{2\mu}\right)}. \tag{4.22}$$

The real part of γ gives the damping factor associated with the quasi–normal mode at hand, while the purely imaginary part will be the angular frequency of vibration. On the other hand, the spatial part of toroidal modes for the Kelvin-Voigt solid, by virtue of equation (4.21), *is identical to that of the elastic solid* (cf. equations (3.43) and (3.44)), so that the internal friction, when modelled in this way, alters only the time–dependence of the vibrations. Regarding this dependence, we shall be interested in the special case of small internal damping, that is, in the approximation

$$\frac{\mu'}{\mu} \approx \frac{\lambda'}{\mu} << \frac{1}{\omega}. \tag{4.23}$$

When this approximation is assumed, we obtain from (4.22):

$$\gamma = i\omega - \omega^2\frac{\mu'}{2\mu} + o(\mu'\omega/\mu), \tag{4.24}$$

which shows that, when (4.23) holds, the angular frequency of vibration remains also unaltered, and the only effect of viscosity is the introduction of a damping factor of the form $\exp(-(\omega^2\mu'/2\mu)t)$.

Summing up, let $\mathbf{s}^T_{KV}(\mathbf{x},t)$ denote a Kelvin-Voigt, toroidal quasi–normal mode, and $\mathbf{s}^T_E(\mathbf{x},t)$ an elastic, toroidal normal mode. We have proved that, under requisite approximations, they are related by:

$$\mathbf{s}^T_{KV}(\mathbf{x},t) = \mathbf{s}^T_E(\mathbf{x},t)\, e^{-w^T_{nl}t/Q_{nl}}, \qquad Q_{nl} = \frac{2\mu}{\mu' \omega^T_{nl}}, \tag{4.25}$$

where, due to (4.23), the quality factor will satisfy $Q >> 1$, as is the case with the actual metallic alloys of our concern here [28, 74, 14]. Thus, all the properties regarding the spectrum and the spatial field of displacements associated with toroidal quasi–normal modes of a Kelvin–Voigt solid are the same as those of toroidal normal modes of an elastic solid (cf. x3.3.3).

4.2.4 Spheroidal modes

A second way to make the linear system (4.18) compatible is to impose the condition

$$\beta_4\left(\mathcal{Q}R, \frac{\lambda+\gamma\lambda'}{\mu+\gamma\mu'}\right)\, \beta_3(\mathcal{K}R) - l(l+1)\,\beta_1(\mathcal{Q}R)\beta_1(\mathcal{K}R) = 0. \tag{4.26}$$

By virtue of equations (4.11), this relationship can be translated into a condition to be fufilled by γ, and depending on the ratios λ/μ, λ'/λ and μ'/μ, as well as on the multipolar index l. In this case, as we are not dealing with an eigenvalue problem of a selfadjoint operator, complex solutions to equation (4.26) are allowed (and, indeed, expected). An exact solution of that equation would imply a separation of its real and imaginary parts, followed by numerical calculations which would determine the angular frequency and quality factor of the quasi–normal mode at hand. But, as we are interested in materials with a high decay time, we shall try a perturbative solution of equation (4.26), using

$$\epsilon \equiv \frac{\mu'\omega}{\mu} \tag{4.27}$$

as the perturbative parameter (that is, assuming that the approximation (4.23) holds). Here, ω stands for any spheroidal eigenfrequency satisfying (3.27). Obviously, the unperturbed solution, i.e., that corresponding to $\epsilon = 0$, is the elastic solid's solution already discussed in previous chapters. Thus, we shall introduce the perturbative expansion

$$\gamma = \gamma_o + \gamma_1\epsilon + O(\epsilon^2), \qquad \gamma_o = -i\omega, \tag{4.28}$$

Using equations (4.11) and (4.28), we obtain perturbative expansions for the parameters $\mathcal{K}$ and $\mathcal{Q}$ that can be written as

$$\mathcal{K} = k_o + k_1\epsilon + O(\epsilon^2), \qquad \mathcal{Q} = q_o + q_1\epsilon + O(\epsilon^2), \tag{4.29}$$

where

$$k_o = k = \omega\sqrt{\tfrac{\rho}{\mu}}, \qquad k_1 = i\sqrt{\tfrac{\rho}{\mu}}\left(\gamma_1 + \tfrac{\omega}{2}\right)$$
$$q_o = q = \omega\sqrt{\tfrac{\rho}{\lambda+2\mu}} \qquad q_1 = i\sqrt{\tfrac{\rho}{\lambda+2\mu}}\left(\gamma_1 + \tfrac{h'+2}{h+2}\tfrac{\omega}{2}\right) \tag{4.30}$$

In the above equations, k and q are the parameters appearing in the elastic sphere's case, and we have introduced the non–dimensional quotients

$$h \equiv \frac{\lambda}{\mu} \qquad h' \equiv \frac{\lambda'}{\mu'}, \tag{4.31}$$

which are both zero–order quantities. We can now perform the perturbative expansion of the eigenvalue equation. In order to ease the resulting expressions, let us introduce the following notation:

$$\begin{aligned}
\beta_4\left(\mathcal{Q}R, \frac{\lambda+\gamma\lambda'}{\mu+\gamma\mu'}\right) &= \beta_4(qR,h) + \left[\beta_4'(qR,\lambda/\mu)q_1R - \frac{i}{2}(h-h')\,j_l(qR)\right]\epsilon \\
&\equiv A_o + [A_1 q_1 R - iA_1']\,\epsilon, \qquad (4.32)\\
l(l+1)\beta_1(\mathcal{K}R) &= l(l+1)\beta_1(kR) + l(l+1)\beta_1'(kR)k_1R\epsilon \\
&\equiv B_o + B_1 k_1 R\,\epsilon, \qquad (4.33)\\
\beta_1(\mathcal{Q}R) &= \beta_1(qR) + \beta_1'(qR)q_1R\,\epsilon \equiv C_o + C_1 q_1 R\,\epsilon, \qquad (4.34)\\
\beta_3(\mathcal{K}R) &= \beta_3(kR) + \beta_3'(kR)k_1R\,\epsilon \equiv D_o + D_1 k_1 R\,\epsilon, \qquad (4.35)
\end{aligned}$$

where a prime over a β–function denotes differentiation with respect to its first argument. We note that the uppercase constants introduced above are real. With this notation, the zeroth order form of equation (4.26) is

$$A_oD_o - C_oB_o = 0,$$

which is simply the condition of ω being a spheroidal eigenvalue of the purely elastic case. On the other hand, the first order expansion of (4.26) yields

$$(A_oD_1 - C_oB_1)k_1R + (A_1D_o - C_1B_o)q_1R = iA_1'D_o,$$

whence, using the form of k_1 and q_1, the value of γ_1 ensues. It can be written as

$$\gamma_1 = -\frac{\omega}{2}f(kR,h,h'), \tag{4.36}$$

where the dimensionless function f has the form [3]

$$f(kR,h,h') = -\frac{2A_1' D_o (kR)^{-1} - A_o D_1 + C_o B_1 - (A_1 D_o - C_1 B_o)\,(h'+2)(h+2)^{-3/2}}{A_o D_1 - C_o B_1 + (A_1 D_o - C_1 B_o)(h+2)^{-1/2}}. \tag{4.40}$$

We note that the first order correction obtained for γ is real. Therefore, to this order of approximation, the frequencies of vibration remain unaltered, and are the same as those obtained for the elastic solid. Moreover, k_1 and q_1 happen to be purely imaginary. Therefore, the modulus of the radial functions appearing in the spatial part of spheroidal quasi–normal modes of vibration will also be the same as those of the elastic solid, for the correction to k and q will just introduce, to first order, a complex phase.

Summing up, we have shown that while the spheroidal normal modes of vibration of an elastic solid are given by an expression of the form (3.29), i.e.

$$\mathbf{s}_E^P(\mathbf{x},t) = e^{i\omega_{nl}^P t}(A_{nl}(r)\,Y_{lm}\,\mathbf{n} - B_{nl}(r)\,i\,\mathbf{n}\times\mathbf{L}Y_{lm}) \tag{4.41}$$

the spheroidal quasi–normal modes of vibration of a Kelvin–Voigt solid having the same Lamé coefficients $\mathbf{s}_{KV}^P$ are obtained from the normal modes of the elastic solid according to the following equation

$$\mathbf{s}_{KV}^P(\mathbf{x},t) = e^{i\omega_{nl}^P t - \omega_{nl}^P t/Q_{nl}}\left(e^{i\chi_1(r)}A_{nl}(r)\,Y_{lm}\,\mathbf{n} - e^{i\chi_2(r)}B_{nl}(r)\,i\,\mathbf{n}\times\mathbf{L}Y_{lm}\right) \tag{4.42}$$

the qualitity factor being given by

$$Q_{nl} = \frac{2\mu}{\mu'\omega_{nl}^P}\frac{1}{f}, \tag{4.43}$$

where we should remember that f is a function of the mode and the coefficients characterizing the body (cf. (4.40)). The real phases $\chi_{1,2}(r)$ can be computed from equations

[3] The case in which f takes its simplest form is that of monopolar modes. We know, from the calculations of the previous chapter, that when $l = 0$ equation (4.26) is no longer valid, and must be replaced by

$$\beta_4\left(\mathcal{Q}R, \frac{\lambda+\gamma\lambda'}{\mu+\gamma\mu'}\right) = 0. \tag{4.37}$$

Using now the expansion (4.32) and the fact that $A_o = 0$ for the uperturbed monopolar eigenfrequencies, we obtain for the first order correction to $\mathcal{Q}$,

$$q_1 = iA_1' A_1^{-1}, \tag{4.38}$$

and therefore, using the notation of equation (4.36) and the relation (4.30):

$$f(qR,h,h') = \frac{h'+2}{h+2} - \frac{2\,A_1'}{qR\,A_1}. \tag{4.39}$$

(4.14), (4.15) and (4.30). Nevertheless, the explicit (and cumbersome) form of these phases is largely irrelevant and whe shall not write it down here (it can be found in appendix B.1). They merely introduce a position–dependent shift in the phase of vibrations which is of order ϵ, and, therefore, they are not likely to give rise to measurable effects. More interesting, and physically relevant, is the behaviour of the function f giving the precise dependence of the quality factor on frequency . First of all, it is easily seen that, for the special case $h = h'$, f is equal to 1, and, thus, the quality factor goes as ω^{-1}, as was the case with toroidal modes. But, when the aforementioned equality does not hold, numerical calculations are needed. Figure 4.1 shows the value of this function for $h = 2$ (elastic Poisson ratio 1/3) and some values of h'. We have represented the first twenty eigenvalues of the spheroidal spectrum. It is evident from equation (4.40) that fixing h and kR leaves us with a linear function of h', whose slope varies from root to root. In figure 4.2 we have plotted the quality factor for the same set of eigenvalues.

4.3 Maxwell model

4.3.1 Constitutive relation and construction of solutions

We saw in chapter 2 that the Maxwell model, when a one–dimensional case is considered, amounts to modelling the viscoelastic solid as a spring (elastic behaviour) in series with a dashpot (viscous behaviour). When a three–dimensional body is at hand, and it is also isotropic and homogenous, the constitutive relation can be written as

$$\partial_t \sigma_{ij} + \alpha\, \sigma_{kk} \delta_{ij} + \beta\, \sigma_{ij}. = \partial_t \left(\lambda\, s_{kk}\, \delta_{ij} + 2\mu\, s_{ij} \right) \tag{4.44}$$

Here, the constants λ and μ are again the Lamé coefficients describing the elastic behaviour of the body, while the coefficients α and β parametrize the effects due to internal friction. To construct separable solutions, we must factorize both stress and strain [4]:

$$\sigma_{ij}(\mathbf{x}, t) = e^{\gamma\, t}\, \sigma_{ij}(\mathbf{x}), \qquad s_i(\mathbf{x}, t) = e^{\gamma\, t}\, s_i(\mathbf{x}), \tag{4.45}$$

On the other hand, the constitutive equation is written, after separation of variables and contraction of its free indices, as

$$(\gamma + 3\alpha + \beta)\, \sigma_{jj}(\mathbf{x}) = \gamma\, (2\mu + 3\lambda)\, s_{jj}(\mathbf{x})$$

[4] Due to the equations of motion (4.1), if $\mathbf{s}$ is assumed to be separable in the fashion (4.2), the strain tensor must also be separable, and, due to the constitutive equation, it is easily seen that the only possible time dependence is of the form $\exp(\gamma\, t)$.

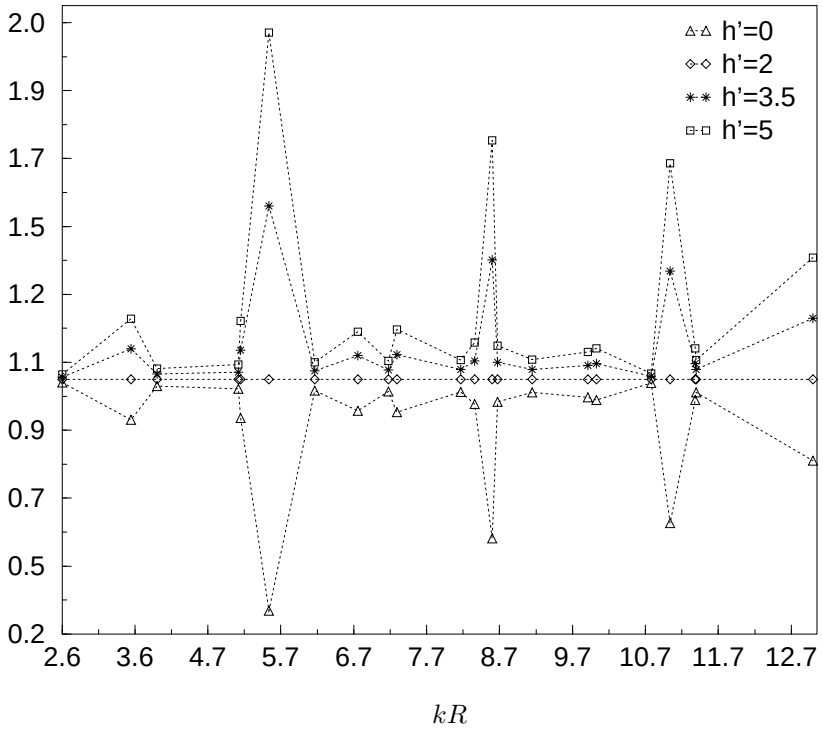

Figure 4.1. *Value of the dimensionless function $f(h, h', kR)$ for $h = 2$ (Poisson ratio $\sigma = 1/3$) and the first few modes of the sphere's spectrum.*

and, hence, we have the following relation between the spatial parts of stress and strain:

$$\left(1 + \frac{\beta}{\gamma}\right) \sigma_{ij}(\mathbf{x}) = \left(\lambda - \alpha \frac{2\mu + 3\lambda}{\gamma + 3\alpha + \beta}\right) s_{kk}(\mathbf{x})\delta_{ij} + 2\mu\, s_{ij}(\mathbf{x}). \tag{4.46}$$

As in the preceeding model, we shall be mainly interested in the case of small internal friction, so that we can assume

$$\frac{\beta}{|\,\gamma\,|} \approx \frac{\alpha}{|\,\gamma\,|} << 1, \tag{4.47}$$

yielding the following constitutive relation

$$\sigma_{ij}(\mathbf{x}) = \lambda \left(1 - \frac{\delta}{\gamma}\right) s_{kk}(\mathbf{x})\delta_{ij} + 2\mu \left(1 - \frac{\beta}{\gamma}\right) s_{ij}(\mathbf{x}), \tag{4.48}$$

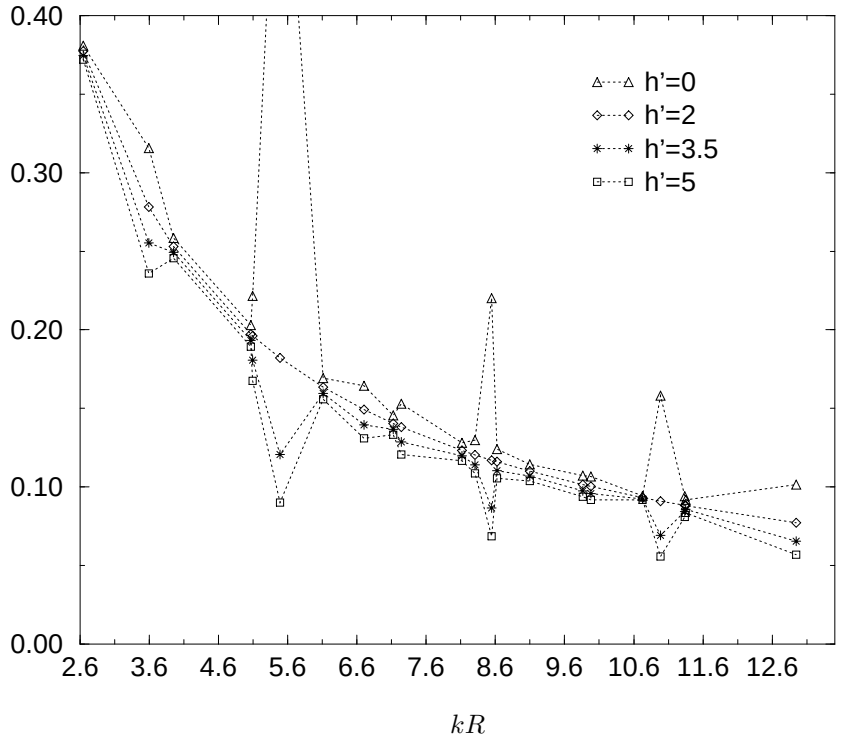

Figure 4.2. *Quality factor Q_{nl} (in units of $\mu R/\mu' v_t$) for some values of the parameter h' and the first modes of the spheroidal spectrum. The viscoelastic solid is described by a Kelvin–Voight model with $h = 2$.*

where we have introduced a new constant, δ, given by

$$\delta = \frac{2\mu + 3\lambda}{\lambda}\alpha + \beta, \tag{4.49}$$

so that we can take, as the parameters characterizing the Maxwell solid, the set consisting of the Lamé coefficients λ, μ, and the parameters β, δ which describe internal friction.

Let us compare equation (4.48) with that of the Kelvin–Voigt model (cf. (4.4)), once the separation of variables has been performed:

$$\sigma_{ij}(\mathbf{x}) = (\lambda + \gamma\lambda')\, s_{kk}(\mathbf{x})\delta_{ij} + 2(\mu + \gamma\mu')\, s_{ij}(\mathbf{x}). \tag{4.50}$$

Comparing equations (4.48) and (4.50), we observe that the resolution of the Maxwell model can be carried out, as regards the spatial part of $\mathbf{s}$, following the method used

in the previous section for the Kelvin–Voigt model. In fact, we can directly take the expressions there derived, and make the substitutions

$$\mu' \longrightarrow -\mu\,\beta\,\gamma^{-2}, \qquad \lambda' \longrightarrow -\lambda\,\delta\,\gamma^{-2}, \tag{4.51}$$

which transform equation (4.50) into (4.48). Thus, the form of the solutions and boundary conditions for a Maxwell viscoelastic sphere is that given in x4.2.2 with constants $\mathcal{K}$ and $\mathcal{Q}$ given now by the following functions of the parameter γ:

$$\begin{aligned} \mathcal{Q} &= i\sqrt{\frac{\rho}{\lambda+2\mu}}\left[\gamma+\frac{1}{h+2}\left(\frac{h}{2}\delta+\beta\right)\right] \\ \mathcal{K} &= i\sqrt{\frac{\rho}{\mu}}\left(\gamma+\frac{\beta}{2}\right), \end{aligned} \tag{4.52}$$

where the approximation (4.47) has been taken into account, and $h=\lambda/\mu$.

Thus, the two families of quasi–normal modes of vibration are also present in this model, and we describe them in the following subsections.

4.3.2 Toroidal modes

As discussed in the previous subsection, the allowed values for γ are again those making the linear system (4.18) compatible. The first possibility are purely tangential ($C_t = C_l = 0$) vibrations satisfying the well–known condition

$$\beta_1(\mathcal{K}R)=0 \Longrightarrow \mathcal{K}=\sqrt{\frac{\rho}{\mu}}\omega_{nl}^T,$$

ω_{nl}^T being a toroidal eigenfrequency of the elastic sphere. Using the relationship between γ and $\mathcal{K}$ for a Maxwell solid given by equation (4.52), we obtain the admitted values γ_{nl}^T as

$$\gamma_{nl}^T = -i\omega_{nl}^T - \frac{\beta}{2}. \tag{4.53}$$

Again, toroidal quasi–normal modes have two fundamental properties. They have the same set of eigenfrequencies as the elastic sphere (to first order in the parameters describing internal friction, β in this case), and also exactly the same spatial part (for *all* values of the viscosity parameters). The only difference between Kelvin–Voigt and Maxwell solids, regarding toroidal modes, appears in the dependence of the quality factor on ω: as equation (4.53) shows, the quality factor of a linear Maxwell solid increases linearly with frequency. We can express all these properties by means of the following formulæ :

$$\mathbf{s}_M^T(\mathbf{x},t)=\mathbf{s}_E^T(\mathbf{x},t)\,e^{-\omega_{nl}^T t/Q_{nl}} \qquad Q_{nl}=\frac{2\omega_{nl}^T}{\beta}, \tag{4.54}$$

relating Maxwell quasi–normal modes of vibration, $\mathbf{s}_M^T(\mathbf{x},t)$, with elastic normal modes, $\mathbf{s}_E^T(\mathbf{x},t)$, for the toroidal family.

4.3.3 Spheroidal modes

In order to handle the spheroidal family, we resort again to the perturbative expansions already used in the Kelvin-Voigt case, and, in fact, when dealing with the toroidal family. The Maxwell model reduces trivially to the perfect elastic case when $\beta = \delta = 0$, and hence we can take as the perturbative parameter

$$\epsilon = \frac{\beta}{\omega}, \tag{4.55}$$

where ω is the elastic eigenfrequency to which γ approachs when both β and δ tend to zero. Perturbative expansions in the fashion of x4.2.4 can be now introduced

$$\gamma = -i\omega + \gamma_1\epsilon, \qquad \mathcal{K} = k + k_1\epsilon, \qquad \mathcal{Q} = q + q_1\epsilon,$$

where the first order corrections k_1 and q_1 are given by equations (4.52) as functions of γ_1:

$$\begin{aligned} k_1 &= i\sqrt{\frac{\rho}{\mu}}\left(\gamma_1 + \frac{\omega}{2}\right) \\ q_1 &= i\sqrt{\frac{\rho}{\lambda+2\mu}}\left(\gamma_1 + \frac{h'+2}{h+2}\frac{\omega}{2}\right) \end{aligned} \tag{4.56}$$

where, now, the zeroth order quotient h' is given by

$$h' = h\frac{\alpha}{\beta}. \tag{4.57}$$

With this definition, together with that of the perturbative parameter, the expressions at hand are formally identical to those of the Kelvin–Voigt model and, therefore, the solutions to the Maxwell model share all the properties with their Kelvin–Voigt counterpart but the dependence of the quality factor on frequency: the product $\gamma_1\epsilon$, which gives the exponential decaying, is now independent of ω.

Summing up, spheroidal quasi–normal modes of the Maxwell solid, $\mathbf{s}_M^P(\mathbf{x},t)$, are related to spheroidal normal modes of perfectly elastic solids by the equations

$$\mathbf{s}_M^P(\mathbf{x},t) = e^{i\omega_{nl}^P t - \omega_{nl}^P t/Q_{nl}}\left(e^{i\chi_1(r)}A_{nl}(r)\,Y_{lm}\,\mathbf{n} - e^{i\chi_2(r)}B_{nl}(r)\,i\,\mathbf{n}\times\mathbf{L}Y_{lm}\right) \tag{4.58}$$

the qualitity factor being now given by

$$Q_{nl} = \frac{2\omega_{nl}^P}{\beta}\frac{1}{f}, \tag{4.59}$$

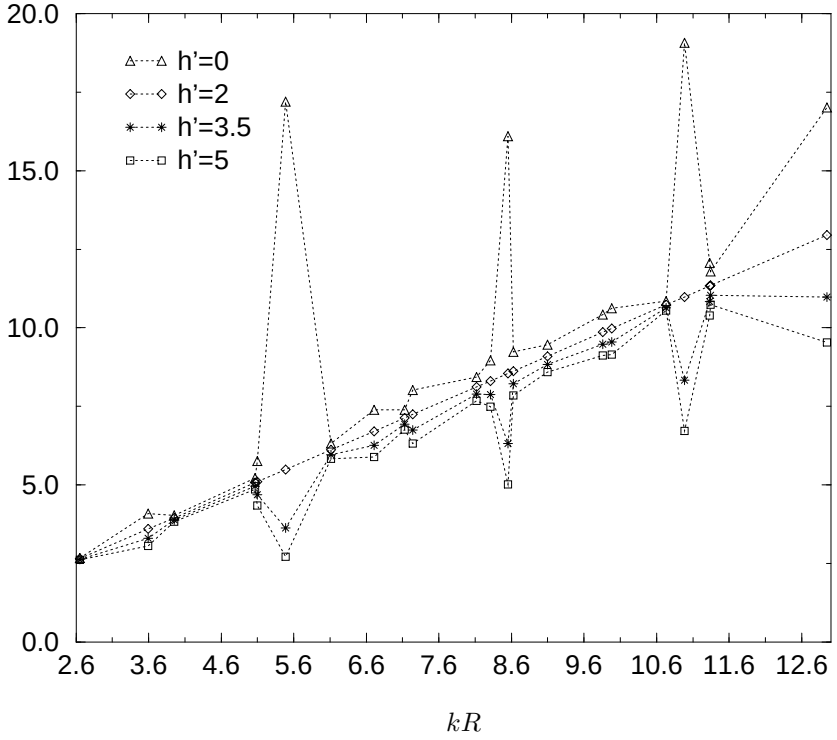

Figure 4.3. *Quality factor Q_{nl} (in units of $v_t/\beta R$) for some values of the parameter h' and the first modes of the spheroidal spectrum. The viscoelastic solid is described by a Maxwell model with $h = 2$.*

where the function $f(kR, h, h')$ is given by (4.40). In figure (4.3) we plot the quality factor of the first twenty eigenfrequencies of a Maxwell solid. We note that this model presents a stronger variability of Q_{nl} with frequency.

As the calculations so far show, the only difference between the behaviour of Maxwell and Kelvin-Voigt viscoelastic solids, when free oscillations are considered and provided the internal friction can be considered small, appears in the dependence of Q on frequency. We should note that, under other conditions (e.g. static load), both models show a greater divergence in their physical behaviour[55].

4.4 Standard Linear Model

4.4.1 Reduction of the SLM

The Standard Linear Model (SLM) for a viscoelastic solid results from the three–dimensional generalization of the mechanical model consisting of a linear, one–dimensional spring in series with a Kelvin–Voigt one–dimensional element (cf. x2.2.2). The corresponding constitutive equation takes the form:

$$\sigma_{ij} + \partial_t \left(\alpha\, \sigma_{kk}\delta_{ij} + 2\beta\, \sigma_{ij}\right) = \left(\lambda + \alpha'\partial_t\right) s_{kk}\delta_{ij} + 2(\mu + \beta'\partial_t)\, s_{ij}, \tag{4.60}$$

where the effects of internal friction are described in this case with the aid of four parameters, namely, the constants α, β, α' and β'. When looking for separable solutions, the equations of motion and the above relation force a time dependence of the form $e^{\gamma\, t}$ for both stress and strain. When such a dependence is introduced in equation (4.60), we obtain the following relation between the spatial parts of the stress and strain tensors:

$$(1 + 2\gamma\beta)\sigma_{ij}(\mathbf{x}) = \left[\lambda + \alpha'\gamma - \alpha\gamma\frac{3\lambda + 2\mu + \gamma(3\alpha' + 2\beta)'}{1 + \gamma(3\alpha + 2\beta)}\right] s_{kk}(\mathbf{x})\delta_{ij} + 2(\mu + \beta'\gamma)s_{ij}(\mathbf{x}).$$

The case of small internal friction is treated by first order approximation in the quantities parametrizing viscous processes, i.e.

$$\alpha,\ \beta,\ \alpha',\ \beta' << 1/\mid \gamma \mid \tag{4.61}$$

When such approximation is made, the above equation reduces to

$$\sigma_{ij}(\mathbf{x}) = (\lambda + \lambda'\gamma)s_{kk}(\mathbf{x})\delta_{ij} + 2(\mu + \mu'\gamma)s_{ij}(\mathbf{x}), \tag{4.62}$$

where we have introduced two new constants given by

$$\mu' = \beta' - 2\beta\mu, \qquad \lambda' = \alpha' - 2\lambda\beta - (3\lambda + 2\mu)\alpha. \tag{4.63}$$

Therefore, when equation (4.61) holds, the SLM reduces to a Kelvin–Voigt one; that is, for small internal friction, both models have the same set of quasi–normal modes of vibration, which are characterized by the constants λ, μ, λ' and μ', the latter being given, for the Standard Linear solid, by equations (4.63).

4.5 Generalized mechanical models

4.5.1 Constitutive equation

The models analysed so far are the simplest ones obtained by three-dimensional generalizations of mechanical viscoelastic models composed of linear springs and dashpots. They give rise to differential constitutive relations, with time derivatives up to the first order. Considering more involved networks of springs and dashpots yields differential relations involving higher order time derivatives of strain and stress (see, e.g., [16, 60]). Thus, quite independently of any reference to the underlying mechanical model, we can consider general differential relations between stress and strain including any number of time derivatives. To ease the formulation of such differential constitutive equations for the case of isotropic and homogenous bodies, we shall introduce the trace–free parts of the strain and stress tensors, s'_{ij}, σ'_{ij} (usually termed *deviatoric* components in the literature on viscoelasticy [16, 60, 51]),and their traces, s and σ (*dilational* components), defined as

$$s'_{ij} = s_{ij} - \frac{1}{3} s \delta_{ij}, \qquad s = s_{kk} \tag{4.64}$$

$$\sigma'_{ij} = s_{ij} - \frac{1}{3} \sigma \delta_{ij}, \qquad \sigma = \sigma_{kk}. \tag{4.65}$$

In terms of the above quantities, the linear Hooke law for an elastic solid takes the form

$$\sigma = (3\lambda + 2\mu) s \qquad \sigma'_{ij} = 2\mu \, s'_{ij}, \tag{4.66}$$

while the constitutuive equation of a SLM is written as

$$[1+(3\alpha+2\beta)\partial_t]\, \sigma = [3\lambda+2\mu+(3\alpha'+2\beta')\partial_t]\, s, \qquad (1+2\beta\partial_t)\sigma'_{ij} = (2\mu+2\beta'\partial_t)\, s'_{ij}. \tag{4.67}$$

The above equation can be now generalized to include higher order time derivatives. We can consider thus viscoelastic models whose constitutive equation is given by

$$R(\partial_t)\sigma = S(\partial_t) s \qquad R'(\partial_t)\sigma'_{ij} = S'(\partial_t) s'_{ij}, \tag{4.68}$$

where we have introduced the polynomials

$$R(x) = \sum_{l=0}^{N} r_l x^l, \qquad R'(x) = \sum_{l=0}^{N} r'_l x^l, \qquad S(x) = \sum_{l=0}^{N} s_l x^l, \qquad S'(x) = \sum_{l=0}^{N} s'_l x^l, \tag{4.69}$$

so that a general differential model is given for each set of $4N$ real constants r_l, r'_l, s_l, s'_l characterizing the solid at hand (some constants may be zero, the polynomials being

then of different order, and N indicating the highest one). It is easily seen that the three preceeding models are special cases of this general class. In the following subsection we shall describe a well–known general procedure, based on Fourier transform techniques, to solve a general differential model, by means of the so–called *Correspondence Principle*, and will just sketch its application to the solid sphere.

4.5.2 The Correspondence Principle

Let $\tilde{\sigma}_{ij}(\mathbf{x},\Omega)$ and $\tilde{s}_{ij}(\mathbf{x},\Omega)$ be the Fourier transforms of the stress and strain tensors, and $\tilde{s}_i(\mathbf{x},\Omega)$ that of the displacement vector field:

$$\tilde{\sigma}_{ij}(\mathbf{x},\Omega) \equiv \int_{-\infty}^{\infty} \sigma_{ij}(\mathbf{x},t)e^{i\Omega t}dt \qquad \tilde{s}_i(\mathbf{x},\Omega) \equiv \int_{-\infty}^{\infty} s_i(\mathbf{x},t)e^{i\Omega t}dt \tag{4.70}$$

$$\tilde{s}_{ij}(\mathbf{x},\Omega) \equiv \int_{-\infty}^{\infty} s_{ij}(\mathbf{x},t)e^{i\Omega t}dt = \tilde{s}_{(i,j)}(\mathbf{x},\Omega). \tag{4.71}$$

In terms of these Fourier transforms, the constitutive equations (4.68) read:

$$\tilde{\sigma} = \frac{R(i\Omega)}{S(i\Omega)}\tilde{s} \qquad \tilde{\sigma}'_{ij} = \frac{R'(i\Omega)}{S'(i\Omega)}\tilde{s}_{ij}, \tag{4.72}$$

while the equations of motion are

$$-\Omega^2\tilde{\mathbf{s}} = \frac{1}{3}\left(\frac{R(i\Omega)}{S(i\Omega)} - \frac{R'(i\Omega)}{S'(i\Omega)}\right)\nabla(\nabla\cdot\tilde{\mathbf{s}}) + \frac{R'(i\Omega)}{2S'(i\Omega)}\nabla^2\tilde{\mathbf{s}}. \tag{4.73}$$

Comparing the above equations with the corresponding ones for normal modes of vibration of elastic solids (see (3.3)), and the constitutive relation (4.72) with (4.66), we note that the problem of finding solutions to the equation of motion of a general viscoelastic differential model reduces to that of finding the normal modes of vibration of an elastic solid having complex Lamé coefficients, given by

$$\tilde{\lambda}(\Omega) = \frac{1}{3}\left(\frac{R(i\Omega)}{S(i\Omega)} - \frac{R'(i\Omega)}{S'(i\Omega)}\right) \qquad \tilde{\mu}(\Omega) = \frac{1}{2}\frac{R'(i\Omega)}{S'(i\Omega)}, \tag{4.74}$$

where the allowed values of Ω are obtained as the solutions to the elastic solid's eigenfrequency equation when the above complex coefficients are used instead of the real, constant Lamé coefficients λ, μ (thus, in general, Ω will take complex values giving rise to damped oscillations). After solving for Ω, the spatial part of the solutions is obtained from that of the normal modes by simply substituting the old, real–valued constants ω, λ and μ by the new complex values Ω, $\tilde{\lambda}$ and $\tilde{\mu}$. This method for solving the viscoelasticity equations is known in the literature on the subject [16, 60, 82] as the *Correspondence Principle*, and, as a matter of fact, our previous derivations of the form of quasi–normal modes for

Kelvin–Voigt, Maxwell and SL models can be seen as special cases of its application. It can be applied to any boundary value problem whose elastic counterpart is solvable. The case of small internal friction (that is, first order approximation in the coefficients of the polynomials given in (4.69)) has been treated by Graffi [82, 58] for one–dimensional wave propagation. As shown in the previous sections, the three–dimensional, spherical case is also solvable. In fact, the toroidal modes are straightforward obtained from their elastic counterparts due to the simple form of their eigenvalue equation, while the spheroidal ones demand more complex algebra, which becomes more cumbersome as the order N of the model increases. Therefore, we shall give the general solution to the toroidal case for any differential viscoelastic model. This solution will give us the dependence of Q on frequency, which will also be the approximated dependence for spheroidal modes.

4.5.3 Toroidal modes

As discussed above, the boundary equation for toroidal modes of a general viscoelastic model is obtained from the eigenvalue equation of the elastic model

$$\beta_1(kR) = 0 \qquad k = \sqrt{\frac{\rho}{\mu}}\omega, \tag{4.75}$$

upon substitution of μ by $\tilde{\mu}$, yielding

$$\beta_1(\mathcal{K}R) = 0 \qquad \mathcal{K} = \Omega\sqrt{\frac{2\rho S'(i\Omega)}{R'(i\Omega)}}. \tag{4.76}$$

We know that the only solutions to the eigenvalue equation (4.75) are the real eigenfrequencies of the elastic sphere, ω_{nl}^T, and therefore the allowed values for Ω are given by the relation

$$\sqrt{\frac{2\mu\, S'(i\Omega)}{R'(i\Omega)}}\Omega = \omega_{nl}^T. \tag{4.77}$$

Let us write the polynomials S' and R' as

$$S'(x) = 1 + \epsilon\sum_{l=1}^{N} s'_l x^l, \qquad R'(x) = 2\mu\left(1 + \epsilon\sum_{l=1}^{N} r'_l x^l\right), \tag{4.78}$$

so that the small internal friction approximation shall be represented by the inequality

$$\epsilon << 1 \tag{4.79}$$

and the quantities $r'_l\omega^l$ and $s'_l\omega^l$ are zero–order in ϵ and dimensionless, ω being a toroidal eigenvalue of the elastic case. We shall introduce also an expansion for Ω in the small

parameter ϵ, whose zero order term will correspond to a toroidal eigenfrequency ω of the elastic solid:

$$\Omega = \omega + \epsilon\Omega_1. \tag{4.80}$$

Under the above approximations, we have

$$\frac{2S'(i\Omega)}{\mu R'(i\Omega)} = 1 + 2i\epsilon \sum_{l=0}^{N} t_l \omega^l, \qquad t_l \equiv i^{l-1}(s'_l - r'_l)/2, \tag{4.81}$$

and the value of Ω_1 follows when introducing the above expansion into equation (4.77), yielding

$$\Omega_1 = \sum_{l=1}^{N} t_l \omega^{l+1}. \tag{4.82}$$

In terms of Ω_1, the quality factor reads

$$Q = -\frac{\omega}{\epsilon} \frac{1}{\mathrm{Im}[\Omega_1]}, \tag{4.83}$$

where $\mathrm{Im}[\cdot]$ denotes the imaginary part of its argument. Thus, we observe that, as regards toroidal modes, using a general differential model gives us a polynomial in ω for $1/Q$, with no independent term (so that constant Q is not allowed by this models) and containing only odd powers of the unperturbed frequency ω. In general, whenever $t_l \neq 0$ for any l even, the real part of Ω_1 will not vanish and the angular frequency of the periodic component of the quasi–normal modes shall undergo first order corrections. Hence, in order to preserve the elastic spectrum to first order, our model must satisfy the conditions

$$t_l = 0 \qquad (l \text{ even}). \tag{4.84}$$

Provided the preceeding equation holds, the corrections to $\mathcal{K}$ will be purely imaginary and, thus, the modulus of the spatial part of the modes will remain unaltered, the only effect of viscosity being the addition of a point–dependent phase in the fashion of equation (4.42) [5].

The calculation for the spheroidal quasi–normal modes could be performed along the same lines, but, as we have seen in the simplest models, the algebra becomes increasingly cumbersome as the order of the model grows. We shall not go into such calculations here.

[5] This correction will appear provided that $N \geq 2$ and, thus, it was absent in the toroidal families of the previously discussed models.

Chapter 5

Sensitivity of spherical detectors

5.1 Introduction

The previous chapters have been devoted to the investigation of the physical properties of elastic and viscoleastic solids when no external forces act upon them, this study being the basis for a detailed analysis of the way such bodies behave under the influence of impinging gravitational waves. We undertake that analysis in the present chapter. As we have shown, the interaction between gravitational radiation and rigid solids takes the form of a tidal driving force entering the equations of motion. Thus, we first address the problem of finding the field of displacements induced in a body by a gravitational wave, and of which are the distinctive features of these deformations. Afterwards, we proceed to an investigation of the efficiency of these resonant detectors, a key point due to the weakness of the expected signals. The sensitivity of a viscoelastic solid as as gravitational wave antenna can be quantitatively described by means of the concept of *absorption cross–section*, a familiar one in many branches of physics, ranging from scattering phenomena in classical electrodynamics [67] to purely quantum phenomena such as neutron absorption [18]. In the present context, the absorption cross–section $\sigma_{\rm abs}$ is defined as the fraction of incoming gravitational energy per unit area absorbed by the detector [127, 93, 105]. More precisely, when considering a finite duration driving force, if dE/dS denotes the total energy per unit area impinging on the detector, we shall compute its absorption cross–section by means of the ratio

$$\sigma_{\rm abs} = \frac{E_{\rm osc}}{dE/dS}, \tag{5.1}$$

where $E_{\rm osc}$ stands for the energy of the oscillations induced by the incoming wave. On the other hand, if a continuous driving force sweeps the detector carrying an energy per unit area and per unit time Φ and causes the resonant body to vibrate with an average mechanical power $< P >$, the absorption cross–section will be defined as the ratio

$$\sigma_{\rm abs} = \frac{< P >}{\Phi}. \tag{5.2}$$

We shall use the concept of cross–section as a useful criterion for evaluating and comparing the suitability of differently shaped bodies to detect gravitational waves. The computation of $\sigma_{\rm abs}$ for spherical bodies is addressed in section 5.3, where we present a rederivation of the sphere's sensitivity parameters within the context of the theory of viscoelastic bodies dealt with in the preceeding chapters. Our approach is alternative to previous derivations, based upon analogies [105], analysis of the scattered wave at infinity [127] or introduction of the dissipation effects parametrically into the equations of motion [93, 119, 88, 91]. The method presented has been previously applied to one–dimensional oscillators [122, 123, 93], and to perfectly elastic bodies [76]. From our point of view, it offers a sound theoretical basis for further research on the perfomance of resonant antennæ. In the last two sections of this chapter, we will take the first steps in this direction, and analyse some issues on the solid and hollow sphere as gravitational wave detectors. There we shall often refer to cylindrical bars for comparison. Although spherical shape was soon recognized as a better choice for a resonant detector's geometry, and has been the object of theoretical attention since the early seventies [48, 5, 119, 69, 76, 27], cylindrical bars are the only resonant detectors actually operative. Therefore, a brief review of their main characteristics is previously given in x5.4.

5.2 Solution to the equations of motion

The aim of this section is to solve the equations of motion governing the interaction of a Kelvin–Voigt solid with a linear gravitational wave. These equations have been derived in chapter 2 and solved for the case of free oscillations in chapter 4. In the calculations presented there, we have seen that solutions for the viscoelastic solid can be constructed relying on the known solutions of the perfectly elastic solid. Now, we shall show that this is also the case when a driving force comes into play, for we will solve the Kelvin–Voigt equations of motion introducing again a perturbative expansion whose zeroth order term corresponds to an elastic solid driven by the same external force. Thus, we begin, after introducing some useful notation, reviewing the general solution to the equations

of motion of an elastic solid in the presence of a driving force [76], while the solution to the viscoelastic problem is derived in x5.2.2.

5.2.1 Elastic solid

As we have seen, when a force per unit volume $\boldsymbol{f}(\mathbf{x},t)$ acts on an elastic solid, it undergoes deformations described by a field of displacements $\boldsymbol{s}(\mathbf{x},t)$ which is a solution of the set of partial differential equations (3.1). Throughout this chapter, we shall perform calculations in the frequency domain, i.e., we shall work with the Fourier transforms of the quantities involved rather than with its time–dependent counterparts. Thus, denoting by $\boldsymbol{F}(\mathbf{x},\omega)$ and $\boldsymbol{S}(\mathbf{x},\omega)$ the Fourier transforms of $\boldsymbol{f}(\mathbf{x},t)$ and $\boldsymbol{s}(\mathbf{x},t)$[1], the equations of motion can be written as

$$\rho\omega^2\boldsymbol{S} + (\lambda+\mu)\nabla\left(\nabla\cdot\boldsymbol{S}\right) + \mu\nabla^2\boldsymbol{S} = -\boldsymbol{F}, \tag{5.4}$$

which must be supplemented by requisite boundary conditions. We shall be interested in the case of no tractions on the body's surface, which gives us the following conditions

$$\lambda(\nabla\cdot\boldsymbol{S})\mathbf{n} + 2\mu\mathbf{n}\cdot\nabla\boldsymbol{S} + \mathbf{n}\times(\nabla\times\boldsymbol{S}) = 0, \tag{5.5}$$

to be satisfied on the solid's surface for any value of ω. Thus, the spatial parts of normal modes of vibration discussed in chapter 3 are the solutions of the homogenous counterparts of the above equations. In order to take advantage of the eigenvalue expansions of Green's functions associated to partial differential equations, let us reformulate our problem in a notation which makes explicit that we are dealing with an eigenvalue problem in a Hilbert space. We shall use the compact notation introduced in chapter 3.

Regarding $\boldsymbol{S}(\mathbf{x},\omega)$ as a one–parameter family of vector fields over V, we can rewrite equations (5.4) and (5.5) describing the driven oscillations of an elastic solid as a linear problem over $\mathcal{H}_h$, namely

$$\mu\mathbb{L}\boldsymbol{S} + \rho\omega^2\boldsymbol{S} = -\boldsymbol{F}, \qquad \boldsymbol{S}\in\mathcal{H}_h. \tag{5.6}$$

where $\mathbb{L}$ and $\mathbb{T}$ are defined by equations (3.85) and (3.86), and are related by equation (3.87). We also recall that the eigenvectors of $\mathbb{L}$ are the normal modes of vibration of the

[1] Uppercase letters will denote, unless stated otherwise, the Fourier transform of their lowercase counterparts, according to the well–known formulæ

$$A(\omega) \equiv \int_{-\infty}^{\infty} a(t)e^{-i\omega t}dt \qquad a(t) = \frac{1}{2\pi}\int_{-\infty}^{\infty} A(\omega)e^{i\omega t}d\omega. \tag{5.3}$$

free solid, cf. (3.89). The above non–homogeneous equation can be immediately solved with the aid of the Green's operator $\mathbb{G}(\mathbf{x}, \mathbf{x}', \omega)$, which is defined [95] to be the solution to

$$\mathbb{L}\mathbb{G} + \frac{\rho\omega^2}{\mu}\mathbb{G} = -\mathbb{I}\frac{1}{\rho}\delta^{(3)}(\mathbf{x} - \mathbf{x}'), \tag{5.7}$$

satisfying homogeneous boundary conditions on S:

$$\mathbb{T}\mathbb{G}|_S = 0. \tag{5.8}$$

Applying both sides of equation (5.7) to $\boldsymbol{S}$ and substracting the resulting equality from $\mathbb{G}$ times equation (5.6), we have, after integration over V,

$$\boldsymbol{S}(\mathbf{x}, \omega) = \frac{1}{\mu}\int_V \rho d\mathbf{x}'\, \mathbb{G}(\mathbf{x}, \mathbf{x}', \omega)\boldsymbol{F}(\mathbf{x}', \omega). \tag{5.9}$$

Combining the above integral representation, with the expansion (3.94) of $\mathbb{G}$ in terms of normal modes of vibration $\mathbf{s}_N(\mathbf{x})$ we finally obtain an expression for $\boldsymbol{S}(\mathbf{x}, \omega)$ as a superposition of normal modes:

$$\boldsymbol{S}(\mathbf{x}, \omega) = \sum_N \frac{F_N(\omega)}{\omega_N^2 - \omega^2}\mathbf{s}_N(\mathbf{x}), \qquad F_N(\omega) \equiv \frac{1}{M}(\mathbf{s}_N, \boldsymbol{F}). \tag{5.10}$$

The above equation gives the general solution to the problem of a driven elastic solid of any shape and for any driving force. Using the convolution theorem for Fourier transforms [30], the form of $\mathbf{s}(\mathbf{x}, t)$ is easily computed from the fact that $\omega_N(\omega_N^2 - \omega^2)^{-1}$ is the Fourier transform of $\Theta(t)\sin\omega_N t$, where $\Theta(t)$ stands for the Heaviside's step function. Thus, the solution in the time domain is written as

$$\mathbf{s}(\mathbf{x}, t) = \sum_N \frac{f_N(t)}{\omega_N}\mathbf{s}_N(\mathbf{x}), \quad f_N(t) \equiv \frac{1}{M}\int_{-\infty}^{t} (\mathbf{s}_N, \boldsymbol{f}(t'))\sin\omega_N(t - t')\, dt', \tag{5.11}$$

which is the expression appearing in [76] for the case of a separable force. We shall make use of these solutions and the formalism introduced to find the solution to the equations of motion of a Kelvin–Voigt solid in the following subsection.

5.2.2 Kelvin–Voigt solid

In order to translate the equations of motion of a Kelvin–Voigt solid into the operational formalism used in the previous subsection, we shall introduce two more linear operators, $\mathbb{L}$' and $\mathbb{T}$', defined as

$$(\mathbb{L}')_{ij} \equiv (1 + h')\partial_i\partial_j + \delta_{ij}\partial_k\partial_k, \tag{5.12}$$

$$(\mathbb{T}')_{ij} \equiv h' n_i \partial_j + 2\delta_{ij} n_k \partial_k + \epsilon_{ikl}\epsilon_{lmj} n_k \partial_m, \tag{5.13}$$

where h' denotes the ratio between the constants characterizing the viscous properties of the solid, i.e., λ' and μ' (cf. chapter 4). With this notation, the equations of motion for the field of displacements $\mathbf{s}(\mathbf{x}, t)$ that a viscoelastic, Kelvin–Voigt solid undergoes under the action of a driving force per unit mass $\boldsymbol{f}(\mathbf{x}, t)$ have the form

$$\rho \frac{\partial^2 \mathbf{s}}{\partial t^2} - \mu \mathbb{L}\mathbf{s} - \mu' \mathbb{L}' \frac{\partial \mathbf{s}}{\partial t} = \boldsymbol{f}, \tag{5.14}$$

with boundary conditions

$$\mu \mathbb{T}\mathbf{s} + \mu' \mathbb{T}' \frac{\partial \mathbf{s}}{\partial t}\bigg|_S = 0. \tag{5.15}$$

In the frequency domain, the above equations translate into

$$\mathbb{L}\boldsymbol{S} + i\alpha \mathbb{L}'\boldsymbol{S} + \frac{\rho\omega^2}{\mu}\boldsymbol{S} = -\frac{\boldsymbol{F}}{\mu}, \quad (\mathbb{T} + i\alpha\mathbb{T}')\boldsymbol{S}|_S = 0, \tag{5.16}$$

where we have introduced the dimensionless, ω-dependent parameter

$$\alpha \equiv \frac{\mu'\omega}{\mu}. \tag{5.17}$$

Before discussing the general solution to equations (5.16), we consider the particularly simple case $h' = h$. When this equality holds the viscoelastic problem is reduced to an elastic–like one:

$$(1 + i\alpha)\mathbb{L}\boldsymbol{S} + \frac{\rho\omega^2}{\mu}\boldsymbol{S} = -\frac{\boldsymbol{F}}{\mu}, \qquad \boldsymbol{S} \in \mathcal{H}_h, \tag{5.18}$$

which is immediately solved following the procedure detailed in the previous subsection, yielding

$$\boldsymbol{S}(\mathbf{x}, \omega) = \sum_N \frac{F_N(\omega)}{(1 + i\alpha)\omega_N^2 - \omega^2}\mathbf{s}_N(\mathbf{x}), \qquad (h = h'), \tag{5.19}$$

where the coefficients $F_N(\omega)$ are defined in (5.10). When the spectrum of the driving force $\boldsymbol{F}(\omega)$ happens to be heavily peaked around a given eigenfrequency ω_K, being zero outside a neighbourhood of $\pm\omega_K$, the above equation can be approximated by

$$\boldsymbol{S}(\mathbf{x}, \omega) = \frac{1}{(1 + i\alpha)\omega_K^2 - \omega^2} \sum_m F_m(\omega)\mathbf{s}_m(\mathbf{x}), \tag{5.20}$$

where the index m ranges over the eigenvectors having the same degenerate eigenfrequency ω_K. Comparing the above solution to that of the purely elastic case (5.10), we see that the effect of viscosity is to remove the real singularities of the spectrum $\boldsymbol{S}(\mathbf{x}, \omega)$

via the new term $i\alpha\omega_K^2 = i\omega\omega_K^2\mu'/\mu$. For small viscosity ($\omega_K\mu'/\mu << 1$), this term has an immediate physical meaning which can be shown notting that it this case we can write

$$[\omega_K^2 - \omega^2 + i(\omega_K^2\mu'/\mu)\omega]^{-1} \approx [\omega_K^2 - \omega^2 + 2i(\omega_K^2\mu'/2\mu)\omega + (\omega_K^2\mu'/2\mu)^2]^{-1}.$$

Now, the right hand member of the above equation is the Fourier transform of

$$\Theta(t)\,\omega_K^{-1}\exp\{-(\omega_K^2\mu'/2\mu)t\}\sin\,\omega_K t,$$

and the convolution theorem gives us the expression of $\boldsymbol{S}(\mathbf{x},\omega)$ in the time domain as

$$\mathbf{s}(\mathbf{x},t) = \sum_N \omega_N^{-1}\exp\{-(\omega_N^2\mu'/2\mu)t\}\int_{-\infty}^{t}\mathbf{f}_N(t')\exp\{t'\omega_N^2\mu'/2\mu\}\sin\,\omega_N(t-t')\,dt'. \tag{5.21}$$

Therefore, the forced solution is damped at each frequency with a quality factor $Q_K = 2\mu/\omega_K\mu'$, *which is the same as the quality factor of free damped oscillations* found in chapter 4.

Returning to the general case $h' \neq h$, we shall look for a solution to equations (5.16) as a power series expansion in α, i.e., having the form

$$\boldsymbol{S}(\mathbf{x},\omega) = \sum_{n=0}^{\infty}\boldsymbol{S}^{(n)}(\mathbf{x},\omega)\alpha^n. \tag{5.22}$$

Obviously, the zeroth order term of the above expansion is the solution corresponding to an elastic solid under the same driving force, given by equation (5.10):

$$\boldsymbol{S}^{(0)}(\mathbf{x},\omega) = \sum_N \boldsymbol{S}_N^{(0)}\mathbf{s}_N(\mathbf{x}), \qquad \boldsymbol{S}_N^{(0)} = \frac{F_N(\omega)}{\omega_N^2 - \omega^2}. \tag{5.23}$$

As regards the contributions $\boldsymbol{S}^{(n)}$ for $n \geq 1$, introducing the expansion (5.22) into the equations of motion and gathering together the terms of the same order in α, we obtain the following iterative set of differential equations to be satisfied for any n greater than zero:

$$\mathbb{L}\boldsymbol{S}^{(n)} + \frac{\rho\omega^2}{\mu}\boldsymbol{S}^{(n)} = -i\mathbb{L}'\boldsymbol{S}^{(n-1)}, \qquad \mathbb{T}\boldsymbol{S}^{(n)}|_S = -i\mathbb{T}'\boldsymbol{S}^{(n-1)}|_S. \tag{5.24}$$

Thus, each $\boldsymbol{S}^{(n)}$ is the solution of a non–homogeneous elastic problem whose driving terms are given by the previous order solution. This problem can be solved with the aid of the Green's operator introduced in the previous subsection once we have coped with the inhomogeneous terms appearing in the boundary conditions. The details of this

calculation, which is performed using standard techniques, are given in appendix (B.2). There it is shown that, *for a driving force with spectrum peaked around* ω_K, the solution to equations (5.24) is given by

$$\boldsymbol{S}^{(n)}(\mathbf{x},\omega) = -i\left(\frac{-i\omega_K^2\zeta}{\omega_K^2-\omega^2}\right)^n \frac{1}{\omega_K^2-\omega^2}\sum_m F_m(\omega)\mathbf{s}_m(\mathbf{x}), \tag{5.25}$$

where m is again a degeneracy index, and the new constant ζ has the value [2]

$$\zeta = 1 + (h'-h)\frac{\mu}{M\omega_K^2}\int_V |\nabla\cdot\mathbf{s}_K|^2\, dV. \tag{5.26}$$

Using (5.25) and the Taylor expansion $(1+ir)^{-1} = \sum_n (-ir)^n$, we can immediately perfom the sumation of the series (5.22) giving the solution to the problem as

$$\boldsymbol{S}(\mathbf{x},\omega) = \sum_m \frac{F_m(\omega)}{(1+i\zeta\alpha)\omega_K^2-\omega^2}\mathbf{s}_m(\mathbf{x}). \tag{5.27}$$

Strictly speaking, the series from which this solution is obtained can be summed only outside a small neighbourhood of ω_K, because $\boldsymbol{S}^{(n)}(\mathbf{x},\omega)$ diverge as $\omega\to\omega_K$. Nevertheless, equation (5.27) has no singularities when $\omega=\omega_K$, and it is a solution of the equations of motion (5.16) for any value of ω, as can be shown by direct substitution. On the other hand, when $h=h'$, $\zeta=\omega_K^2$, so that solution (5.20) is seen to be a special case of the above equation[3]. An argument analogous to that following equation (5.20) can be applied to the general solution (5.27), leading to the following relationship between ζ and the quality factor Q_K^f associated with each frequency component of the forced solution

$$Q_K^f = \frac{2\mu}{\mu'\omega_K}\frac{1}{\zeta}. \tag{5.29}$$

On the other hand, we have shown in chapter 4 that the quality factor Q_K of a quasi–normal mode of vibration of frequency ω_K is given by (cf. x4.2.4)

$$Q_K = \frac{2\mu}{\mu'\omega_K}\frac{1}{f} \tag{5.30}$$

[2]Spherical symmetry is also assumed in this calculation. As easily seen from the explicit form of eigenvectors in this case (cf. chapter 3), ζ does not depend on the degeneracy index m.

[3]For $h\neq h'$ use of the explicit expressions of $\mathbf{s}_K(\mathbf{x})$ gives for a spheroidal mode of the solid with $K=\{n,l,m\}$

$$\begin{aligned}\zeta &= 1+(h'-h)\frac{\mu}{q_{nl}\omega_{nl}^2}\frac{C(n,l)^2}{M}\int_0^{q_{nl}R} j_l(\xi)\xi^2\, d\xi \\ &= 1+(h'-h)\frac{\mu}{q_{nl}\omega_{nl}^2}\frac{C(n,l)^2}{M}\frac{1}{2q_{nl}R}\left\{(j_l(z)/z-j_l'(z))^2+[z^2-(l+1/2)^2]j_l^2(z)\right\}_{q_{nl}R}\end{aligned} \tag{5.28}$$

where the term between braces is computed at $z=q_{nl}R$, and we have used the notation of chapter 3. Analogous expressions for the hollow sphere can be found *mutatis mutandis*.

where f has the somewhat cumbersome form given in (4.40), which by no means resembles the one found for ζ. It is thus most remarkable that numerical computation of ζ according to equation (5.28) shows it *to take exactly the same values as* f, i.e., we have

$$Q_K^f = Q_K. \tag{5.31}$$

Thus, we can rewrite the general solution (5.27) as

$$\boldsymbol{S}(\mathbf{x},\omega) = \sum_m \frac{F_m(\omega)}{\omega_K^2 - \omega^2 + 2i(\omega_K/Q_K)\omega}\mathbf{s}_m(\mathbf{x}). \tag{5.32}$$

5.3 Calculation of the absorption cross–section

5.3.1 Absorbed power

Having now at our disposal the explicit form of the field of displacements undergone by a Kelvin–Voigt solid under the action of an arbitrary driving force, we can proceed to the calculation of expressions giving the absorption cross–section of such a solid. We begin by computing in this subsection the power absorbed by the solid driven by a general force, and spell it out for a separable, periodic one.

The external force $\boldsymbol{f}(\mathbf{x},t)$ acting on the body makes a work per unit time which is given by the instantaneous power:

$$P(t) = \int_V \frac{\partial \mathbf{s}}{\partial t}\cdot \boldsymbol{f}\, dV.$$

We shall not be interested in this instantaneous magnitude, but in the average power absorbed by the solid as a result of the force's action, which is given by

$$< P > \equiv \lim_{T\to\infty}\frac{1}{2T}\int_{-T}^{T} P(t)\, dt = \lim_{T\to\infty}\frac{1}{2T}\int_{-\infty}^{\infty}\chi_T(t)P(t)\, dt, \tag{5.33}$$

where we have introduced the function

$$\chi_T(t) = \begin{cases} 1 & |t| < T \\ 0 & |t| > T \end{cases} \tag{5.34}$$

whose Fourier transform $\tilde{\chi}_T(\omega)$ is

$$\tilde{\chi}_T(\omega) = 2\frac{\sin T\omega}{\omega}. \tag{5.35}$$

With the aid of Parseval's and convolution theorems, equation (5.33) can be written as a double integration over frequencies of the form

$$< P >= \lim_{T\to\infty} \frac{-i}{4\pi^2 T} \int_{-\infty}^{\infty} d\omega \int_{-\infty}^{\infty} d\omega' \int_V dV\, \boldsymbol{F}(\mathbf{x},\omega)\cdot \boldsymbol{S}^*(\mathbf{x},\omega')\omega' \frac{\sin T(\omega-\omega')}{(\omega-\omega')},$$

Making use of the expression for $\boldsymbol{S}(\mathbf{x},\omega)$ derived in the previous section (equation (5.32)), the average power can thus be represented in terms of quantities referred only to the driving force, namely

$$< P >= \lim_{T\to\infty} \frac{-iM}{4\pi^2 T} \int_{-\infty}^{\infty} d\omega \int_{-\infty}^{\infty} d\omega'\, \omega' \frac{\sin T(\omega-\omega')}{\omega-\omega'} \sum_m \frac{F_m(\omega)F_m^*(\omega')}{\omega_K^2-\omega^2-2i(\omega_K/Q_K)\omega}. \tag{5.36}$$

Let us consider a particular form of the driving force (plane wave) for which the above frequency integrations can be performed, and which shall be of interest when dealing with gravitational wave detectors.

By *plane wave* we mean a separable force having sinusoidal time–dependence, i.e.,

$$\boldsymbol{f}(\mathbf{x},t) = \mathbf{f}(\mathbf{x})\sin\Omega t, \tag{5.37}$$

with Ω close to a given eigenfrequency ω_K. Then we have

$$F_m(\omega) = i\pi\, f_m\,[\delta(\omega+\Omega)-\delta(\omega-\Omega)], \qquad f_m \equiv \frac{1}{M}(\mathbf{s}_m,\mathbf{f}). \tag{5.38}$$

The integrations appearing in (5.36) can be now immediately performed to yield

$$< P >_{pw}= \lim_{T\to\infty} \left(1+\frac{\sin 2T\Omega}{2T\Omega}\right) \mathrm{Im}\left[\frac{\Omega}{\omega_K^2-\Omega^2-2i\Omega\omega_K/Q_K}\right] \frac{M}{2}\sum_m |f_m|^2,$$

and the limit is trivially computed, the average power absorbed by a detector under the action of a plane wave being thus

$$< P >_{pw}= \frac{4\omega_K^2\Omega^2/Q_K^2}{\left(\omega_K^2-\Omega^2\right)^2+\left(2\Omega\omega_K/Q_K\right)^2} \frac{M}{2}\sum_m |f_m|^2. \tag{5.39}$$

This equation can be further simplified using the fact that we have assumed Ω very close to ω_K, i.e., $|\Omega-\omega_K| << \omega_K$, so that

$$< P >_{pw}= \frac{M}{4}\frac{\omega_K/Q_K}{\left(\omega_K-\Omega\right)^2+\left(\omega_K/Q_K\right)^2}\sum_m |f_m|^2. \tag{5.40}$$

So far, we have made no assumption regarding the dependence of $\boldsymbol{f}$ on the spatial coordinates. But, as discussed in chapter 2, when considering the action of a gravitational

wave impinging on a (visco)elastic body as observed in a normal reference, this form happens to be of a very concrete type—in fact, it is a tidal force. The next subsection is devoted to the calculation of the coefficients F_m and f_m for such a x–dependence, which, together with the expressions already derived for the power absorbed and those for the incident energy flux carried by an incoming gravitational wave, will finally give us the absorption cross–section of spherical resonant detectors.

5.3.2 Tidal driving force

Let us consider the specific form of the driving force arising from the interaction of a viscoelastic solid with an impinging gravitational wave which is weak enough to allow the use of the linear theory discussed in chapter 2. As shown there in full detail, this interaction is described by a tidal field

$$f_i(\mathbf{x},t) = \rho\, c^2 R_{0i0j}(t) x^j, \tag{5.41}$$

provided we are measuring in a normal frame. In the equation above, R_{0i0j} stands for the components of Riemann's tensor at the center of the detector and are therefore functions of time but not of position. These components are gauge invariant under first order coordinate changes, as those relating normal coordinates with a reference system in which the transverse, traceless gauge (TT–gauge) holds [47, 84]. We can thus compute Riemann's tensor in the TT–coordinate system although we are writing the equations of motion in a normal system. They are given by the well–known expressions [121, 93]

$$R_{0i0j} = -\frac{1}{2c^2}\frac{\partial^2 h_{ij}^{TT}}{\partial\, t^2}, \tag{5.42}$$

where h_{ij}^{TT} denote the metric's first order perturbation due to a linear gravitational wave, as measured by a TT–observer. They have thus the following properties

$$h_{ii}^{TT} = 0 \qquad h_{ij,j}^{TT} = 0. \tag{5.43}$$

Three–dimensional, symmetric and traceless matrices constitute a five–dimensional vector space. Thus, and arbitrary matrix $A_{ij}(t)$ with the aforementioned properties can always be decomposed as a linear combination of the form

$$A_{ij}(t) = \sum_{m=-2}^{m=2} A^{(m)}(t) E_{ij}^{(m)}$$

with $\{E^{(m)}_{ij}\}_{m=-2,\ldots,2}$ a properly chosen set of linearly independent traceless, symmetric matrices. A very convenient choice of this basis is the following [76]:

$$E^{(0)}_{ij} = \sqrt{\tfrac{5}{16\pi}} \begin{pmatrix} -1 & 0 & 0 \\ 0 & -1 & 0 \\ 0 & 0 & 2 \end{pmatrix},$$

$$E^{(\pm 1)}_{ij} = \sqrt{\tfrac{15}{32\pi}} \begin{pmatrix} 0 & 0 & \mp 1 \\ 0 & 0 & -i \\ \mp 1 & -i & 0 \end{pmatrix}, \qquad E^{(\pm 2)}_{ij} = \sqrt{\tfrac{15}{32\pi}} \begin{pmatrix} 1 & \pm i & 0 \\ \pm i & -1 & 0 \\ 0 & 0 & 0 \end{pmatrix}. \quad (5.44)$$

This basis is particularly suitable to bring out the spin features of the tidal driving term, due to the following properties

$$E^{(m)}_{ij} n_i n_j = Y_{2m}(\theta, \phi) \quad (5.45)$$

where $\mathbf{n} = \mathbf{x}/|\mathbf{x}|$ is the radial unit vector and Y_{2m} denotes spherical harmonics. This is also an orthogonal basis, i.e., the E matrices satisfy the orthogonality relationships

$$E^{(m)*}_{ij} E^{(m')}_{ij} = \frac{15}{8\pi} \delta_{mm'}, \quad (5.46)$$

so that the driving force (5.41) can be represented as the linear combination

$$\boldsymbol{f}(\mathbf{x}, t) = \sum_{m=-2}^{m=2} \mathbf{f}^{(m)}(\mathbf{x})\, g^{(m)}(t), \quad (5.47)$$

with

$$\mathrm{f}^{(m)}_i(\mathbf{x}) = \rho E^{(m)}_{ij} x_j, \qquad g^{(m)}(t) = \frac{8\pi c^2}{15} E^{(m)*}_{ij} R_{0i0j}(t). \quad (5.48)$$

Using this representation, the calculation of the coefficients F_m introduced in the previous subsection becomes straightforward. First of all, let us remember that, as shown in chapter 2, the eigenvectors for a spherical body are labelled by four indices, namely P or T (indicating spheroidal or toroidal family) and the triad $\{n, l, m\}$, m being the degeneracy index. Thus, the eigenfrequencies can be labelled as ω^S_{nl}, with S standing for P or T, and the aformentioned coefficients should be labelled F^S_{nlm}, with the triad $\{S, n, l\}$ playing the part of the generic index K previously used. Thus, we have

$$F^S_{nlm}(\omega) = \frac{1}{M} \sum_{m'=-2}^{m'=2} G^{(m')}(\omega)(\mathbf{s}^S_{nlm}, \mathbf{f}^{(m')}), \quad (5.49)$$

where $G^{(m)}(\omega)$ stands for the Fourier transform of $g^{(m)}(t)$. On the other hand, the scalar products $(\mathbf{s}^S_{nlm}, \mathbf{f}^{(m')})$ are easily computed from the explicit expressions derived in chapter 3 for the sphere's eigenmodes in terms of vector spherical harmonics. Thus, for toroidal modes,

$$\begin{aligned}(\mathbf{s}^T_{nlm}, \mathbf{f}^{(m')}) &= \int_V T_{nl}(r)\mathbf{f}^{(m')} \cdot (\, i\,\mathbf{L}Y_{lm}\,)^* \rho\, dV \\ &= \int_V T_{nl}(r)\epsilon_{irs}E^{(m')}_{ij}x_j x_r \partial_s Y^*_{lm}(\theta,\phi)\,\rho\, dV.\end{aligned}$$

The above integral can be cast into the following sum of three terms

$$\begin{aligned}(\mathbf{s}^T_{nlm}, \mathbf{f}^{(m')}) &= \int_V \partial_s \left(T_{nl}\epsilon_{irs}E^{(m')}_{ij}x_j x_r Y^*_{lm}\right)\,\rho\, dV \\ &\quad - \int_V (\partial_r T_{nl}) n_s \epsilon_{irs}E^{(m')}_{ij}x_j x_r Y^*_{lm}\,\rho\, dV \\ &\quad - \int_V T_{nl}\epsilon_{irs}\left(E^{(m')}_{is}x_r + E^{(m')}_{ij}x_j\delta_{rs}\right) Y^*_{lm}\,\rho\, dV.\end{aligned}$$

The first integral of the above equality's right hand member can be transformed into a surface integration, in which a term of the form $\epsilon_{irs}x_r n_s$ appears. Therefore, due to the antisymmetry of ϵ_{irs}, this term vanishes identically. For the same reason, the second and third integrands are also identically zero, the matrices $E^{(m)}_{ij}$ and δ_{ij} being symmetric. Therefore,

$$F^T_{nlm}(\omega) = 0, \tag{5.50}$$

for *all* values of n, l, m, that is, *there is no power absorbed at toroidal eigenfrequencies*, and thus the absorption cross–section at such frequencies vanishes. As regards spheroidal modes, the scalar products $(\mathbf{s}^P_{nlm}, \mathbf{f}^{(m')})$ are given by

$$\begin{aligned}(\mathbf{s}^P_{nlm}, \mathbf{f}^{(m')}) &= \int_V \mathbf{f}^{(m')} \cdot [A_{nl}(r)\, Y_{lm}\,\mathbf{n} - B_{nl}(r)\, i\,\mathbf{n}\times\mathbf{L}Y_{lm}\,]^*\, dV \\ &= \int_V \rho\, r\left[A_{nl}Y^*_{lm}Y_{2m'} + B_{nl}E^{(m')}_{ij}x_j\partial_i Y^*_{lm}\right] dV,\end{aligned}$$

where use has been made of (5.45) and the identity $(\, i\,\mathbf{n}\times\mathbf{L}Y_{lm}\,)_i = -r\partial_i Y_{lm}$ (cf. equation (A.1)). Angular integration of the term involving A_{nl} is straightforward due to the ortoghonality of spherical harmonics, while the term proportional to B_{nl} can be tackled writing it as a divergence (which is transformed into a surface integral) plus additional terms, as we did in the toroidal case. The final result is then reducible to purely radial integrations:

$$(\mathbf{s}^T_{nlm}, \mathbf{f}^{(m')}) = \delta_{l2}\delta_{mm'}\, M\, a_n, \qquad a_n \equiv \frac{1}{M}\int_a^R r^3[A_{n2}(r) + 3\, B_{n2}(r)]\,\rho\, dr, \tag{5.51}$$

where a and R denote the inner and outer radii of the spherical detector at hand. Therefore combining the above equation with (5.49), we have

$$F^P_{nlm}(\omega) = \delta_{l2} a_n \, G^{(m)}(\omega). \tag{5.52}$$

An immediate and remarkable consequence of this equation is that, when acted upon by a tidal driving force, a viscoelastic solid absorbes power *only at quadrupolar, spheroidal frequencies*. It must also be stressed that this fact is independent of the actual time–dependence of the incoming wave, that is, Fourier components of the tidal driving force outside the spheroidal quadrupolar spectrum do not interact with a (visco)elastic body[4].

On the other hand, the explicit form of the radial functions $A_{n2}(r)$, $B_{n2}(r)$, given in x3.3.2 and x3.4.2, allows the integration defining the coefficient a_n, both for the solid and the hollow sphere. For the former case, its value has already been given in [76]:

$$\frac{a^s_n}{R} = -\frac{3\,C(n,2)}{4\pi}\left[\beta_3(k_{n2}R)\frac{j_2(q_{n2}R)}{q_{n2}R} - 3\frac{q_{n2}}{k_{n2}}\beta_1(q_{n2}R)\frac{j_2(k_{n2}R)}{k_{n2}R}\right], \tag{5.53}$$

where we use the superscript s to indicate the solid sphere's case, and we have dropped the superscript P denoting the spheroidal family in k^P_{n2} and q^P_{n2} to ease the notation (which is that of chapter 3). The expression for the hollow sphere's case is obtained along the same lines[5]

$$\frac{a^h_n}{R} = -\frac{3C(n,2)}{4\pi}\,[\Xi(R) - \Xi(a)], \tag{5.54}$$

where we have introduced the dimensionless function

$$\Xi(z) \equiv \frac{z^3}{R^3 - a^3}\left[\frac{1}{q_{n2}R}j_2(q_{n2}z) - \frac{3C_{tl}}{k_{n2}R}j_2(k_{n2}z) + \frac{D_{ll}}{q_{n2}R}y_2(q_{n2}z) - \frac{3D_{tl}}{k_{n2}R}y_2(k_{n2}z)\right]. \tag{5.55}$$

[4]This conclusion relies upon two assumptions, namely, the tidal structure of the driving force (which is common to all metric theories of the gravitational field [129, 33]) and the property of Riemann's tensor of being traceless (which is specific to General Relativity). Relaxing the latter assumption gives room to excitation of monolopolar as well as quadrupolar spheroidal modes [76, 12, 78].

[5]Equation (5.53) is obtained as follows. From the explicit form of A_{n2} and B_{n2}, and the recurrence relationship $3z^{-1}j_2(z) + j_2'(z) = j_1(z)$, we have

$$A_{n2}(r) + 3B_{n2}(r) = C(n,0)\left[\beta_3(k_{nl}R)j_1(q_{nl}r) - 3\frac{q_{nl}}{k_{nl}}\beta_1(q_{nl}R)j_1(k_{nl}r)\right],$$

and the integration over r is immediately performed with the aid of the identity

$$z^3 j_1(z) = -\frac{d}{dz}\left[z^3 j_2(z)\right].$$

Analogous relationships hold for spherical Bessel functions of the second kind, from which (5.54) ensues.

Let us turn our attention to the time–dependence of the driving force, given by $g^{(m)}(t)$. Vacuum Einstein's equations admit plane wave solutions in the linear regime, which in a transverse, traceless coordinate system take the form

$$h_{ij}^{TT}(\mathbf{x},t) = h_{ij}\sin[\Omega(t-\hat{\mathbf{k}}\cdot\mathbf{x}/c)], \tag{5.56}$$

where $\hat{\mathbf{k}}$ is the unit propagation vector, Ω will be taken close to a spheroidal eigenfrequency, and h_{ij} is a constant matrix. The gauge conditions (5.43) translate into

$$h_{ii} = 0, \qquad h_{ij}\hat{k}_j = 0, \tag{5.57}$$

and the Riemann's tensor at the detector's centre is given by

$$R_{0i0j}(t) = \frac{\Omega^2}{2c^2}h_{ij}\sin\Omega t. \tag{5.58}$$

Due to the ommidirectionality of the detector, we can choose without loosing generality $\hat{k}_i = \delta_{i3}$ (that is, a plane wave propagating along the z-axis). Then, the matrix h_{ij} can be written in terms of the well–known 'plus' and 'cross' gravity–wave amplitudes (cf. x1.3) as

$$h_{ij} = \begin{pmatrix} h_+ & h_\times & 0 \\ h_\times & -h_+ & 0 \\ 0 & 0 & 0 \end{pmatrix}, \tag{5.59}$$

and we immediately obtain[6]

$$g^{(0)}(t) = g^{(\pm1)}(t) = 0, \qquad g^{(\pm2)}(t) = \sqrt{\frac{2\pi}{15}}(h_+ \mp ih_\times)\Omega^2\sin\Omega t, \tag{5.60}$$

so that, in the notation of (5.38),

$$f_m = \sqrt{\frac{2\pi}{15}}\left[(\delta_{-2m}+\delta_{2m})h_+ + i(\delta_{-2m}-\delta_{2m})h_\times\right]\Omega^2 a_n. \tag{5.61}$$

Whence, by virtue of equation (5.40), the power absorbed by a spherical detector when excited by a gravitational plane wave of frequency Ω which is close to a spheroidal, quadrupolar eigenfrequency ω_{n2} is

$$< P >_{pw} = \frac{\pi\Omega^4}{15}(h_+^2+h_\times^2)Ma_n^2\,\frac{\omega_{n2}/Q_{n2}}{(\omega_{n2}-\Omega)^2+(\omega_{n2}/Q_{n2})^2}. \tag{5.62}$$

[6]The vanishing of $g^{(0)}$ and $g^{(\pm1)}$ can be seen as an outcome of the spin–two character of Riemann's tensor in General Relativity, according to the general classification procedure used in field theory[41].

5.3.3 Incident energy flux and absorption cross–section

Once the power absorbed by a viscoelastic body from an impinging gravitational wave has been calculated, the only magnitude left to compute the absorption cross–section is the amount of energy carried in by the incoming radiation. The energy–momentum tensor of a gravitational wave is given by [65, 66]

$$T^{GW}_{\mu\nu} = \frac{c^5}{32\pi G} < \partial_\mu(h^{\alpha\beta})\,\partial_\nu h_{\alpha\beta} >, \tag{5.63}$$

where $< \ldots >$ denotes space–time average over several wavelengths[7]. This quantity happens to be gauge invariant (as should be expected on physical grounds), and can thus be calculated using the metric potentials, h^{TT}_{ij}, as measured in a TT reference. For the plane wave (5.56), the above equation yields

$$T^{GW}_{\mu\nu} = \frac{c^5}{64\pi G}(h_{ij}h_{ij})\,k_\mu k_\nu, \tag{5.64}$$

with $k_\mu \equiv \frac{\Omega}{c}(1, \hat{\mathbf{k}})$ the wave four–vector. The energy flux (energy per unit time per unit area) sweeping the detector for an impinging plane wave propagating along the z–axis is then

$$\Phi = T^{GW}_{0i}\hat{k}_i = \frac{c^3}{32\pi G}\Omega^2(h^2_+ + h^2_\times). \tag{5.65}$$

We can now write down the final expression for the absorption cross–section of a spherical gravitational detector acted upon by a gravitational plane wave. We have, from equations (5.62) and (5.65),

$$\sigma^{pw}_{\rm abs}(\Omega) = \frac{< P >_{pw}}{\Phi} = \frac{16\pi^2}{15}\frac{GMv_t^2}{c^3}(k_{n2}a_n)^2\frac{2\omega_{n2}/Q_{n2}}{(\omega_n-\Omega)^2 + (\omega_{n2}/Q_{n2})^2}, \tag{5.66}$$

where the impinging wave's frequency Ω is assumed close to a quadrupolar frequency ω_{n2} belonging into the spheroidal spectrum, $v_t = \sqrt{\mu/\rho}$ is the velocity of transverse sound waves in the detector, and the coefficients a_n are given by equations (5.54) and (5.53).

For future reference, we quote here also the value of the integrated cross–section σ, given by

$$\sigma \equiv \frac{1}{2\pi}\int_{-\infty}^{\infty}\sigma_{\rm abs}(\Omega)d\Omega = \frac{16\pi^2}{15}\frac{GMv_t^2}{c^3}(k_{n2}a_n)^2. \tag{5.67}$$

[7] The average procedure (known as Brill–Hartle averaging[19, 4]) is fully described in the references given, and must be tackled with some care when the gravitational wave propagates in a curved background. When the underlying space–time is flat or static (which is the case of interest here), Brill–Hartle average reduces to a simple space–time average. This smearing endows the quantity between brackets in (5.63) with the property of gauge invariance, so that it cannot be made to vanish by a coordinate transformation, unlike the case of the energy pseudotensor.

which will be relevant when computing the sphere's sensitivity to short duration bursts.

We should note that, when deriving the above formulæ for absorption cross–sections, we have also disregarded the power re–radiated by the detector due to the oscillations induced by the impinging wave, which should be substracted from the power (or energy) gained by the solid as a result of the driving force acting on it. This is nevertheless an excellent approximation, for while the solid looses energy by internal friction at a rate $\omega/Q \approx 10^{-4}\,\mathrm{Hz}$, the emission of gravitational radiation causes the oscilator to loose energy at a rate $\Gamma_{\rm grav} \approx 10^{-35}\,\mathrm{Hz}$ (see below).

5.3.4 Alternative views

The rest of this chapter is devoted to an analysis of the performance of spherical viscoelastic bodies as detectors of gravitational waves, which is largely based upon the formulæ just derived for their absorption cross–section. But, before delving into this discussion, a few comments on equation (5.66) are in order. Analogous expressions describing the sensitivity of spherical detectors can be found elsewhere in the literature [127, 93, 5], although they are derived in a by no means analogous way. Thus, Weinberg [127] makes use of an optical theorem (which is a consequence of the conservation of energy), together with two supplementary assumptions: that the free vibrations of solid have the time dependence $\exp\{i\omega_n t - \omega_n t/Q\}$, and that the effect of a plane wave with frequency Ω close to ω_n is merely to excite the aforementioned free vibration[8]. Relying upon these hypotheses, it is possible to derive the following form for the absorption cross–section of a spherical detector acted upon by a plane wave

$$\sigma_{\rm abs}^{pw} = \frac{5\,\pi\,c^2\,\Gamma_{\rm grav}}{2\,\omega_n^2}\,\frac{2\,\omega_n/Q}{(\Omega-\omega_n)^2+(\omega_n/Q)^2}. \tag{5.68}$$

Here, $\Gamma_{\rm grav}$ stands for the decay rate of the oscillations owing to emission of gravitational radiation. The key idea behind the reasoning yielding (5.68) is to derive the absorption capabilities of the detector by studying the scattered wave at infinity, along essentially the same lines as done in electrodynamics or quantum mechanics. Such an approach circumvents the detailed analysis of the interaction between gravitational waves and viscoelastic solids, which has been the conducting line of the derivation presented here.

Let us show that equation (5.68) is identical to our expression for the absorption cross–section (5.66), a reassuring and remarkable conclusion. By definition, the rate of

[8] We have seen in chapter 4 that the first hypothesis is fully justified, while the second one holds only when ω_n happens to be a quadrupole spheroidal eigenfrequency.

energy loses due to emission of gravitational radiation is given by the ratio

$$\Gamma_{\rm grav} = \frac{P_{\rm rad}}{E_{\rm osc}}, \tag{5.69}$$

where $P_{\rm rad}$ is the radiated power and $E_{\rm osc}$ stands for the energy of the acoustic oscillations induced in the solid. Provided these vibrations are given by a normalized normal mode of vibration $\mathbf{s}(\mathbf{x},t)$ with frequency ω, the mechanical energy is immediately computed

$$E_{\rm osc} = \frac{1}{2}\int_V \left\{\rho\, s_i s_i^* + s_{i,j}\sigma_{ij}^*\right\}\, dV = M\,\omega^2. \tag{5.70}$$

On the other hand, the emitted power can be safely computed with the aid of the well–known quadrupolar approximation [73, 15], which gives

$$P_{\rm rad} = \frac{G}{5c^5}\frac{d^3Q_{ij}}{d\,t^3}\frac{d^3Q_{ij}^*}{d\,t^3}, \tag{5.71}$$

where Q_{ij} denotes the solid's quadrupolar moment, defined as

$$Q_{ij}(t) \equiv \int_V \rho(\mathbf{x},t)\, r^2 d_{ij}(\theta,\phi)\, dV, \qquad d_{ij}(\theta,\phi) \equiv n_i n_j - \frac{1}{3}\delta_{ij}, \tag{5.72}$$

and the symmetric, traceless tensor d_{ij} can be written in terms of the E–matrices (5.44) as

$$d_{ij}(\theta,\phi) = \frac{8\pi}{15}\sum_{m=-2}^{m=2} Y_{lm}^*(\theta,\phi)E_{ij}^{(m)}. \tag{5.73}$$

The homogenous, underformed sphere has vanishing quadrupolar moment, but, when it is vibrating in a normal mode, Q_{ij} varies as a result of two effects, namely, changes in the sphere's density and changes in the sphere's *shape* due to radial displacements. Thus, the variation of quadrupolar moment, δQ_{ij}, is, to first order in the deformation,

$$\begin{aligned}\delta Q_{ij} &= \int_0^{R+\delta R} r^4\, dr \int d\Omega\,(\rho+\delta\rho)\, d_{ij} \\ &\approx \int d\Omega\, d_{ij}\left\{\rho\delta R\, R^4 + \int_0^R r^4\delta\rho\, dr\right\},\end{aligned} \tag{5.74}$$

where $d\Omega \equiv \sin^2\theta\, d\theta d\phi$, and δR and $\delta\rho$ stand, respectively, for the normal displacement at the sphere's surface and the variation of density due to the deformation[9]. These variations are given by

$$\delta R = \mathbf{n}\cdot\mathbf{s}|_{r=R}, \qquad \delta\rho = -\rho\nabla\cdot\mathbf{s}. \tag{5.75}$$

[9]For the sake of clarity, we limit ourselves to the case of a solid sphere. The calculation for the hollow sphere can be tackled analogously.

From the discussion in previous chapters, we know that the above variations both vanish when **s** belongs into the toroidal family. On the other hand, when spheroidal modes are considered, it is immediately seen that δR and $\delta\rho$ are proportional to $Y_{lm}(\theta,\phi)$, with (l,m) the indices labelling the mode at hand. From equation (5.73) it is thus apparent that the angular integrations giving δQ_{ij} are zero unless $l=2$. Therefore, we again draw the conclusion that only quadrupole spheroidal modes have a non–vanishing absorption cross–section. While in our previous derivation this was shown as a result of the tidal form of interaction between gravitational waves and viscoelastic solids, here it follows from the fact that the sphere emits gravitational waves only at the aforementioned frequencies. For quadrupole spheroidal modes we have, in the notation of chapters 3 and 4,

$$\begin{aligned}\delta R &= e^{-i\omega_{n2}t}\, A_{n2}(R) Y_{2m}(\theta,\phi),\\ \delta\rho &= e^{-i\omega_{n2}t}\, C(n,2)\, \beta_3(k_{nl}R)\, q_{n2} j_2(q_{n2}r) Y_{2m}(\theta,\phi)\end{aligned}$$

whence, using (5.74) and the explicit expression for $A_{n2}(R)$, [10]

$$\delta Q_{ij} = e^{-i\omega_{n2}t}\frac{4\,C(n,2)}{5} MR\left[\beta_3(k_{n2}R)\frac{j_2(q_{n2}R)}{q_{n2}R} - 3\frac{q_{n2}}{k_{n2}}\frac{j_2(k_{n2}R)}{k_{n2}R}\right] E_{ij}^{(m)},$$

or, using the coefficient a_n^s defined in (5.53),

$$\delta Q_{ij} = -e^{-i\omega_{n2}t}\frac{16\pi}{15} M\, a_n^s\, E_{ij}^{(m)}. \tag{5.76}$$

Introducing this value for δQ_{ij} into equation (5.71) and making use of the orthogonality equations (5.46), we obtain

$$P_{\rm rad} = \frac{32\pi G}{75c^5}(M a_n^s)^2 \omega_n^6, \tag{5.77}$$

whence

$$\Gamma_{\rm grav} = \frac{32\pi G}{75c^5} M (a_h^s)^2 \omega_n^4, \tag{5.78}$$

and combining the above equation with (5.68) we recover the expression (5.66) previously derived for the absorption cross-section.

5.4 Review of cylindrical bar sensitivity

The use of resonant rigid bodies as gravitational wave antennæ has now a long history, starting in the pioneering works, both theoretical and experimental, of Weber in the early

[10] The r–integration appearing in (5.74) is immediately performed with the aid of the identity $[z^4 j_3(z)]' = z^4 j_2(z)$, and the expression given for δQ_{ij} is then obtained using the recurrence relationship $j_2'(z) + j_3(z) = 2j_2(z)/z$.

sixties (cf. chapter 1 and references therein). The problem of detection of gravitational waves by a resonant antenna has been thus clarified in its main aspects [96, 54, 122, 123], with special emphasis in the case of long cylindrical bodies. This is the only antenna geometry actually made operative by experimental reasearchers, and it is relatively simple to be tackled theoretically. By "long cylindrical body" we mean a cylindrical bar of length L very long compared to its diameter. The only modes of vibration to be considered for such a detector are the longitudinal ones, whose frequencies are

$$\omega_n = \frac{v_s}{L}\,\pi\,n, \qquad n = 1, 2, \ldots,$$

with v_s the velocity of sound in the bar. The effects of internal friction are taken into account by introducing a quality factor Q associated to each normal mode of vibration in the fashion of our equations for quasi–normal modes of viscoelastic solids. When the body is acted upon by a plane gravitational wave of frequency ω close to ω_n (for some fixed n), the equations of motion are easily solved, and the magnitudes entering the definition of absorption cross–section can be explicitly computed [108, 105], yielding, *for odd* n,

$$\sigma_{\rm abs}^{\rm cyl} = \frac{8}{n^2\pi}\frac{GMv_s^2}{c^3}\,\sin^4\theta\cos^2 2\psi\,\frac{2\omega_n/Q_n}{(\omega-\omega_n)^2+(\omega_n/Q_n)^2}, \tag{5.79}$$

where M is the mass of the bar, θ stands for the angle between the direction of propagation of the gravitational wave and the cylinder longitudinal axis, and ψ describes the wave's polarization. When the resonance frequency has even n, the absorption cross–section vanishes. The above equation shows that, due to the n^2 decay, the cylinder is only operative at its first longitudinal eigenfrequency[11], and that its sensitivity is highly dependent on the direction and polarization of the impinging wave (in fact, the bar is blind to waves propagating along its longitudinal axis or having the wrong polarization state). This strong directionality imposes a serious penalty in the performance of cylindrical bars as gravitational wave detectors, and six bars are needed at least to attain isotropic sky coverage at one frequency[25]. A more accurate measure of a single cylinder's sensitivity is therefore obtained after averaging of equation (5.79) over polarisations and incidence directions:

$$\sigma_{\rm abs,avg}^{\rm cyl} = \frac{32}{15\,n^2\pi}\frac{GMv_s^2}{c^3}\,\frac{2\omega_n/Q_n}{(\omega-\omega_n)^2+(\omega_n/Q_n)^2}. \tag{5.80}$$

[11] Rasband and Hier [104, 62] have computed the normal modes of vibration of a cylinder for a finite length–diameter ratio, and have shown that the absorption cross–section is also very small for non–longitudinal modes and the actual dimensions of operative cylindrical detectors.

When a broadband burst with spectrum energy density $F(\omega)$ hits the cylinder, the energy it absorbs can be computed as

$$E_a \approx F(\omega_1) \int \sigma_{\rm abs}(\omega) \frac{d\omega}{2\pi}, \tag{5.81}$$

where $\sigma_{\rm abs}(\omega)$ stands for the absorption cross–section for plane waves (5.79). After performing the integration we obtain

$$\frac{E_a}{F(\omega_1)} = \frac{8}{\pi} \frac{GMv_s^2}{c^3} \sin^4\theta \, \cos^2 2\psi. \tag{5.82}$$

The energy absorbed, E_a, must be compared to the variance of the noise energy fluctuations, E_n, of the detector. This energy noise can be written as the sum of two contributions, originating from two uncorrelated Gaussian processes: the thermal noise in the resonant mass and the electronic noise of the readout system [56, 103, 117]. We assume that a fraction β of the antenna energy is converted into electromagnetic energy by a noiseless transducer; the signal is then fed to an amplifier, assumed to have an additive noise at its output, whose spectral density is S_q; the amplifier also exerts a back action noise force onto the antenna mode with spectral density S_f. The energy fluctuations in the readout system can then be expressed by the noise temperature $T_n = k_B^{-1}(S_f \omega^2 S_q)^{1/2}$, where k_B is the Boltzmann constant. If antenna and transducer are correctly matched, it is found that

$$E_n = \frac{k_B T}{\beta Q} + k_B T_n, \tag{5.83}$$

where T is the thermodynamic temperature of the cylindrical bar. It is costumary to express the energy noise as the Boltzmann constant times a *detector noise temperature* $T_{\rm eff}$, writting $E_n = k_B T_{\rm eff}$. The detector's signal–to–noise ratio (SNR) is defined by

$$SNR \equiv \frac{E_a}{k_B T_{\rm eff}}, \tag{5.84}$$

and the sensitivity of the detector, i.e., the minimum detectable gravitational amplitude $h_{\rm min}$ (SNR=1), can be written as

$$h_{\rm min} = \sqrt{\frac{4}{\pi} \frac{G k_B T_{\rm eff}}{c^3 \sigma}}, \tag{5.85}$$

where σ stands for the integrated cross–section. The detector bandwith, defined by the width of the SNR resonance curve, is of order $\beta\omega_1$, much larger than the purely mechanical resonance linewidth ω_1/Q of the vibrational mode. Since the beginning of

the gravitational wave research, all efforts for improving the sensitivity have been focused on the reduction of the effective noise temperature $T_{\rm eff}$. The use of cryogenic technologies permitted to reduce $T_{\rm eff}$ by a factor of 10^4, from the tens of Kelvin to a few millikelvin. Further developements are in progress in order to improve the energy resolution up to one vibrational quantum ($\hbar\omega_1$ at 1 kHz corresponds to $T_{\rm eff} \approx 10^{-7}K$).

The above considerations can be applied to transducers attached to any resonant antenna. As we shall see, spherical detectors offer the possibility of further improvement in $h_{\rm min}$ via a higher value of σ.

5.5 Sensitivity of the solid sphere

We have seen in the previous sections that the solid sphere's sensitivity to gravitational waves is basically described by the dimensionless factor

$$\mathcal{F}_n(\lambda/\mu) = (a_n^s k_{2n})^2. \tag{5.86}$$

As the above notation explicitly displays, this is only a function of the quadrupole mode at hand (n), and the elastic properties of the sphere, via the ratio of its Lamé coefficients (or, if preferred, its Poisson ratio). Owing to the symmetry of the spherical shape, neither the angle of incidence of the incoming wave nor its polarization make any difference in the sphere's capabilities of detection, this being the first and more apparent advantage of such a detector over cylindrical bars (and also over interferometric detectors). For the sake of comparision, we shall rewrite the cylinder's cross–section (5.79) as

$$\sigma_{\rm abs}^{\rm cyl} = \mathcal{F}_n^{\rm cyl}(\lambda/\mu,\theta,\psi)\frac{16\pi^2}{15}\frac{GMv_t^2}{c^3}\frac{2\omega_n/Q}{(\omega-\omega_n)^2+(\omega_n/Q)^2} \tag{5.87}$$

where $\mathcal{F}_n^{\rm cyl}$ depends now also on the incoming wave's polarisation and angle of incidence. For an optimally oriented ($\theta = \pi/2$) and polarized ($\psi = 0$) wave, it attains the maximum value

$$\mathcal{F}_n^{\rm cyl,max}(\lambda/\mu) = \frac{1}{n^2}\frac{8}{\pi}\frac{15}{16\pi^2}\frac{v_s^2}{v_t^2} = \frac{1}{n^2}\frac{15}{2\pi^3}\frac{3\lambda+2\mu}{\lambda+\mu}, \tag{5.88}$$

where we recall that n must be odd. Averaging over polarizations and incidence angles reduces $\mathcal{F}_n^{\rm cyl}$ to the value

$$\mathcal{F}_n^{\rm cyl,avg}(\lambda/\mu) = \frac{1}{n^2}\frac{2}{\pi^3}\frac{3\lambda+2\mu}{\lambda+\mu}. \tag{5.89}$$

In the case of the sphere's $\mathcal{F}_n$ we cannot write down closed expressions like the one above, and numerical calculation is needed. Table 5.1 displays the results of such calculation

n	$\omega_{\rm sph}$	$\omega_{\rm cyl}$	$\mathcal{F}_n/\mathcal{F}_1$	$\mathcal{F}_n^{\rm cyl,max}/\mathcal{F}_1$	$\mathcal{F}_n^{\rm cyl,avg}/\mathcal{F}_1$
1	2.6501	2.6501	1.0000	0.8545	0.2279
2	5.0966	5.3001	0.3819	0	0
3	8.6255	7.9502	0.0369	0.0949	0.0253
4	10.9857	10.6002	0.0113	0	0
5	12.2916	13.2503	0.0390	0.0342	0.0091
6	15.3502	15.9003	0.0150	0	0
7	17.8584	18.5504	0.0027	0.0174	0.0046
8	18.6765	21.2005	0.0166	0	0
9	21.7505	23.8505	0.0078	0.0105	0.0028
10	24.4042	26.5006	0.0012	0	0
11	25.0053	29.1506	0.0092	0.0071	0.0016
12	28.0915	31.8007	0.0047	0	0
13	30.8383	34.4507	0.0007	0.0051	0.0013
14	31.3148	37.1008	0.0058	0	0
15	34.4096	39.7509	0.0032	0.0038	0.0010

Table 5.1. *First eigenfrequencies and normalised $\mathcal{F}$–factors for the absorption cross–section of a sphere and a cylinder with $\lambda/\mu = 2$. The normalization factor takes the value $\mathcal{F}_1 = 0.755$. The frequencies are expressed in units of v_t/R, and the cylinder's length is assumed to be $L = R/0.516$, so that both detectors are tunned to the same fundamental frequency.*

(which has been performed with the aid of the C-library *sphere* described in appendix C) for the common case $\lambda/\mu = 2$ (corresponding to a Poisson ratio equal to 1/3). We have chosen $R/L = 0.516$, which makes the first eigenfrequency of the sphere equal to that of the cylinder, although it must be remembered that the values of the $\mathcal{F}$–factors are independent of the dimensions of the detector. A glance at the given figures shows that, for equal masses, the solid sphere is slightly better that the cylinder for optimal orientation. If we consider the averaged sensitivity, the sphere's cross–section becomes a factor of 6 better for equal masses. We also find a remarkable sensitivity at the sphere's second mode, only about half the maximum for the fundamental mode. So a spherical antenna is potentially sensitive at *two* frequencies, this being a new advantage of this kind of antenna over cylindrical ones. For higher modes, both detectors show very low

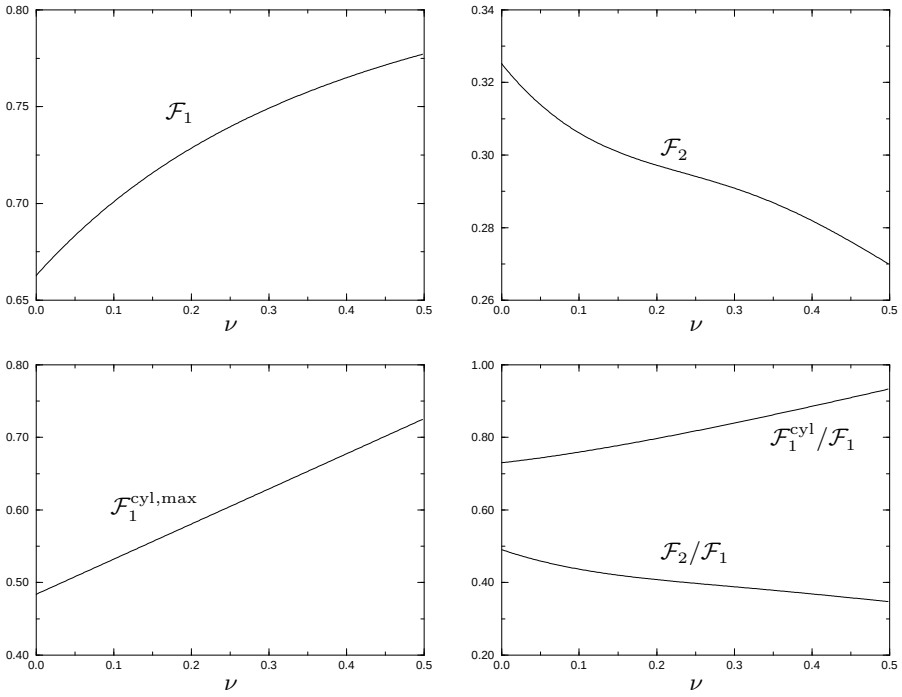

Figure 5.1. *Sensitivity parameters as a function of Poisson ratio ν. The last graphic displays the second sphere's and the first cylinder's modes over the first mode of the sphere, which has the better sensitivity at any ν.*

sensitivity[12].

Regarding the dependence of $\mathcal{F}_n$ on the material's elastic properties (which is again explicit in $\mathcal{F}_n^{\rm cyl}$), we have plotted in figure 5.1 these parameters as a function of Poisson ratio ν [13] for the first and second modes of the sphere and the cylinder's first one for optimal incidence and polarization. We observe that while $\mathcal{F}_1$ monotonically increases with ν, $\mathcal{F}_2$ presents just the opposite behaviour, so that the relative sensitivity $\mathcal{F}_2/\mathcal{F}_1$ shows little variability.

Let us turn again our attention to the use of spherical antennæ as multifrequency detectors. The resonant detectors being narrow–band, it has been suggested[69, 89, 88] the use of a so–called *xylophone* consisting of an array of solid spheres with decreasing

[12] In fact, it is easily shown using the asymptotic expansions given in chapter 2, that $\mathcal{F}_n$ falls also as n^{-2} for high frequencies.

[13] We remind the reader of the relationship between the Poisson ratio, which has been denoted σ in the previous chapters, and the Lamé coefficients—equation (3.32): $\lambda/\mu = 2\nu/(1-2\nu)$. Therefore, $\mathcal{F}_n^{\rm cyl,max} = (15/\pi^3)(1+\nu)$.

Frequency (Hz)	Diameter (m)	CS ratio
910	3.10	1
1747	1.61	2.72
2959	0.95	1.23
3750	0.75	0.92
4217	0.67	3.81
5217	0.54	2.84

Table 5.2. *A xylophone of spheres of Al 5056 whose fundamental frequencies are equal to the succesive harmonics of the larger one. In the third column, the ratio of the cross–section of the larger sphere to that of the smaller one at the corresponding frequency.*

sizes, so that their fundamental frequencies form an ascending series. A xylophone would constitute a wide–band detector, which is shown to present even better sensitivity than planned interferometric detectors (like, e.g. LIGO[1] or VIRGO[53]) in the range of frequencies over 750 kHz. Consider now a xylophone consisting of several solid spheres made of the same material, such that sphere 2 has its fundamental frequency at the *second* frequency of sphere 1 (which will be the larger one), sphere 3 has its fundamental frequency at the *third* frequency of sphere 1, and so on. In other words, we are considering a xylophone of spheres whose fundamental frequencies are equal to succesive harmonics of a larger one. Table 5.2 shows the frequencies and diameters of these spheres (which, for the sake of concreteness, have been supposed of the common alloy Al 5056). Also, in the third column, we display the ratio of the cross–section of the largest sphere at each frequency to that of the respective smaller ones in their first mode, as obtained from the data in table 5.1. These numbers indicate that, except for the nonsignificant exception of the fourth mode, *the single sphere has better sensitivity than the xylophone*. In order to graphically display the situation, we plot in figure 5.2 the *strain noise spectrum* $\tilde{h}(\omega)$, for

the first two spheres[14]. It has been calculated with the aid of the model for the readout arrangement proposed by Johnson and Merkowitz [69, 89]. The figures correspond to 3.1 and 1.6 m diameter spheres of Al 5056 operated at the quantum limited noise level. The just described "single detector xylophone" has the limitation that its frequencies are fixed and too widely spaced; still, xylophone proposals [69, 89] should benefit from the above considerations in the sense of reducing the number of required elements in them.

Actual spherical antennæ working on the same frequency range as operative cylindrical bars would have the further advantage of being far more massive, and, therefore, presenting an even better cross–section. Standard aluminium cylinders have typically length–diameter ratios around 5. If a sphere made of the same material has to be tunned to such a cylinder, it must have a diameter close to the bar's length, and, therefore, the mass of the sphere will be 14 times that of the cylinder. This is displayed in table 5.3, together with the integrated cross–section, for projected spheres and existing cylinders[15], always under the assumption of optimal orientation of the latter. We see that, at the first mode, the sphere has an energy sensitivity over 20 times that of a cylinder, and that the second mode absorbs over 15 times more energy than the fundamental mode of a cylinder.

As mentioned in x5.4, the amplitude sensitivity for broadband bursts of a resonant antenna is a function of the detector noise temperature, $T_{\rm eff}$, which describes the energy fluctuations in the readout system and the thermal noise in the resonant mass, and of the integrated cross–section, according to equation (5.85). For a detector working at the quantum limit[56]

$$T_Q = 4.8 \times 10^{-8}\, K \left(\frac{f}{1000\,\mathrm{Hz}}\right),$$

where f is the frequency of resonance, and using equation (5.85), we have that the

[14]The strain noise spectrum is defined as the square root of the fictitious strain noise spectral density needed to mimic the observed noise at the detector's noise. Thus, when the detector is swept by a plane wave of frequency ω and amplitude h_o, the signal-to-noise ratio is given by [117]

$$SNR = \frac{h_o}{\tilde{h}(\omega)} \frac{1}{\sqrt{2\Delta f}}$$

, where Δf stands for the inverse of the integration time, i.e., the bandwith at which the detector output is analyzed. We note that $\tilde{h}$ has dimensions of $\mathrm{Hz}^{-1/2}$.

[15]The quoted numbers correspond to the detectors Explorer at CERN Geneva[7], Nautilus at INFN Frascati[9], Auriga at INFN Legnaro[24], and Allegro at LSU[112].

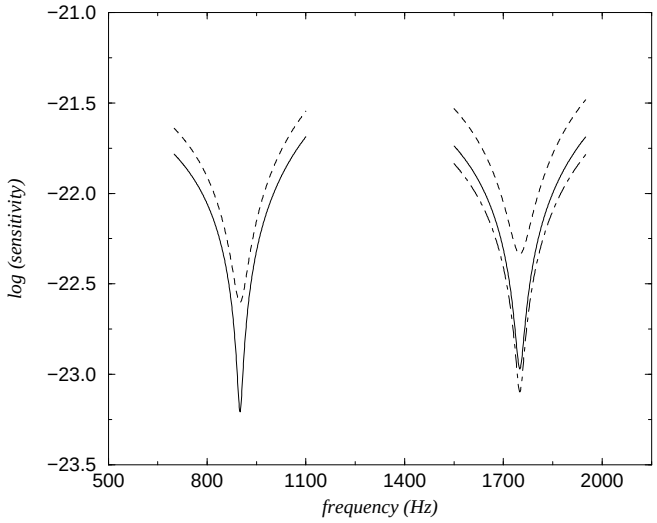

Figure 5.2. *Strain noise spectrum $\tilde{h}$ for various detectors at the quantum limit:* solid *lines for the lowest quadrupole mode of Al 5056 spherical detectors 3.1 and 1.6 m diameter, respectively;* dot–dashed *for the second quadrupole mode of the 3.1 m sphere, which is seen to present better sensitivity that the second sphere's first mode, and* dashed *lines for the equivalent cylindrical bar optimally oriented (3 m long and 0.6 m diameter).*

minimum burst amplitude detectable by a resonant antenna can be written as

$$h_{\min} = 2 \times 10^{-22} \left(\frac{T_{\rm eff}}{T_Q}\right)^{1/2} \left(\frac{100\,{\rm t}}{M}\right)^{1/2} \left(\frac{f}{1000\,{\rm Hz}}\right)^{1/2} \left(\frac{\mathcal{F}_n}{\mathcal{F}_1}\right)^{1/2} \tag{5.90}$$

This gives $h_{\min} \approx 10^{-21}$ for cylindrical bars optimally oriented at the fundamental mode and spheres at its second mode, while the amplitude sensitivity of the sphere's first mode would be of order 10^{-22}. This should be enough to see supernova events out to the Virgo cluster, with an estimated event rate of a few per week[111].

Cylinder	Sphere
$f_1 = 910$ Hz	$f_1 = 910$ Hz $f_2 = 1747$ Hz
$L = 3.0$ metres $D = 0.6$ metres	$\phi = 3.1$ metres
$M_c = 2.3$ tons	$M_s = 42$ tons
$\sigma_1 = 4.3\times10^{-21}$ cm^2 Hz	$\sigma_1 = 9.2\times10^{-20}$ cm^2 Hz $\sigma_2 = 3.5\times10^{-20}$ cm^2 Hz
(Optimal orientation)	(Omnidirectional)

Table 5.3. *Integrated cross–section for a typical Al 5056 cylinder in its first longitudinal mode with* optimal *orientation with respect to the incoming radiation, and for a sphere of the same material and fundamental frequency in its first two quadrupole modes. Antenna dimensions are also specified.*

5.6 Sensitivity of the hollow sphere

The key parameter describing the hollow sphere's sensitivity is the counterpart of $\mathcal{F}_n$, i.e.,

$$\mathcal{F}_n^h(\lambda/\mu, \eta) = (a_n^h k_{2n})^2, \tag{5.91}$$

where the coefficient a_n^h has the somewhat cumbersome form given in equation (5.54). We make explicit the existence of a new parameter: the ratio between the sphere's inner and outer radii, η. We have seen that, due to the fact that they share the same group of symmetries, the only difference between the formulæ describing the sensitivity of a solid and a hollow sphere is the numerical value of this coefficient. Resorting again to the C–library *sphere* (appendix C), we have plotted in figure 5.3 the value of $\mathcal{F}_n^h(2, \eta)$ for the first quadrupole modes and variable η.

We obtain, to begin with, that the better sensitivity is attained at the fundamental mode of a solid sphere (in fact, we use $\mathcal{F}_1^h(2, 0)$ to normalize the factors plotted), and that $\mathcal{F}_1^h$ decreases monotonically with increasing η. But, as the graphic shows, the second mode sensitivity presents just the opposite behaviour. Indeed, for $\eta \geq 0.38$ the detector's sensitivity is *larger* at the *second* quadrupole mode than it is at the first. It always keeps

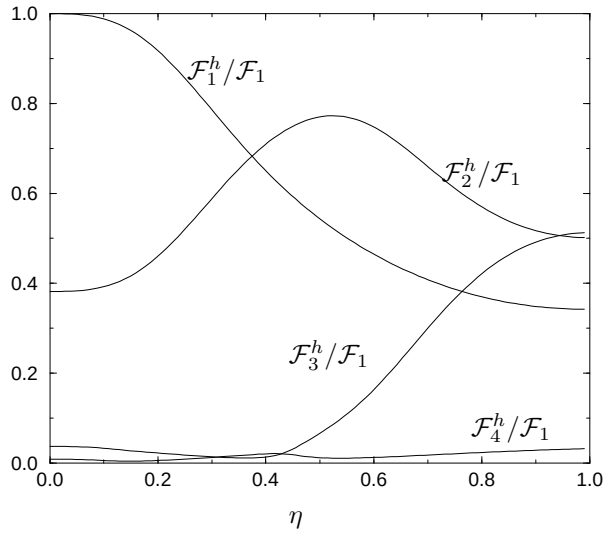

Figure 5.3. *Sensitivity parameter $\mathcal{F}_n^h$ for a hollow sphere with Poisson ratio $\nu = 1/3$, as a function of $\eta = a/R$. It has been normalized to $\mathcal{F}_1^h(2,0) = \mathcal{F}_1(2) = 0.775$.*

below that of a solid sphere, but, for a given mass, thinner shells have lower resonance frequencies, and this is a very desirable property for a gravitational wave detector. Let us be more specific at this point. If we vary η maintaining M constant (so that $\mathcal{F}_n^h$ gives us the absorption cross–section up to a multiplicative factor), we are bound to increase the outer radius of the hollow sphere. As we have seen in chapter 3, this implies a lower resonance frequency because the dimensionless eigenvalue kR depends only on η for a given material. To put it in other words, the resonance frequency of a hollow sphere of constant mass depends on η through the equation

$$\omega(\eta) = \frac{kR}{v_t}(1-\eta^3)^{1/3}, \tag{5.92}$$

where kR has the η–dependence described in x3.4.2. The situation is depicted in figure 5.4, where the first two eigenfrequencies of an Al 5056 hollow sphere of constant mass M=100 tons are plotted as a function of η.

Inspection of the data represented in figures 5.4 and 5.3 shows that a thin hollow

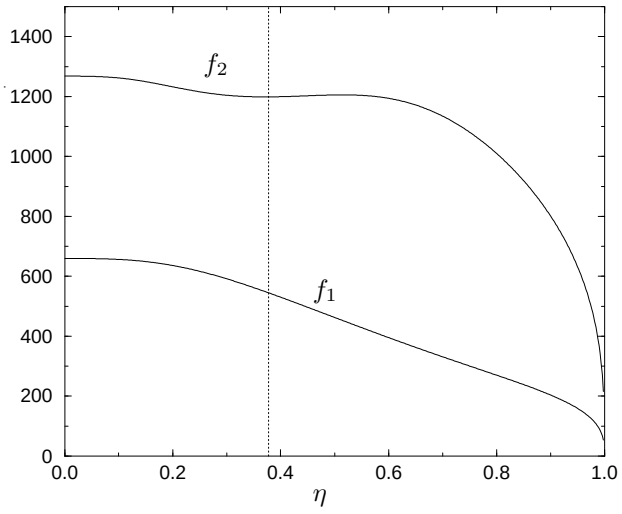

Figure 5.4. *First and second eigenfrequencies (in Hz) for an Al 5056 sphere of constant mass* $M = 100$ *tons. The dotted line indicates the value of equal sensitivity* $\eta \approx 0.38$.

sphere ($\eta \approx 0.9$) can operate as a gravitational wave antenna with high sensitivity at a (remarkably low) frequency of 200–300 Hz *and also* at a frequency around 1 kHz[16]. We have picked up three possible values for η in table 5.4, where we present a few characteristics of hollow Al 5056 spheres of a fixed mass of 100 tons: diameter, thickness, resonance frequencies and normalized sensitivities. These figures open the possibility of using omnidirectional detectors at frequencies in the range 200–800 Hz, typically covered by interferometric antennæ such as LIGO or VIRGO which do not offer isotropic sky coverage. Moreover, these thin shells can be used *simultaneously* in the frequency range over 1 kHz, usually covered by resonant antennæ. Thus, a xylophone of hollow spheres would offer the possibility of covering, with isotropic sensitivity, virtually any frequency over 200 Hz.

[16] Although the third quadrupole mode also presents very high sensitivity for the thin shell—see figure 5.3– $k_{32}R$ belongs to the group of divergent eigenvalues for $\eta \to 1$. This resonance frequency is thus too high ($\approx 10^4$ Hz) to be of interest.

Diam. (m)	Thick. (cm)	f_1 (Hz)	f_z (Hz)	$\mathcal{F}_1^h/\mathcal{F}_1$	$\mathcal{F}_2^h/\mathcal{F}_1$
5.06	60	300	1093	0.38	0.60
5.62	44	250	960	0.36	0.54
6.65	29	200	790	0.35	0.51

Table 5.4. *Three proposals of 100 ton, hollow sphere detectors operating at two frequencies. The sensitivities are normalized to that of a solid sphere of the same mass.*

Resorting again to equation (5.85) giving us the minimum burst amplitude detectable by a resonant detector, we obtain, taking into account that a burst presents a broadband spectrum and can be monitored at two frequencies—200 Hz and 760 Hz, say—, a burst sensitivity of

$$h_{\min} \approx 10^{-22} - 10^{-23}. \tag{5.93}$$

This sensitivity is perfectly comparable with that of projected long baseline interferometers [1, 53], which gives a very attractive possibility of making observations in coincidence between the two classes of gravitational wave antennas.

Chapter 6

Gravitational wave astronomy

We present in this chapter a brief review of some issues laying somewhat out the logic scope of our work, but which are nevertheless of great importance to the subject of gravitational wave detection.

The first section gives a sketchy discussion on the deconvolution problem for spherical detectors, which has been extensively treated in the literature (see [119] for the first approach to this subject, and new discussions in [89] and references therein). Properly chosen transducer configurations endow a single spherical detector with isotropic sky coverage. Nevertheless, one sphere gives us not *all* the properties of the incoming gravitational wave. The missing information can be obtained by means of a two–sphere observatory, which offers a number of additional capabilities. These are summarized in section 6.2. We end this final chapter with a brief catalogue of expected sources of gravitational waves reaching the Earth, and the way spherical detectors would *see* these signals.

6.1 Signal deconvolution

Once the vibration modes of the sphere are accurately known, we need a suitable readout system to monitor them. This is accomplished by means of a set of transducers attached to the sphere. And once we know that such and such modes have been excited and how much they have been excited, we want to use this information to trace back the causes of their being excited in that particular way or, as we shall say, to *deconvolve* the signal.

We now describe a deconvolution procedure on the basis of the observation of the vibrations of a spherical antenna. Let us consider the simpler situation, to begin with, in which we know the direction of incidence of the gravitational wave, e.g., because the source is known from astronomical observations or even a network of other gravitational wave antennæ. Direct measurement of the sphere vibration states will then produce a complete deconvolution of all the coefficients h_{ij} in a purely phenomenological way, i.e., *independently* of any underlying assumption about a particular theory of gravity. The data obtained in this way can then be compared to the predictions of the theory in order to either confirm or discard it.

If, more realistically, the direction of incidence is unknown, then knowledge of the sphere's vibrations is insufficient to decide on whether this or that theory is confirmed by the observations made. This is because each theory is characterised by a specific mode pattern, or by a *canonical* form of the matrix h_{ij}. Such canonical form shows in a coordinate frame suitably adapted to the propagation direction of the wave (e.g. the TT frame oriented along the wave's propagation direction, when General Relativity is the theory to be checked), and this frame will in general be *rotated* with respect to the laboratory frame. Not knowing the rotation angles is therefore a strong limitation to establish the validity of a given theory.

A possible way out consists in *assuming* a certain theory, for example General Relativity, and *then* determine the rotation angles on that hypothesis. This idea was suggested by Wagoner and Paik [119], and is as follows. As we have seen in x5.2 when solving the equations of motion for a viscoelastic solid under the action of a driving force $\boldsymbol{f}$, only those modes $\mathbf{s}_N$ with non–null scalar product $(\mathbf{s}_N, f)$ are excited as a result of such action. It has also been shown that, if a tidal force is assumed, only quadrupole spheroidal modes have a non–vanishing scalar product with $\boldsymbol{f}$; in fact, when the wave is travelling down the z–axis of the detector (that is, when the adapted TT and the laboratory frames have the same orientation, and thus the metric perturbation h_{ij} takes the form (5.59)), the field of displacements $\mathbf{s}(\mathbf{x}, t)$ is written as the sum of two terms

$$\mathbf{s}(\mathbf{x}, t) = f_{n22}(t)\mathbf{s}^P_{n22}(\mathbf{x}) + f_{n2-2}(t)\mathbf{s}^P_{n2-2}(\mathbf{x}), \tag{6.1}$$

where n labels the spheroidal eigenfrequency being monitored, and $f_{n2\pm2}(t)$ have Fourier transforms $F^P_{n2\pm2}(\omega)$ given by equation (5.52). Provided the transducers measure radial displacements only, we shall be interested in the normal projection of $\mathbf{s}$ at the sphere's surface:

$$a(\theta, \phi, t) \equiv \mathbf{s}(\mathbf{x}, t) \cdot \mathbf{n}|_{r=R} = a_{-2}(t)Y_{2-2}(\theta, \phi) + a_2(t)Y_{22}(\theta, \phi), \tag{6.2}$$

where the amplitudes $a_{\pm 2}(t)$ are obtained from (6.1) and the explicit expresion of $\mathbf{s}^P_{nlm}$,

$$a_{\pm 2}(t) = A_{2\pm 2}(R)\, f_{n2\pm 2}(t). \tag{6.3}$$

But, in general, the wave's propagation direction and polarization will be rotated by three Euler angles (α, β, ψ) with respect to the laboratory frame[1]. Thus, the matrix h_{ij} will look in this frame as a full 3x3 traceless matrix, and the field of normal displacements will be given by a linear combination of the form

$$a(\theta, \phi, t) = \sum_{m=-2}^{m=2} a_m(t)\, Y_{2m}(\theta, \phi). \tag{6.4}$$

The $a_m(t)$ amplitudes can then be monitored by measuring $a(\theta, \phi, t)$ at five positions on the sphere's surface and making linear combinations of the output[2].

Let $a_m(t)$ (m=−2,...,2) be the *measured* amplitudes of the five quadrupole modes of the sphere. If a helicity–2 gravitational wave is responsible for the excitation of these amplitudes —as would happen should General Relativity be true— then we are guaranteed that a rotation of the coordinate axes exists which reduces the set of measured modes to the canonical set $\hat{a}_m(t)$= ($\hat{a}_{-2}(t)$,0,0,0,$\hat{a}_2(t)$). If, following standard notation [43], we call $\mathcal{D}^{(2)}_{mm'}(\alpha, \beta, \psi)$ the coefficients of the rotation matrix, then we can write

$$\hat{a}_m(t) = \sum_{m'=-2}^{2} \mathcal{D}^{(2)}_{mm'}(\alpha, \beta, \psi)\, a_{m'}(t) \qquad , \qquad m = -2, \ldots, 2 \tag{6.5}$$

and so, by setting $\hat{a}_{-1}(t)$=$\hat{a}_0(t)$=$\hat{a}_1(t)$=0 we have a homogeneous system of three equations to determine, e.g., the angles (α-ψ,β). Once these are known, the other two equations define $\hat{a}_{-2}(t)$ and $\hat{a}_2(t)$ up to a polarisation angle, and these in turn determine $h_+(t)$ and $h_\times(t)$ [119].

[1]The first two of these angles define the source direction in the laboratory frame, while the third defines the wave's polarisation ellipse with respect to the line of nodes.

[2]If tangential transducers are available, it is possible to find five positions each one being a node for all the modes but one in a certain direction. For instance, fixing the laboratory frame, only the $(2, 0)$ mode has radial displacements at the north and south poles; only the $(2, \pm 1)$ modes have non–zero displacements along the local meridian at locations (θ=π/2,φ=0) and (θ=π/2,φ=π/2); and only the $(2, \pm 2)$ modes have non-zero displacements along the equator at locations (θ=π/2,φ=π/4) and (θ=π/2,φ=π). A complete set of transducers can then be constituted by one radial plus four tangential transducers. Each quadrupole mode is equipped with its transducer and its amplifier, forming an independent detection channel. The five independent channels act as five independent detectors with different orientations. Sets of radial transducers have been proposed by Forward [48], Johnson and Merkowitz [69], Michelson and Zou [91] and recently by J.A. Lobo and M.A. Serrano [79]

It must however be cautioned that the viability of this procedure *is strongly dependent on General Relativity being true*: we can use e.g. (6.5) to determine $(\alpha - \psi, \beta)$, but this will yield the *wrong* answer for the actual angles if General Relativity fails to be correct. Should that happen, we are expected to find algebraic incompatibilities as we proceed further to evaluate h_+ and $h_\times$; such incompatibilities are to be held as *vetoes* on the hypothesis that General Relativity is true.

In order to unambiguously assign a sudden excitation of the detector to a gravitational wave, several types of tests can be applied. The most general involves monitoring the detector also at frequencies other than the l=2 spheroidal modes. One can for instance look at toroidal modes, which, as we have rigorously proved, are never excited by gravitational waves. The lowest quadrupole toroidal frequency is so near the lowest spheroidal (less than 6%) that a veto based on the excitation of this mode is extremly efficient: any event which is seen at this frequency *cannot* be due to an impinging gravitational wave. This would require a 6% wideband transducer, or an extra number of transducers to monitor the sphere's vibration at the toroidal frequency.

We should note that the signal deconvolution of one resonant antenna will not provide all the information about the impinging gravitational wave that is needed to unambigously determine its physical properties. In the next subsection, we describe which are the parameters not obtanaible from deconvolution of a single antenna readout, and how *two* spherical detectors would constitute a complete gravitational wave observatory.

6.2 Two sphere observatory

There are certain details in the signal deconvolution process which cannot be sorted out with a *single* sphere. For example, if the direction of incidence is unknown and the procedure just described is applied, there is an unavoidable ambiguity: one cannot possibly tell a given source from a source in its antipode in the sky.

Also, nothing can be said with a single gravitational wave antenna about the propagation speed of gravitational waves.

An array of two spheres provides the necessary means to tackle these problems: if the two antennas are placed in strategic places on the earth's surface so that most potential sources are seen under sufficiently different angles, this would remove the direction ambiguity; on the other hand, if the signal arrival time can be determined accurately [25], then the time delay between detection at the two antennas, together with the in-

formation on the source position, enables the direct determination of the gravitational wave propagation speed. This measurement may be used as an additional check of our theoretical predictions.

A two sphere array will help solving these problems, but it will also produce redundant information. The latter can be used as a *local disturbance* veto on possible signals, thus improving detection probability. Let us be more specific on this point.

A coincidence experiment requires that all the detectors have signals above a given threshold at the same arrival time within a certain time window. An observatory of two spherical detectors has two advantages over other proposed observatories, such as the one constituted by six cylindrical bars [25] or that consisting of three laser interferometers [37, 38]. First, in the presence of a signal the two spheres will measure the same energy. Six bars or three interferometers will have different individual orientations, and therefore cannot use this criterion for vetoing possible signals, except at larger *SNR*'s [91]. And second, the application of the orientational deconvolution procedure to the two individual spheres provides the additional criterium of equal source direction.

These properties of a two sphere observatory provide criteria which can be used to drastically reduce the chances of accidental coincidences, thereby increasing the confidence level of detection. For instance, when accidental events from cosmic rays are considered (over 10^4 are expected per day in a several ton resonant detector operated at the quantum limit[3]), it is enough to place *just one* detector in an underground laboratory to reduce the number of random coincidences to about one in three years.

We can briefly summarise the essential additional features of a two-sphere observatory:

- it enables unambiguous determination of the source position in the sky,
- it enables determination of the gravitational wave propagation speed, and
- it provides powerful vetoes against local disturbances.

Obviously, an observatory with more than two antennæ (in the spirit of the xylophe previously discussed) will further reliability of detection. Also, a network of several antennæ can determine the direction of the wave, which will facilitate the procedure described in the previous section.

6.3 Likely sources: their detectability

A gravitational wave detector should be designed looking to the features of potential sources giving a reasonable rate of observable events. The subject of astrophysical sources of gravitational waves is widely discussed in the literature [117, 110, 77]. We give here a very brief survey of the "classical" sources of gravitational waves—namely, supernovæ coalescing binaries, pulsars and stochastic background—and the suitability of spherical resonant antennæ to detect them.

6.3.1 Supernovæ

It is generally accepted that the most intense gravitational waves reaching the Earth must come from dynamic deformed systems near their gravitational radius. Perhaps the most favourable source is a star collapsing across its gravitational radius in a highly non–spherical process.

Such kind of source involves a considerable mass compressed to very high density in a very short timescale. In particular, the usual assumption about *supernovæ* is that they produce a burst of radiation in a timescale characteristic of the bounce, of the order of 1 millisecond. This would result in a burst at about 1 kHz. It is possible, however, that considerable radiation from a collapse event emerges at a frequency below 1 kHz, if rotation is involved. In fact rotational effects slow down the collapse and thereby lower the dominant frequency at which the radiation comes out. The radiation amplitude produced in a galaxy a distance r from the Earth by a collapse in which an energy E is converted into gravitational radiation in a time τ, can be estimated as [111]

$$h = 1.4 \times 10^{-21} \left(\frac{E}{10^{-2}\, M_\odot c^2} \right)^{1/2} \left(\frac{\nu}{1\,\mathrm{kHz}} \right)^{-1} \left(\frac{\tau}{1\,\mathrm{ms}} \right)^{-1/2} \left(\frac{r}{15\,\mathrm{Mpc}} \right)^{-1} \tag{6.6}$$

Assuming that the duration of the burst is the timescale of the rebound, i.e., about one millisecond, and that the strongest possible burst would emit the entire binding energy of a neutron star, around $0.1 M_\odot c^2$, then this event would produce an amplitude of $3{\times}10^{-18}$ if it ocurred in our Galaxy, and $3{\times}10^{-21}$ if in the Virgo cluster. A more moderate and plausible event, converting to gravitational radiaton $0.01 M_\odot c^2$, would give an amplitude of about $8{\times}10^{-22}$ at 20 Mpc. The expected rate of these events is several per month.

We refer the reader to our previous discussion of the burst sensitivity of solid and hollow spheres in chapter 5, which show that they would be within the threshold set by the above theoretical estimates.

6.3.2 Coalescing binaries

Binary star systems, whose components are neutron stars or black holes, have received great theoretical attention because of the existence of of PSR 1913+16 [115] and because a large fraction of stars are in close binary systems. Since very recently, the almost exclusive interest in this source has been connected with projected large interferometers, for resonant detectors had insufficient sensitivity to detect them. Recent theoretical research by E. Coccia and V. Fafone [26] shows, however, that solid spherical antennæ monitored at their first two quadrupole modes can be advantageously used to detect signals from binary systems, and to determine some of the parameters characterizing it. Let us briefly review this issue, and show how hollow spherical detectors enter the picture.

The waveform of the gravitational radiation emitted by a binary system in the Newtonian regime—usually called *chirp*— is a sinusoidal with time–increasing frequency and amplitude. The time–dependent frequency of the gravitational wave is given by [94]

$$\omega_g(t) = 2\left(\frac{256}{5}\frac{G^{5/3}}{c^5}\right)^{-3/8} M_c^{-5/8}(t_c - t)^{-3/8}, \tag{6.7}$$

where t_c denotes the time at which coalescence is expected, and M_c is the *chirp mass*, which is related to the two stars' masses, m_1 and m_2 through the equation

$$M_c \equiv (m_1 m_2)^{3/5}(m_1 + m_2)^{-1/5}. \tag{6.8}$$

The 'plus' and 'cross' amplitudes of the chirp are then,

$$h_{+,\times}(t) = A_{+,\times}(t)\,\sin\int^t \omega_g(t')\,dt', \tag{6.9}$$

where

$$A_+(t) = \frac{1}{2r}\left(\frac{5G^5}{c^{11}}\right)^{1/4} M_c^{5/4}(t_c - t)^{-1/4}(1 + \cos^2\imath) \tag{6.10}$$

$$A_\times(t) = \frac{1}{r}\left(\frac{5G^5}{c^{11}}\right)^{1/4} M_c^{5/4}(t_c - t)^{-1/4}\cos\imath, \tag{6.11}$$

$\imath$ being the angle of inclination of the orbit to the line of sight and r the source distance. Figure 6.1 shows a typical chirp waveform.

The above formulæ are not valid when we are close to t_c. We must restric ourselves to frequencies over the five–cycle limit

$$\omega_{5c} = 2\pi(1525\text{Hz})(M_\odot/M_c), \tag{6.12}$$

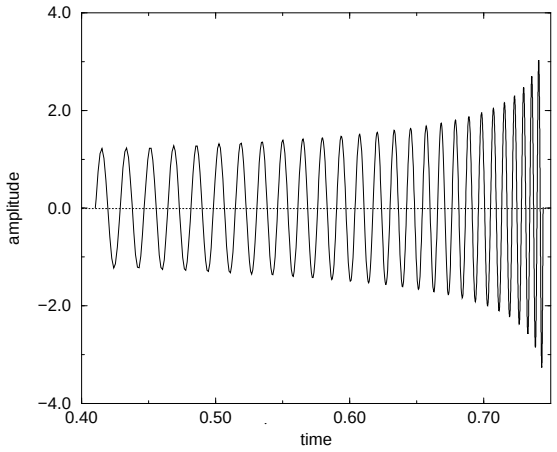

Figure 6.1. *Typical chirp waveform.*

which is the frequency of the inspiralling motion when there are less than five cycles remaining to coalescence.

The idea of Coccia and Fafone is as follows. If the chirp is detected at time t_1 with frequency ω_1 equal to the first quadrupole mode of the sphere, and at time t_2 with frequency ω_2 (second sphere quadrupole mode), then we can easily determine the chirp mass with the aid of equation (6.7). As this equation has a range of validity given by (6.12), the measurable chirp masses are limitted by the condition $\omega_{1,2} \geq \omega_{5c}$. For instance, a 3m–diameter solid sphere has an upper chirp mass limit around one solar mass. Hollow spherical detectors working at lower figures for $\omega_{1,2}$ would push upward this upper limit. Moreover, as the stars spend more time at lower frequencies, the signal monitoring would be easier for the hollow sphere than for the solid detector.

Work on this issue in collaboration with Coccia and Fafone is currently underway.

6.3.3 Pulsars

Rotating stars presenting deviations from symmetry around its rotation axis would emit gravitational radiation at several frequencies. Such deviations could arise from a number of causes. Namely, deformations owing to the star's past history—e.g., non–

symmetric collapse—; distortions induced by the star's internal magnetic field; or differential rotation inducing hydrodinamical waves in the star. However, at present there is no observational evidence in any known pulsar for sufficient non–axisymmetry to produce potentially measurable gravitational radiation.

Waves coming from pulsars would be emitted at twice their rotation frequency, so that resonant antennæ can only detect millisecond pulsars. This also limits the potentially observable sources. Again, the lower resonance frequency of a hollow sphere will widen the possibilities of detection, for the number of pulsars expected rotating at lower frequencies is larger.

6.3.4 Stochastic background

An isotropic stochastic background of gravitational radiation is expected to bath the Earth. It would be the outcome of a number of causes—binary stars in the low frequency range, Population III stars, relic gravitational waves from string cosmology and phase transitions associated with quantum cromodynamics interactions and with electroweak interactions [117].

As the waves are stochastic, a single detector cannot differentiate them from noise. Therefore, correlation between the outputs of at least two detectors is needed [90]. To get a good correlation, detectors should be as close together as possible, so that they respond to the same random gravitational waves at the same time. Therefore, the use of two different types of antenna to perform the correlation will help to avoid spurious local noise correlations between the detectors. Coincidence experiments between interferometers and resonant bars have recently recieved theoretical attention [8, 118, 20]. As two different detectors can only respond to the background in a correlated way if they look at signals in the same bandwith, the broadband interferometer data must be filtered to resonant antenna's bandwidth before performing a cross–correlation search for stochastic background.

The use of spherical detectors in coincidence experiments will ease the aligment of the two antennæ and offer the possibility of cross–correlation search at lower frequencies, where the interferometer's sensitivity is better.

Conclusions

We close this work with a brief summary of its main results, and a few words on possible extensions.

Its main objective has been the study of some fundamental aspects of the performance of spherical gravitational wave detectors from a theoretical point of view. In other words, we have addressed the question of how realistic rigid bodies interact with gravitational radiation, assuming the latter is correctly described by General Relativity.

A list of our main contributions follows.

- We have obtained the General Relativity equations of elasticity and viscoelasticity in a normal reference frame, and argued that these are the suitable ones to describe laboratory observations. We have also produced concrete equations of motion for a solid elastic or viscoelastic detector.

- We present a thorough, exact analysis of free sphere's normal modes of vibration, with unprecedentedly complete tables.

- The analysis has been extended to encompass general spherically symmetric bodies. Normal modes of vibration of hollow spheres are fully described for *arbitrary* ratios of inner to outer radii.

- We have addressed and solved the perturbative analysis of small deviations from spherical symmetry and/or homogeneity.

- The pertubative formulation is applied to the threefold splitting of the sphere's first quadrupole mode ensuing from its suspension in the terrestrial gravitational field.

- A thorough and complete analysis of the quasi—normal modes of vibration of Kelvin–Voigt, Maxwell and Standard Linear viscoelastic solids is given. Closed

expressions for their bandwith, as a function of frequency and the parameters entering the model, open the possibility of experimental fitting of the models. Possible generalizations are discussed.

- Analytical solutions to the equations of motion for a gravitational wave driven Kelvin–Voigt solid are given, allowing a clarification of the coupled modes.
- A direct computation of the absorption cross–section is given. Alternative views are reassessed and checked.
- The sensitivity of spherically symmetric detectors is studied, and new capabilities are found:
  - the solid sphere has high sensitivity also at is second quadrupole mode, giving the possibility of two—frequency resonant detectors;
  - applications of the above property to xylophone proposals are given;
  - the sensitivity of *hollow* spheres is investigated and good performance at two frequencies is also obtained for this new type of detectors;
  - thin hollow spheres are shown to be operative at very low frequencies, considered so far unreacheable by resonant detectors.
- Detectability of classical gravitational wave sources by spherical antennæ is reviewed, with special emphasis in their specific capabilities.

Appendix A

A.1 Normal modes: calculations

In this section we give the details of the computations yielding the transverse and longitudinal components of normal modes of vibration given in equations (3.17), (3.18) and (3.19), as well as the action of the operator $\boldsymbol{b}$ on these components (equations (3.23)). Our aim is to present a derivation as compact as possible of the expressions involved.

A.1.1 Computation of $\mathbf{s}_l$, $\mathbf{s}_t$ and $\mathbf{s}_{t'}$

When using a spherical coordinate system, it will be very helpful the following splitting of the nabla operator:

$$\nabla = \mathbf{n}\,\frac{\partial}{\partial r} - \frac{i}{r}\,\mathbf{n}\times\mathbf{L} \tag{A.1}$$

(where the vector $\mathbf{n} \equiv \boldsymbol{x}/r$ depends only on θ and ϕ), as well as the property of the "angular momentum" differential operator $\mathbf{L} = -ir\mathbf{n}\times\nabla$ of having no component along ∂_r, so that

$$\mathbf{L}G(r) = 0 \qquad\qquad (G(r) \text{ arbitrary}). \tag{A.2}$$

The above properties make the derivation of equations (3.17) and (3.19) straightforward:

$$\begin{aligned} \mathbf{s}_l &= \nabla\phi_{lm} = \left(\mathbf{n}\,\frac{\partial}{\partial r} - \frac{i}{r}\,\mathbf{n}\times\mathbf{L}\right) j_l(qr)Y_{lm}(\theta,\phi) \\ &= \frac{dj_l(qr)}{d\,r}\,Y_{lm}\,\mathbf{n} - \frac{j_l(qr)}{r}\,i\,\mathbf{n}\times\mathbf{L}Y_{lm}\,. \end{aligned} \tag{A.3}$$

$$\mathbf{s}_{t'} = i\mathbf{L}\varphi_{lm} = i\mathbf{L}j_l(kr)Y_{lm}(\theta,\phi) = j_l(kr)\,i\,\mathbf{L}Y_{lm}\,. \tag{A.4}$$

As regards $\mathbf{s}_t$, we have, from its definition,

$$\mathbf{s}_t = i\nabla \times \mathbf{L}\varphi_{lm} = \nabla \times (r\mathbf{n} \times \nabla\varphi_{lm}).$$

Using now the vector identity

$$\nabla \times (\mathbf{A} \times \mathbf{B}) = (\mathbf{B} \cdot \nabla)\mathbf{A} - (\nabla \cdot \mathbf{A})\mathbf{B} - (\mathbf{A} \cdot \nabla)\mathbf{B} + (\nabla \cdot \mathbf{B})\mathbf{A}, \tag{A.5}$$

we obtain

$$\mathbf{s}_t = -\left(2\nabla + r\partial_r\nabla + rk^2\mathbf{n}\right)\varphi_{lm},$$

where use have been made of the fact the φ satisfies a Helmholtz equation. Introducing the split (A.1) in the above equation, we are left with

$$\mathbf{s}_t = -\,Y_{lm}\,\mathbf{n}\left(2\frac{d}{dr} + r\frac{d^2}{d\,r^2} + rk^2\right)j_l(kr) + \,i\,\mathbf{n}\times\mathbf{L}Y_{lm}\,\left(2 + r\frac{d}{dr}\right)r^{-1}j_l(kr).$$

Using finally the differential equation satisfied by spherical Bessel functions

$$z^2\frac{d^2 j_l(z)}{d\,z^2} + 2z\frac{dj_l(z)}{d\,z} + [z^2 - l(l+1)]j_l(z) = 0, \tag{A.6}$$

we obtain the expression quoted in the text for $\mathbf{s}_t$:

$$\mathbf{s}_t = -l(l+1)\frac{j_l(kr)}{r}\,Y_{lm}\,\mathbf{n} + \left(\frac{j_l(kr)}{r} + \frac{dj_l(kr)}{d\,r}\right)\,i\,\mathbf{n}\times\mathbf{L}Y_{lm}\,. \tag{A.7}$$

A.1.2 Calculation of the boundary conditions

The action of the operator $\boldsymbol{b}$ on $\mathbf{s}_l$ is computed immediately. As the longitudinal solution is irrotational, we have, from the definition of $\boldsymbol{b}$,

$$\boldsymbol{b}[\mathbf{s}_l] = \lambda(\nabla \cdot \mathbf{s}_l)\,\mathbf{n} + 2\mu\,\partial_r\mathbf{s}_l. \tag{A.8}$$

The first of equations (3.23) is obtained simply using $\nabla \cdot \mathbf{s}_l = \nabla^2\phi_{lm} = -k^2\phi_{lm}$ in the above expression.

On the other hand, as $s_{t'}$ is divergence free,

$$\boldsymbol{b}[s_{t'}] = 2\mu\,\partial_r\mathbf{s}_{t'} + \mathbf{n} \times (\nabla \times \mathbf{s}_{t'}). \tag{A.9}$$

But, by definition, $\nabla \times \mathbf{s}_{t'} = \mathbf{s}_t$, so that, using (A.7), we get the desired expression:

$$\begin{aligned}\boldsymbol{b}[\mathbf{s}_{t'}] &= 2\mu\frac{dj_l(kr)}{d\,r}\,i\,\mathbf{L}Y_{lm} + \left[\frac{j_l(kr)}{r} + \mu\frac{dj_l(kr)}{d\,r}\right]\,\mathbf{n}\times(\,i\,\mathbf{n}\times\mathbf{L}Y_{lm}\,)\\ &= -\mu\,r\,\frac{d}{dr}\frac{j_l(kr)}{r}\,i\,\mathbf{L}Y_{lm}\,.\end{aligned} \tag{A.10}$$

As regards $\boldsymbol{b}[\mathbf{s}_t]$, we have an expression analogous to (A.9), in which appears a trivial term $(\partial_r \mathbf{s}_t)$ and the more involved one $\mathbf{n} \times (\nabla \times \mathbf{s}_t)$. From equation (A.7) and standard properties of the rotational, we obtain

$$\begin{aligned} \nabla \times \mathbf{s}_t &= -l(l+1)[\nabla(\frac{j_l(kr)}{r} Y_{lm})] \times \mathbf{n} + \left[\frac{j_l(kr)}{r} + \frac{dj(kr)}{d\,r}\right] \nabla \times (\, i\,\mathbf{n} \times \mathbf{L} Y_{lm}\,) \\ &\quad + \frac{d}{dr}\left[\frac{j_l(kr)}{r} + \frac{dj_l(kr)}{d\,r}\right] \mathbf{n} \times (\, i\,\mathbf{n} \times \mathbf{L} Y_{lm}\,). \end{aligned} \tag{A.11}$$

The first term of the RHM of the above equation can be computed using (A.1), resulting the expression

$$[\nabla(r^{-1} j_l(kr) Y_{lm})] \times \mathbf{n} = -r^{-2} j_l(kr)\, i\, \mathbf{L} Y_{lm}\,,$$

while the second term in the RHM of (A.11) is calculated applying the identity (A.5):

$$\nabla \times (\, i\,\mathbf{n} \times \mathbf{L} Y_{lm}\,) = (\, i\,\mathbf{L} Y_{lm}\, \cdot \nabla)\mathbf{n} - (\nabla \cdot \mathbf{n})\, i\, \mathbf{L} Y_{lm}\, = -r^{-1}\, i\, \mathbf{L} Y_{lm}\,,$$

where use has been made of the fact that $i\,\mathbf{L} Y_{lm}$ does not depend on r, is irrotational, and orthogonal to $\mathbf{n}$. Thus, the final expression for the rotational of $\mathbf{s}_t$ is

$$\nabla \times \mathbf{s}_t = \left[(l+2)(l-1)\frac{j_l(kr)}{r^2} - 2\frac{d}{dr}\frac{j_l(kR)}{r} - \frac{d^2 j_l(kr)}{d\,r^2}\right] i\, \mathbf{L} Y_{lm}\,, \tag{A.12}$$

and from this equation and the explicit form of $\mathbf{s}_t$ we obtain the desired result:

$$\begin{aligned} \boldsymbol{b}[\mathbf{s}_t] &= 2\mu\, \partial_r \mathbf{s}_t + \mu\, \mathbf{n} \times (\nabla \times \mathbf{s}_t) \\ &= -2\mu\, l(l+1)\frac{d}{dr}\frac{j_l(kr)}{r}\, Y_{lm}\, \mathbf{n} + \mu \left[\frac{d^2}{dr^2} + (l+2)(l-1)\frac{1}{r^2}\right] j_l(kr)\, i\, \mathbf{n} \times \mathbf{L} Y_{lm}\,. \end{aligned} \tag{A.13}$$

Appendix B

B.1 Explicit form of $\chi_{1,2}(r)$

The explicit form of the phase functions appearing in spheroidal quasi–normal modes of vibration for the Kelvin–Voigt solid is obtained from the expression of their spatial part. This can be readily written down taking the corresponding equations for the normal modes and replacing the constants k and q by their viscoelastic counterparts $\mathcal{K}$ and $\mathcal{Q}$, as discussed in chapter 4. Thus, referring to equation (3.29), the spatial part of spheroidal quasi–normal modes can be written as

$$\mathbf{s}^{P}_{nlm}(r,\theta,\phi) = \mathcal{A}_{nl}(r)Y_{lm}(\theta,\phi)\mathbf{n} - \mathcal{B}_{nl}(r)\, i\, \mathbf{n}\times\mathbf{L}Y_{lm}\,(\theta,\phi), \tag{B.1}$$

where the radial functions $\mathcal{A}_{nl}$ and $\mathcal{B}_{nl}$ are obtained from equations (3.30) and (3.31) upon the aformentioned substitutions, yielding:

$$\mathcal{A}_{nl}(r) = C(n,l)\left[\beta_3(\mathcal{K}R)\frac{d\, j_l(\mathcal{Q}r)}{d\,(\mathcal{Q}r)} - l(l+1)\frac{\mathcal{Q}}{\mathcal{K}}\beta_1(\mathcal{Q}R)\frac{j_l(\mathcal{K}r)}{\mathcal{K}r}\right] \tag{B.2}$$

$$\mathcal{B}_{nl}(r) = C(n,l)\left[\beta_3(\mathcal{K}R)\frac{j_l(\mathcal{Q}r)}{\mathcal{Q}r} - \frac{\mathcal{Q}}{\mathcal{K}}\frac{\beta_1(\mathcal{Q}R)}{\mathcal{K}r}\frac{d}{dr}\{r\, j_l(\mathcal{K}r)\}\right]. \tag{B.3}$$

Making use of the approximated expressions (4.29) for $\mathcal{K}$ and $\mathcal{Q}$, the first order expansion of the above radial functions shall be

$$\mathcal{A}_{nl}(r) = A_{nl}(r) - i\epsilon A^{(1)}_{nl}(r) \qquad \mathcal{B}_{nl}(r) = B_{nl}(r) - i\epsilon B^{(1)}_{nl}(r), \tag{B.4}$$

where $A_{nl}(r)$ and $B_{nl}(r)$ are the radial functions corresponding to the elastic solid, while the corrections $A^{(1)}_{nl}(r)$ and $B^{(1)}_{nl}(r)$ are given by the following expressions

$$A^{(1)}_{nl}(r) = i\left(\frac{\partial\mathcal{A}_{nl}}{\partial\,\gamma}\right)_{\gamma=w_{nl}}\gamma_1 \qquad B^{(1)}_{nl}(r) = i\left(\frac{\partial\mathcal{B}_{nl}}{\partial\,\gamma}\right)_{\gamma=w_{nl}}\gamma_1. \tag{B.5}$$

When applying the chain rule to the derivatives with respect of γ in the above equation, the following derivatives will come into play

$$\frac{\partial \mathcal{K}}{\partial \gamma} = k_1 + O(\epsilon) \qquad\qquad \frac{\partial \mathcal{Q}}{\partial \gamma} = q_1 + O(\epsilon), \tag{B.6}$$

which, as is immediately inferred from the fact that γ_1 is real (cf. (4.36)), are purely imaginary magnitudes. As a result of this fact, the functions defined by equations (B.5) *are real*, so that rewriting the radial functions (B.4) as

$$\mathcal{A}_{nl}(r) = |\mathcal{A}_{nl}(r)|e^{i\chi_1(r)} \qquad\qquad \mathcal{A}_{nl}(r) = |\mathcal{A}_{nl}(r)|e^{i\chi_2(r)} \tag{B.7}$$

it is readily obtained

$$|\mathcal{A}_{nl}| = A_{nl}(r) \qquad\qquad |\mathcal{B}_{nl}| = B_{nl}(r) \tag{B.8}$$

$$\chi_1(r) = \arctan\left(-\epsilon\frac{A^{(1)}_{nl}(r)}{A_{nl}(r)}\right) \approx -\epsilon\frac{A^{(1)}_{nl}(r)}{A_{nl}(r)} \tag{B.9}$$

$$\chi_2(r) = \arctan\left(-\epsilon\frac{B^{(1)}_{nl}(r)}{B_{nl}(r)}\right) \approx -\epsilon\frac{B^{(1)}_{nl}(r)}{B_{nl}(r)}. \tag{B.10}$$

For the sake of completeness, it must be remembered that the equations given so far are not valid for the case of monopolar modes. When $l = 0$, the spatial part of quasi–normal modes is obtained from equation (3.33), which gives the spatial part of monopolar normal modes of vibration, after making the requisite substitutions:

$$\mathbf{s}^P_{KV}(r) = \mathcal{A}_{n0}(r)\mathbf{n}, \tag{B.11}$$

where, now,

$$\mathcal{A}_{n0}(r) = C(n,0)\frac{dj_0(\mathcal{Q}r)}{d\left(\mathcal{Q}r\right)} = C(n,0)\left(\frac{dj_0(q_{n0}r)}{d\left(q_{n0}r\right)} + q_1 R\frac{d^2 j_0(q_{n0}r)}{d\left(q_{n0}r\right)^2}\epsilon\right) = A_{n0}(r)e^{i\chi(r)}, \tag{B.12}$$

and, making use of the form of q_1 for monopolar modes given by equation (4.38),

$$\chi(r) = \arctan(j_0''(q_{n0}r)/j_0'(q_{n0})\epsilon) \approx \epsilon\, j_0''(q_{n0}r)/j_0'(q_{n0}) \tag{B.13}$$

where a prime denotes derivative with respect to the argument.

As discussed in the main text, the expressions derived in this appendix happen to be valid *mutatis mutandis* to all the viscoelastic models presented.

B.2 General solution to the Kelvin–Voigt model

As shown in the main text of x5.2.2, the general solution to the equations of motion of a driven Kelvin–Voigt solid can be written as a series in the parameter α (cf. (5.22)) whose coefficients are solutions of the non–homogeneous elastic problem

$$\mathbb{L}\boldsymbol{S}^{(n)} + k^2\boldsymbol{S}^{(n)} = -i\mathbb{L}'\boldsymbol{S}^{(n-1)}, \quad \mathbb{T}\boldsymbol{S}^{(n)}|_S = -i\mathbb{T}'\boldsymbol{S}^{(n-1)}, \tag{B.14}$$

where $k^2 \equiv \rho\omega^2\mu^{-1}$ and $n > 0$, while the zero–order term is written as a linear superposition of the form

$$\boldsymbol{S}^{(0)} = \sum_N \boldsymbol{S}_N^{(0)}\mathbf{s}_N(\mathbf{x}), \qquad \boldsymbol{S}_N^{(0)} = \frac{F_N(\omega)}{\omega_N^2 - \omega^2},$$

where $F_N(\omega)$ is the component of the driving force along $\mathbf{s}_N$, cf. (5.10).

Let us have a look at the driving terms appearing in equations (B.14) for $n = 1$. Due to the fact that $\mathbf{s}_N$ is an eigenvector of $\mathbb{L}$ and that

$$(\mathbb{L} - \mathbb{L}')_{ij} = (h - h')\partial_i\partial_j, \qquad (\mathbb{T} - \mathbb{T}')_{ij} = (h - h')n_i\partial_j, \tag{B.15}$$

the following relationships ensue:

$$\mathbb{L}'\boldsymbol{S}^{(0)} = \sum_N \boldsymbol{S}_N^{(0)}\left[(h' - h)\nabla\left(\nabla\cdot\mathbf{s}_N\right) - k_N^2\mathbf{s}_N\right],$$

$$\mathbb{T}'\boldsymbol{S}^{(0)} = (h' - h)\sum_N \boldsymbol{S}_N^{(0)}(\nabla\cdot\mathbf{s}_N)\mathbf{n}.$$

Due to the linearity of the problem (B.14), it is clear that in order to find $\boldsymbol{S}^{(1)}$ we must simply solve the following equations

$$\mathbb{L}\boldsymbol{A}_N + k^2\boldsymbol{A}_N = \nabla f_N(\mathbf{x}) - ik_N^2\mathbf{s}_N, \qquad \mathbb{T}\boldsymbol{A}_N|_S = -f_N(S)\mathbf{n}, \tag{B.16}$$

where $f_N(\mathbf{x}) = (h' - h)\nabla\cdot\mathbf{s}_N(\mathbf{x})$, the desired solution for $n = 1$ being then the linear superposition

$$\boldsymbol{S}^{(1)} = -i\sum_N \boldsymbol{S}_N^{(0)}\boldsymbol{A}_N. \tag{B.17}$$

Before using the Green's operator $\mathbb{G}$ for solving equations (B.16), we must get rid of the inhomogeneous boundary conditions thereof. Assuming spherical symmetry, this can be done writting $\boldsymbol{A}_N$ as the sum

$$\boldsymbol{A}_N = \boldsymbol{A}'_N + \frac{f_N(S)}{f'_N(S)}\mathbf{s}'_N(\mathbf{x}), \tag{B.18}$$

where $\mathbf{s}'_N$ denotes an eigenfunction of $\mathbb{L}'$ satisfying $\mathbb{T}\mathbf{s}'_N|_S = 0$, and f'_N stands for $(h'-h)$ times its divergence. It is then straightforward to show, using the second (B.15)[3], that when applying the operator $\mathbb{T}$ to both sides of equation (B.18) we obtain

$$\mathbb{T}\boldsymbol{A}_N|_S = \mathbb{T}\boldsymbol{A}'_N|_S - f_N(S)\mathbf{n} \tag{B.19}$$

Thus, introducing the decomposition (B.18) into equations (B.16) we obtain the following equations for $\boldsymbol{A}'_N$:

$$\mathbb{L}\boldsymbol{A}'_N + k^2\boldsymbol{A}'_N = -\boldsymbol{B}_N, \qquad \boldsymbol{A}'_N \in \mathcal{H}_h, \tag{B.20}$$

where we have introduced the vector field $\boldsymbol{B}_N$, defined as

$$\boldsymbol{B}_N(\mathbf{x},\omega) = -\nabla f_N(\mathbf{x}) + k_N^2\mathbf{s}_N(\mathbf{x}) + \frac{f_N(S)}{f'_N(S)}\left(\mathbb{L}\mathbf{s}'_N(\mathbf{x}) + k^2\mathbf{s}'_N(\mathbf{x})\right).$$

As have been shown in x5.2.1, the solution to (B.20) can be written as

$$\boldsymbol{A}'_N(\mathbf{x},\omega) = \sum_L \frac{B_L^N(\omega)}{\omega_L^2-\omega^2}\mathbf{s}_L(\mathbf{x}), \qquad B_L^N(\omega) = \frac{\mu}{\rho M}(\mathbf{s}_L, \boldsymbol{B}_N).$$

Using equation (3.87) and the definition of $\boldsymbol{B}_N$, we can rewrite the coefficients B_L^N in the form

$$B_L^N(\omega) = C_L^N + (\omega_L^2-\omega^2)\,D_L^N,$$

where we have introduced the constant, ω-independent coefficients

$$C_L^N = \delta_L^N\omega_N^2 + \frac{\mu}{M}(h'-h)\int_V (\nabla\cdot\mathbf{s}_L^*)(\nabla\cdot\mathbf{s}_N),, \qquad D_L^N = -\frac{f_N(S)}{f'_N(S)}\frac{1}{M}\int_V \rho\, d\mathbf{x}\; \mathbf{s}_L^*(\mathbf{x})\cdot\mathbf{s}'_N(x).$$

Therefore, the final form of $\boldsymbol{A}_N$ is

$$\boldsymbol{A}_N(\mathbf{x},\omega) = \frac{f_N(S)}{f'_N(S)}\mathbf{s}'_N(\mathbf{x}) + \sum_L\left(\frac{C_L^N}{\omega_L^2-\omega^2} + D_L^N\right)\mathbf{s}_L(\mathbf{x}),$$

and, according to (B.18), we finally obtain the rather involved equality:

$$\begin{aligned}\boldsymbol{S}^{(1)}(\mathbf{x},\omega) = \quad & -i\sum_L\left[\sum_N \frac{F_N(\omega)}{\omega_N^2-\omega^2}\left(C_L^N + (\omega_L^2-\omega^2)D_L^N\right)\right]\frac{1}{\omega_L^2-\omega^2}\mathbf{s}_L(\mathbf{x}) \\ & -i\sum_N \frac{F_N(\omega)}{\omega_N^2-\omega^2}\frac{f_N(S)}{f'_N(S)}\mathbf{s}'_N(\mathbf{x}).\end{aligned} \tag{B.21}$$

[3]The assumption of spherical symmetry is needed for deriving (B.19), because in this case the quotient f/f' is constant on S.

The method just described for obtaining the first-order contribution $\boldsymbol{S}^{(1)}$ to the solution, can be followed iteratively to obtain $\boldsymbol{S}^{(n)}$ for any n. Nevertheless, the general expression we would arrive at is a cumbersome expansion of nested summatories which is far from being easy to handle. There is, however, a very interesting particular case in which these expressions are greatly simplified; namely, the case of a driven force whose spectrum $\boldsymbol{F}(\omega)$ is peaked around a ressonant frequency ω_K, being zero outside a small neighbourhood of $\pm\omega_K$. Under such assumption, we must only consider equation (B.21) for $|\omega| \approx \omega_K$. For such values of ω, we can drop all terms except the dominant quadratic one in $(\omega_N^2 - \omega^2)^{-1}$, obtaining

$$\boldsymbol{S}^{(1)}(\mathbf{x}, \omega) \approx \frac{-i\, C_K^K}{(\omega_K^2 - \omega^2)^2} \sum_m F_m \mathbf{s}_m(\mathbf{x}),$$

where the summation extends over the eigenvectors having the same (degenerated) eigenfrequency ω_K. The above equation is easily generalized for any value of n:

$$\boldsymbol{S}^{(n)}(\mathbf{x}, \omega) \approx \left(\frac{-iC_K^K}{\omega_K^2 - \omega^2}\right)^n \frac{1}{\omega_K^2 - \omega^2} \sum_m F_m(\omega) s_m(\mathbf{x}),$$

which is formula (5.25) used in the main text.

Appendix C

Part of the work described in the main text relies on numerical calculations. These calculations have been performed with the aid of an HP Workstation of the *Apollo* series, which ran some routines in the C programming language [70] written specifically for the problem at hand. Although none of the computations required heavy numerical analysis, we ended up with a small library of functions, which has proved useful and handy thorough our work on spherical gravitational wave detectors, and which is described in this Appendix.

All the routines are written according to the Standard ANSI C conventions [70], so that they can be compiled and used on any plataform or operative system. In the first section we give a list of the functions developed and a description of their performance. The second section is devoted to the presentation of the algorithms through their listings in C.

C.1 The library *sphere*

Any programme using this library must be linked with the compiled version of the listings in the next section, as well as include the header file *sphere.h*, containing the prototypes of our functions. This header is the following:

```
    /** header sphere.h **/
#ifndef __sphere__
#define  __sphere__

#include <math.h>
```

```
/** Function prototypes for the library **/

void beta(int l, double z, double* bet, double* tbet,
  double* dbet, double* dtbet, double eta , double pr);
void matrixP(int l ,double z,double* Ap, double eta, double pr);
void matrixT(int l, double z,double* At, double eta);
double rootP(int l, int n, double eta, double pr);
double rootT(int l, int n, double eta);
double rootivP(int l, double iv, double eta, double pr);
double rootivT(int l, double iv, double eta);
void weightsP(int l, int n, double* p, double eta , double pr);
void radP(int l, int n, double z, double* A, double* B,
  double eta, double pr);
void dradP(int l, int n, double z, double* dA, double* dB,
   double eta, double pr);
void radT(int l, int n, double z, double* T, double* dT,
  double eta);
double normP(int l, int n, double eta, double pr);
double normT(int l, int n, double eta);
double cross(int n, double eta, double pr);

/**  Auxiliar functions  **/

void sphbes(int ,double ,double*, double*, double*, double*);
double deter(double*, int);
double rtbis(double (*func)(double), double, double);
void gauleg(double, double, double *,double *,int);
void triangular(double*, int, int, int*);
void error(char*);


#endif
```

The routines termed `Auxiliar functions` are used by the rest of the library. They perform general purpose tasks. We shall give here a description of each especific function, avoiding technical details of their implementation, which are left for the next section. In

the descriptions hereafter, the following arguments have always the same meaning:

int l Integer denoting the multipole index l. It can take any non-negative value.

int n Integer denoting the index n of normal modes. It can take any positive value.

double eta Double–precision variable giving the value of $\eta = a/R$, i.e., the ratio between the inner and outer radii of the hollow sphere. It ranges from 0 to 1.

double pr Value of the material's Poisson's ratio. It must be in the interval $[-1, 0.5]$.

Functions of the library

- `void beta(int l, double z, double *bet, double *tbet, double *dbet, double *dtbet, double eta, double pr)`

  This function computes the functions β and $\tilde{\beta}$, given by equations (3.25) and (3.56), at the point z. The result is stored in the five-dimensional arrays pointed by `bet` and `tbet` according to the following formulæ:

  $$\texttt{bet[n]} = \beta_n(z) \qquad \texttt{tbet[n]} = \tilde{\beta}_n(z)$$
  $$\texttt{bet[0]} = z^{-2} j_l(z) \qquad \texttt{tbet[0]} = z^{-2} y_l(z)$$

  When `eta`=1 (thin shell limit), the derivatives of the above functions are also computed and stored in the five–dimensional arrays pointed by `dbet` and `dtbet`. Otherwise, as they are not used in the calculations when $\eta < 1$, these pointers are reset to `NULL`.

- `void matrixP(int l, double z, double *A, double eta, double pr)`

  This function computes the matrix $\mathbb{A}_P$ given in (3.54), and stored it, sorted by arrows, in the sixteen-dimensional array pointed by `A`, according to the following relations:

  $$\texttt{A[(i-1)*4+j-1]} = (\mathbb{A}_P)_{ij},$$

  valid when $0 < \eta < 1$ and $l \neq 0$. The limiting cases are treated as follows:

  - $0 < \eta < 1$, $l = 0$

    In this case, the relevant matrix is the 2×2 one appearing in (3.61). Thus, `A`

is assumed to point to a four-dimensional array in which the matrix is stored:

$$\texttt{A[0]} = \beta_4(zq/k) \qquad \texttt{A[1]} = \tilde{\beta}_4(zq/k)$$
$$\texttt{A[2]} = \beta_4(\eta zq/k) \quad \texttt{A[3]} = \tilde{\beta}_4(\eta zq/k).$$

– $\eta = 0$, $l \neq 0$
For the solid sphere, the matrix whose determinant vanishes is again 2×2, and is given by equation (3.27). It is stored rowwise in `A`:

$$\texttt{A[0]} = \beta_4(zq/k) \qquad \texttt{A[1]} = -l(l+1)\beta_1(z)$$
$$\texttt{A[2]} = -\beta_1(zq/k) \quad \texttt{A[3]} = \beta_3(z)$$

– $\eta = 0$, $l = 0$
The monopolar modes of the solid sphere satisfy equation (3.34). `A` is assumed again four-dimensional, and the following values are stored in it:

$$\texttt{A[0]} = \beta_4(zq/k) \qquad \texttt{A[1]} = \texttt{A[2]} = 0 \qquad \texttt{A[3]} = 1.$$

– $\eta = 1$
In the thin shell limit, the corresponding matrix is $\mathbb{A}_P$ (or the 2×2 matrix appearing in the monopolar case) with the functions taking values at $z\eta$ replaced by their derivatives taken at z.

The values stored in `A` are such that the eigenvalue equation is always $det(A) = 0$, and `A` is considered a function of $z = kR$.

- `void matrixT(int l, double z, double *A, double eta)`

This function stores in `A` the matrix $\mathbb{A}_T$ (cf. (3.55)), corresponding to toroidal modes:

$$\texttt{A[(i-1)*2+j-1]} = (\mathbb{A}_T)_{ij}.$$

In the case of the solid sphere ($\eta = 0$), the toroidal eigenvalue equation is (3.40), so that the values stored by `matrixT` in `A` are:

$$\texttt{A[0]} = \beta_1(z) \qquad \texttt{A[1]=A[2]} = 0 \qquad \texttt{A[3]} = 1.$$

The thin shell limit in the toroidal family can be solved analytically, so that no numerical calculations are needed for $\eta = 1$.

This function cannot be called for $l = 0$ (there are no monopolar modes in the toroidal family).

- `weightsP(int l, int n, double *p, double eta, double pr)`

  This function calculates, for the spheroidal normal mode (n,l), the coefficients defined in equation (3.67) and stores them in the 3–dimensional array pointed by `p`:

  $$\texttt{p[0]} = C_{tl} \qquad \texttt{p[1]} = D_{ll} \qquad \texttt{p[2]} = D_{tl}.$$

  When `eta`=1, the quotient $C_t q/C_l k$ is stored in `p[0]`.

- `void radP(int l, int n, double z, double *A, double *B,`
  `double eta, double pr)`

  This function evaluates the radial functions $A_{nl}(r)$ and $B_{nl}(r)$, given by equations (3.69) and (3.70), at $r/R =$ `z(1-eta)+eta` and taking $C(n,l) = 1/\beta_3(k^P_{nl}R)$. Their values are stored in the variables pointed by `A` and `B`. In the case of a solid sphere, equations (3.30) and (3.31) are used. The variable `z` can take values within the interval $[0,1]$.

- `void dradP(int l, int n, double z, double *dA, double *dB,`
  `double eta, double pr)`

  This function stores in `dA` and `dB` the derivatives $dA_{nl}/d(kr)$ and $dB_{nl}/d(kr)$ at $r/R =$ `z(1-eta)+eta`.

- `void radT(int l, int n, double z, double *T, double *dT, double eta)`

  The functions $T_{nl}(r)$ for the solid (equation (3.44)) and hollow (equation (3.81)) sphere are calculated, as well as its derivative. Their values are stored in the variables pointed by `T` and `dT`, and `z` has the same meaning as in `radP`.

- `double normP(int l, int n, double eta, double pr)`
  `double normT(int l, int n, double eta)`

  These functions return values which are proportional, respectively, to the normalization constants $C(n,l)$ and $C'(n,l)$, when the normalization conditions (3.74) and (3.83) are imposed. In fact, they perform the numerical integration. Thus, if

  $$x = \texttt{normP(l,n,eta,pr)}$$

  $$y = \texttt{normT(l,n,eta)},$$

  the following relations hold

  $$C(n,l) = x\beta_3(k^P_{nl}R)\sqrt{4\pi(k^P_{nl}R)^3(1-\eta^3)/3}$$

$$C'(n,l) = y\sqrt{4\pi(k_{nl}^T R)^3(1-\eta^3)/3}.$$

- `double rootP(int l, int n, double eta, double pr)`
  `double rootT(int l, int n, double eta)`

  These functions return, respectively, the eigenvalues $k_{nl}^P R$ and $k_{nl}^T R$.

- `double rootivP(int l, double iv, double eta, double pr)`
  `double rootivT(int l, double iv, double eta)`

  These functions return the first spheroidal and toroidal eigenvalue greater than the value of `iv`.

- `double cross(int n, double eta, double pr)`

  This function returns the value $(a_n^s k_{2n}^P)^2$ when `pr`=0 and $(a_n^h k_{2n}^P)^2$ otherwise. These values determine, up to a multiplicative constant, the absorption cross–sections of spherical detectors (cf. chapter 5)

C.2 Source code of the library

C.2.1 Auxiliar functions

The routines described in the previous section make use of some auxiliar functions, whose listings are given below: `rtbis` (a root finder using the method of bisection), `deter`, `gauss`, `triangular` (computation of determinants and solution of linear systems), `gauleg` (quadratures using Gauss–Legendre interpolation) and `sphbes` (spherical Bessel functions and their derivatives). They are general purpose routines based on well-known numerical algorithms [32, 101]. Thus, `rtbis` and `gauleg` are almost identical to those found in [101], and we give their listings just for the sake of completeness. On the other hand, although `deter`,`gauss`, `triangular` and `sphbes` use standard algorithms and source code for them can be found in the literature, we have prefered writting the code ourselves. As the calculations involved are not exceedingly time or memory demanding, our aim has been to provide programmes which were simple rather than computationally optimized.

- `rtbis`

  This routine uses the usual bisection method [101] for searching a root of the function pointed by `func` in the interval `x1<x<x2`. The macro `NMAX` gives the

maximum number of bisections allowed to attain a precision in the value returned of one part in `1e(-PREC)`.

The source code of this function is the following:

```
#define NMAX 100
#define PREC 1e-10

double rtbis(double (*func)(double),double  x1,double  x2)
{
int j;
double dx,f,fmid,xmid,rtb;

f=(*func)(x1);
fmid=(*func)(x2);
if (f*fmid >= 0.0)
       error("rtbis: root must be bracketed for bisection");
rtb = f < 0.0 ? (dx=x2-x1,x1) : (dx=x1-x2,x2);
for (j=1;j<=NMAX;j++) {
fmid=(*func)(xmid=rtb+(dx *= 0.5));
if (fmid <= 0.0) rtb=xmid;
if (fabs(dx) < PREC || fmid == 0.0) return rtb;
}
error("rtbis: NMAX exceeded");
return 0.0;
}
#undefine NMAX
#undefine PREC
```

This and the following routines make use of a simple error handler:

```
void error(char *s)
{
      fprintf(stderr,"\nError:%s\n",s);
      exit(1);
}
```

- `gauleg`

  This routine stores in `x` and `w` the points and weights used in the Gaussian quadrature approximation [32, 101]

$$\int_a^b f(x)\,dx \approx \sum_{i=0}^{n-1} w_i f(x_i),$$

  where the points are the zeros of the Legendre polynomial $P_n(x)$ considered in the interval (a, b), and the weights are given by

$$w_i = 2(1 - x_i^2)^{-1}[P_n'(x_i)]^{-2}.$$

  The source code [101] is the following:

```
#define PREC 1e-10

void gauleg(double x1, double x2, double x[], double w[], int n)
{
int m,j,i;
double z1,z,xm,xl,pp,p3,p2,p1;

m=(n+1)/2;
xm=0.5*(x2+x1);
xl=0.5*(x2-x1);
for (i=1;i<=m;i++) {
/* calculus of the zero by Newton's method */
z=cos(3.141592654*(i-0.25)/(n+0.5));
do {
```

```
       /* computation of the polynomial by recurrence*/
p1=1.0;
p2=0.0;
for (j=1;j<=n;j++) {
p3=p2;
p2=p1;
p1=((2.0*j-1.0)*z*p2-(j-1.0)*p3)/j;
}
                        /* derivative of the polynomial */
pp=n*(z*p1-p2)/(z*z-1.0);
                        /* Newton's method */
z1=z;
z=z1-p1/pp;
} while (fabs(z-z1) > PREC;
x[i]=xm-xl*z;
x[n+1-i]=xm+xl*z;
w[i]=2.0*xl/((1.0-z*z)*pp*pp);
w[n+1-i]=w[i];
}
}
#undefine PREC
```

- `triangulation`

  This routine transforms the matrix stored rowwise in the address pointed by `d` into its upper-triangular equivalent by Gaussian elimination (if $n < m$, the programme makes upper-triangular the embedded $n \times n$ matrix). Thus, if, say, a_{ij} is the `nxm` matrix to be stored, the routine expects that the following equality holds:

  $$\texttt{a[i*(m-1)+j-1]} = a_{ij}, \tag{C.1}$$

  and, after its action, the equivalent matrix stored in `a` will satisfy

  $$a_{ij} = 0 \qquad \text{if} \qquad i, j < n.$$

  The programme uses the method of *partial pivoting* (see, e.g., [32] chapter 5), which may also imply changes in the original order of the rows. The parity of these permutations is stored in the address pointed by `par`.

```
 void triangular(double *d,int n, int m, int *par)
 {
  double akk,x;
  int i,j,k;

  *par=1;

  for (k=0;k<n;k++)
   {
    /* choosing the pivot */
    akk=d[k*m+k]; j=k;
    for (i=k;i<n-1;i++)
      if (akk<d[i*m+k]) {akk=d[i*m+k]; j=i;}
    if (akk==0) continue;
    /* interchanging rows if necessary */
    if (j!=k)
      {
for(i=k;i<m;i++)
       {  x=d[k*m+i]; d[k*m+i]=d[j*m+i]; d[j*m+i]=x;}
*par*=-1;/* change of parity */
      }
    /* pivoting */
    for (i=k+1;i<n;i++)
       for (j=k+1; j<m; j++)
             d[i*m+j]-=d[i*m+k]*d[k*m+j]/akk;

    for (i=0; i<k; i++)
       for (j=k+1;j<n;j++)
     d[j*m+i]=0;
    }
}
```

- `deter`

This routine returns the determinant of an `nxn` matrix stored rowwise (cf. (C.1)) in the address pointed by `d`.

The routine constructs a triangular matrix by the aid `triangular`, and then computes its determinant multiplying the diagonal components of the new matrix.

The source code of `deter` is the following:

```
double deter(double *d,int n)
{
 double det=1, *a;
 int k,par;

 if (n==2) return d[0]*d[3]-d[1]*d[2];

 if ((a=malloc(n*n*sizeof(double)))==NULL)
     error("deter: memory allocation.");
 for (k=0;k<n*n;k++) a[k]=d[k];

 triangular(a,n,n,&par);
 for (k=0;k<n;k++) det*=a[k*n+k];
 free(a);
 return par*det;
}
```

- `gauss`

  This routine solves the linear system $\mathbb{A} \cdot \boldsymbol{X} = \boldsymbol{B}$, where $\mathbb{A}$ is a `nxn` matrix stored in the address `a` and $\boldsymbol{B}$ is an `n`-dimensional vector stored in the address `b`. The solution $\boldsymbol{X}$ is stored in `b`. The routine reduces the system to its triangular form and then uses the well–known algorithm of *back substitution* (cf. [32], chapter 5) to solve it. The source code is given below.

```
void gauss(double *a, double *b, int n)
{
 double *d;
 int i,j;

 if ((d=malloc(n*(n+1)*sizeof(double)))==NULL)
     error("gauss: memory allocation error");

 /* making up an nx(n+1) matrix */
 for (i=0; i<n; i++) {
      d[i*(n+1)+n]=b[i];
      for (j=0;j<n;j++) d[i*(n+1)+j]=a[i*n+j]; }

 triangular(d,n,n+1,&i);

 /* back substitution on a triangular matrix */

 for (i=n-1;i>-1;i--){
   b[i]=d[i*(n+1)+n];
   for(j=i+1;j<n;j++) b[i]-=d[i*(n+1)+j]*b[j];
   b[i]/=d[i*(n+1)+i];}

free(d);
}
```

- `sphbes`

  The function `sphbes` computes spherical Bessel functions of the first and second kind, and their derivatives, at the point `z`, and stores them in the variables pointed by `j, y, dj, dy` (see listing below).

  This routine computes spherical Bessel functions of the second kind with the use of the recurrence relations [2]

  $$y_l(z) = (2l-1)z^{-1}y_{l-1}(z) - y_{l-2}(z), \tag{C.2}$$

  by forward iteration starting with $y_0(z)$ and $y_1(z)$. This method is hampered by numerical instability when applied to spherical Bessel functions of the first kind.

To compute them recursively we use a method due to J.C. Miller [92]. It makes use of the backwards recursive formula

$$j_{l-2}(z) = (2l-1)z^{-1}j_{l-1}(z) - j_l(z), \tag{C.3}$$

starting from some $L > l$ and the tentative values $\tilde{j}_L(z) = 0$, $\tilde{j}_{L-1}(z) = 1$. Using these values and the above recursive relation, we obtain a series of values $\tilde{j}_{L-2} \cdots \tilde{j}_0$. The true value of $j_l(z)$ is then given by

$$j_l(z) = \tilde{j}_l \frac{j_0(z)}{\tilde{j}_0}, \tag{C.4}$$

due to the fact that different solutions to second order difference equations are proportional to each other [32].

The derivative of spherical Bessel functions is computed using the recurrence relation [2]

$$h_l'(z) = h_{l-1}(z) - (l+1)z^{-1}h_l(z), \tag{C.5}$$

which is valid for $h_l = j_l,\ y_l$.

The chosen value for L is `50+(int)z`, which has been proved to give correct values for, at least, ten decimal places when $z \leq 100$ and $l \leq 10$.

The code for `sphbes` is thus the following:

```
void sphbes(int l, double z, double *j, double *y,
    double *dj, double *dy)
{
 int sbj(int,double,double*,double*);
 int sby(int,double,double*,double*);
 if (sbj(l,z,j,dj)) printf("\nWarning: bad arguments in sbj\n");
 if (sby(l,z,y,dy)) printf("\nWarning: bad arguments in sby\n");
}

/* spherical bessel functions of the first kind */

int sbj(int l, double x, double *j, double *dj)
{
```

```
 int  k;
 double fl, fl_1, fk_1, fk=1, fk1=0;

 if ( x<0 || l<0) return 1; /* bad arguments: returns 1 */
 if (x==0) { *j=(l==0 ? 1:0); *dj=0; return 0; }

 *j=sin(x)/x;
 if (l==0) { *dj=-*j/x+cos(x)/x; return 0;}

 /* backward recurrence */

 for (k=50+(int) x; k>0; k--) {
  fk_1=(2*k+1)*fk/x-fk1;
        if (k==l) { fl=fk; fl_1=fk_1;}
        fk1=fk; fk=fk_1;
 }
 fl/=fk; fl_1/=fk;

 *dj=*j*fl_1-(l+1)*fl*(*j)/x;
 *j*=fl;
 return 0;
}

/* spherical Bessel functions of the second kind */

int sby(int l, double x, double *y, double *dy)
{
 int k;
 double  sy0, sy1,yk;

 if ( x<=0 || l<0 ) return 1; /* bad arguments: return 1 */

 sy0=-cos(x)/x;
 if (l==0) { *y=sy0; *dy=sin(x)/x+cos(x)/(x*x); return 0; }

 sy1=-sin(x)/x-cos(x)/(x*x);
 if (l==1) { *y=sy1; *dy=-2*sy1/x+sy0; return 0;}
```

```
 /*forward recurrence */
 for (k=2; k<l; k++){
     yk=(2*k-1)*sy1/x-sy0;
     sy0=sy1; sy1=yk;
 }  /* sy1=bessel of order l-1 */

 *y=(2*l-1)*sy1/x-sy0;
 *dy=sy1-(l+1)*(*y)/x;
 return 0;
}
```

C.2.2 Specific functions

In this subsection we give the listings and technical details of the routines specifically programmed to deal with functions and magnitudes appearing in the theory of spherical detectors of gravitational radiaton.

- `beta`

  The expressions used in this routine to compute the functions β and $\tilde{\beta}$, as well as their derivatives, are easily obtained from their definitions (equations (3.25) and (3.56)) and recurrence relations (C.2) and (C.4).

  The source code for this routine is thus self–explanatory:

```
void beta(int l, double x, double *b, double *bb,double *db,double *dbb,
  double eta, double pr)
{
 double j,y,dj,dy,H;

 if ( (x<=0)||(l<0)||(pr>0.5)||(pr<-1) )
     error("betaP:bad arguments");

 /* computing the value of H=lambda/mu from pr */
```

```
 H=2*pr/(1-2*pr);


   sphbes(l,x,&j,&y,&dj,&dy);
   b[0]=j/(x*x);          bb[0]=y/(x*x);
   b[1]=dj/x-j/(x*x);     bb[1]=dy/x-y/(x*x);
   b[2]=l*b[1]-j*(1-l*(l+2)/(x*x))-dj*(l+2)/x;
                          bb[2]=l*bb[1]-y*(1-l*(l+2)/(x*x))-dy*(l+2)/x;
   b[3]=0.5*b[2]+(0.5*l*(l+1)-1)*b[0];
                          bb[3]=0.5*bb[2]+(0.5*l*(l+1)-1)*bb[0];
   b[4]=b[2]-H*0.5*j;
                          bb[4]=bb[2]-H*0.5*y;

   /* spherical shell limit: the derivatives of the
    beta functions will be needed.    */

   if (eta>0.99999)
   {
    db[0]=(b[1]-b[0])/x;  dbb[0]=(bb[1]-bb[0])/x;
    db[1]=(b[2]-2*b[1])/x;
                          dbb[1]=(bb[2]-2*bb[1])/x;
    db[2]=l*db[1]-dj+l*(l+2)*db[0]-(l+2)*(b[2]-dj/x)/x;
                          dbb[2]=l*dbb[1]-dy+l*(l+2)*dbb[0]
-(l+2)*(bb[2]-dy/x)/x;
    db[3]=0.5*db[2]+(0.5*l*(l+1)-1)*db[0];
                          dbb[3]=0.5*dbb[2]+(0.5*l*(l+1)-1)*dbb[0];
    db[4]=db[2]-H*0.5*dj;
                          dbb[4]=dbb[2]-H*0.5*dy;
    }
      else db=dbb=NULL;

}
```

- `matrixP` and `matrixT`

These routines calculate the matrices $\mathbb{A}_P$ and $\mathbb{A}_T$ according to the prescriptions given in section C.1. Once the functions β and $\tilde{\beta}$ have been provided, the code is merely a translation in C of the correspondig formulæ for the members of these matrices.

```
/** matrixP **/

void matrixP(int l,double x,double *a, double eta, double pr)
{
 double b[5],bb[5],db[5],dbb[5],y,S;
 int s,t;


 if ((pr<-1)||(pr>0.5)) error("matrixP: pr out of bounds");
 if ((eta<0)||(eta>1))  error("matrixP: eta out of bounds");

 /* Computation of S=k/q from pr */

 S=sqrt((2-2*pr)/(1-2*pr));

 if (eta==0)
  {
    beta(l,x/S,b,bb,db,dbb,0,pr);
    if (l==0) { a[0]=b[4]; a[3]=a[1]=1; a[2]=0; return;}
    a[0]=b[4]; a[2]=-b[1];
    beta(l,x,b,bb,db,dbb,0,pr);
    a[1]=-l*(l+1)*b[1]*S; a[3]=b[3]*S);
    return;
   }
 y=x/S;
 beta(l,y,b,bb,db,dbb,eta,pr);
 if (l==0) { a[0]=b[4]; a[1]=bb[4];
     beta(l,eta*y,b,bb,db,dbb,eta,pr);
     if (eta>0.999) { a[2]=S*db[4]; a[3]=S*dbb[4]; return;}
     a[2]=b[4]; a[3]=bb[4];
     return;
```

```
          }
 a[0]=b[4]; a[2]=bb[4];
 a[4]=-b[1]; a[6]=-bb[1];
 if (eta>0.99999)  /* eta=1 -> spherical shell approximation */
 {
  a[8]=db[4]; a[10]=dbb[4];
  a[12]=-db[1]; a[14]=-dbb[1];
 }
      else
      {
       beta(l,eta*y,b,bb,db,dbb,eta,pr);
       a[8]=b[4]; a[10]=bb[4];
       a[12]=-b[1]; a[14]=-bb[1];
 }
 beta(l,x,b,bb,db,dbb,eta,pr);
 t=l*(l+1);
 a[1]=-t*b[1]*S; a[3]=-t*bb[1]*S;
 a[5]=b[3]*S; a[7]=bb[3]*S;
 if (eta>0.99999)
 {
  a[9]=-t*db[1]*S; a[11]=-t*dbb[1]*S;
  a[13]=db[3]*S; a[15]=dbb[3]*S;
 }
      else
      {
       beta(l,eta*x,b,bb,db,dbb,eta,pr);
       a[9]=-t*b[1]*S; a[11]=-t*bb[1]*S;
       a[13]=b[3]*S; a[15]=bb[3]*S;
 }
}

/** matrixT **/

void matrixT(int l, double x, double *a, double eta)
{
 double b[5],bb[5],db[5],dbb[5];

 if (l==0) error("matrixT: there are no toroidal modes for l=0");
```

```
 if ((eta<0)||(eta>1))  error("matrixT: eta out of bounds");

 beta(l,x,b,bb,db,dbb,eta,0);
 if (eta==0) { a[0]=b[1]; a[1]=a[3]=1; a[2]=0; return;}
 a[0]=b[1]; a[1]=bb[1];
 if (eta>.999) { a[2]=db[1]; a[3]=dbb[1]; return; }
 beta(l,x*eta,b,bb,db,dbb,eta,0);
 a[2]=b[1]; a[3]=bb[1];
}
```

- `rootP`, `rootivP`, `rootT` and `rootivP`

  These are root finders for spheroidal and toroidal modes. They use the function `rtbis` described in the previous subsection, and the auxiliar functions `cf` and `tf`, which return the determinants vanishing when their argument is the desired eigenvalue. While `rootP` and `rootT` look for the `n`th mode with multipole index `l`, their "`iv`" counterparts find the first eigenvalue greater than `vi` for the given `l`.

  The code is thus the following:

```
double cf(double);      /* auxiliar functions */
double tf(double);
static double L, R, PR; /* parameters for cf and tf */

/* spheroidal finders */

double rootP(int l, int n, double eta, double pr)
{
 double x1,vi,kR,x0=0.5,h=0.1;
 int m;


 if ((n<1)||(l<0)||(eta<0)||(eta>1)||(pr<-1)||(pr>0.5))
    error("rootP: bad arguments");
```

```
 L=l; R=eta; PR=pr; /* parameters of cf */

 for (m=0; m<n;m++,x0=kR+h)
 {
  x1=x0; vi=cf(x0);
  while((cf(x1+=h)* vi>0)&&(x1<x0*151));

 if (x1>x0*151)
  { fprintf(stderr,"\nrootP: cannot find next root\n");
    return x1; }

  kR=rtbis(cf,x0,x1);
 }
 return kR;
}

double rootivP(int l, double vi, double eta, double pr)
{
 double x1,kR,val,h=0.1;

 if ((n<1)||(l<0)||(eta<0)||(eta>1)||(pr<-1)||(pr>0.5))
    error("rootP: bad arguments");

 L=l; R=eta; PR=pr;

 x1=vi; val=cf(vi);
 while((cf(x1+=h)*val>0)&&(x1<vi*151));

 if (x1>vi*151)
 { fprintf(stderr,"\nrootivP: cannot find next root\n");
   return x1; }

 kR=rtbis(cf,vi,x1);
 return kR;
}

/* cf(x): function which must vanish when
```

```
   x is a spheroidal root            */

double cf(double x)
{
  double m[16],y;
  int n;

  if ((R==0)||(L==0)) n=2; else n=4;

  matrixP(L,x,m,R,PR);

  return deter(m,n);
}


/* toroidal finders */

double rootT(int l, int n, double eta)
{
 double x1,vi,kR,x0=0.5,h=0.1;
 int m;

 if ((n<1)||(l<1)||(eta<0)||(eta>1))
    error("rootP: bad arguments");


 L=l; R=eta; /* parameters of tf */

 for (m=0; m<n; m++, x0=kR+h)
 {
  vi=tf(x0); x1=x0;
  while((tf(x1+=h)* vi>0)&&(x1<151*x0));

 if (x1>151*x0)
 { fprintf(stdout,"\nrootT: cannot find next root\n");
   return x1; }

  kR=rtbis(tf,x0,x1);
```

```
 }

 return kR;
}


double rootivT(int l, double vi, double eta)
{
 double x1,kR,val,h=0.1;

 if ((n<1)||(l<1)||(eta<0)||(eta>1))
    error("rootP: bad arguments");

 L=l; R=eta;

 x1=vi; val=tf(vi);
 while((tf(x1+=h)*val>0)&&(x1<vi*151));

 if (x1>vi*151)
 { fprintf(stdout,"\n rootivT: cannot find next root\n");
   return x1; }

 kR=rtbis(tf,vi,x1);
 return kR;
}

/* tf(x): function that must vanish when x
  is a toroidal eigenvalue            */

double tf(double x)
{
  double m[4], y;

  matrixT(L,x,m,R);

  return deter(m,2);
}
```

- `weightsP`

  The resolution of the indeterminated system with matrix of coefficients `matrixP`, taking as independent terms its first row, is carried out by this routine with the aid of `rtbis` and `gauss` (see preceeding subsection).

```
void weightsP(int l, int n, double *p,double eta, double pr)
{
   double a[16],d[9],kR;
   int i,j;

   kR=rootP(l,n,eta,pr);
   matrixP(l,kR,a,eta,pr);

   /* especial cases */

   if (l==0) { p[0]=p[2]=0; p[1]=-a[0]/a[1]; return;}
   if (eta==0) { p[0]=-a[0]/a[1]; p[1]=p[2]=0; return; }

   /* general case */

   /* matrix of the system */

   for (i=0;i<3;i++)
      for(j=0;j<3;j++)
         d[3*i+j]=a[4*i+j+1];

   /* vector of independent terms= coeficients of C_l */

   for (i=0;i<3;i++)  p[i]=-a[4*i];

   /* solving the system and storing the result in p */

   gauss(d,p,3);
```

```
}
```

- `radP`, `radT` and `dradP`

  The following code computes the radial functions of spheroidal as well as toroidal normal modes from their definitions. The arbitrary normalization factor is chosen here as $C(n,l) = 1/\beta_3(k_{nl}^P R$. It must be remembered that the argument `x` always runs from 0 to 1. The routine translates this value into the interval $[ka, kR]$ in which the functions are defined, according to the transformation $x \to kR[\eta + x(1-\eta)]$. As the functions which use these routines do not admit the value $kr = 0$, this point (which is only present in the case of a solid sphere) is treated especifically in an `if` statement.

```
void radT(int l, int n, double x, double *t, double *dt, double eta)
{
 double j,y,dj,dy,b[5],bb[5],db[5],dbb[5],p=0,kR;

 if (l==0) error("radT: there are no toroidal modes for l=0.");
 if ((l<0)||(n<1)||(eta<0)||(eta>1)||(x<0)||(x>1))
     error("radT: bad arguments.");

 kR=rootT(l,n,eta);

 x=kR*(eta+x*(1-eta)); /* transformation from [0,1] to [kR*eta,kR] */

 sphbes(l,x,&j,&y,&dj,&dy);
 if (eta!=0) { beta(l,kR,b,bb,db,dbb,0,0); p=b[1]/bb[1];}
 *t=j-p*y;
 *dt=dj-p*dy;
}

void radP(int l, int n, double x, double *A, double *B,
```

```
  double eta, double pr)
{
 double j,y,dj,dy,jq,yq,djq,dyq,p[3],S,kR;

 if ((l<0)||(n<1)||(eta<0)||(eta>1)||(x<0)||(x>1))
     error("radP: bad arguments.");

 kR=rootP(l,n,eta,pr);
 S=sqrt((1-2*pr)/(2-2*pr)); /* S=q/k */

 if ((x==0)&&(eta==0))
 { if (l==1) { weightsP(l,n,p,0,pr);
   *A=*B=(1-2*p[0]*S/3)/3.; }
                         else *A=*B=0;
          return;
         }

 x=kR*(eta+x*(1-eta)); /* transformation from [0,1] to [kR*eta,kR] */

 sphbes(l,x,&j,&y,&dj,&dy);
 sphbes(l,x*S,&jq,&yq,&djq,&dyq);
 weightsP(l,n,p,eta,pr);

 *A= djq+p[1]*dyq-l*(l+1)*(p[0]*j+p[2]*y)/x;
 if (l==0) *B=0; else
 *B= (jq+p[1]*yq)/(S*x)-(p[0]*j+p[2]*y)/x-(p[0]*dj+p[2]*dy);

}

void dradP(int l, int n, double x, double *dA, double *dB,
   double eta, double pr)
{
  double b[5],bb[5],a[5],aa[5],db[5],dbb[5],p[3],kR,S;

  if ((l<0)||(n<1)||(eta<0)||(eta>1)||(x<0)||(x>1))
     error("radT: bad arguments.");

  kR=rootP(l,n,eta,pr);
```

```
  S=sqrt((1-2*pr)/(2-2*pr)); /* S=q/k */

  if ((x==0)&&(eta==0)
    { if (l>2 || l==1) { *dA=*dB=0; return;}
               weightsP(l,n,p,0,pr);
               if (l==2) { *dA=S*(1-3*p[0])/15.; *dB=2*(*de);}
               else {*dA=0; *dB=-S/3;}
               return;
              }

  x=kR*(eta+x*(1-eta)); /* transformation from [0,1] to [kR*eta,kR] */

  beta(l,x,b,bb,db,dbb,eta,pr);
  beta(l,S*x,a,aa,db,dbb,eta,pr);
  weightsP(l,n,p,eta,pr);

  *dA= S*(a[2]+p[1]*aa[2]-l*(l+1)*(p[0]*b[1]+p[2]*bb[1]));
  *dB= S*(a[1]+p[1]*aa[1]-(p[0]*b[1]+p[2]*bb[1])-(p[0]*b[2]+p[2]*bb[2]));
}
```

- `normP` and `normT`

  The normalization constants of toroidal and spheroidal normal modes of vibration are returned by these functions, which compute them by means of Gauss-Legendre interpolation (cf. section C.2.1).

```
double normT(int l, int n, double eta)
{
 double *x,*w,t,dt,y,kR,norm=0;
 int m,np;

 if (l==0) error("radT: there are no toroidal modes for l=0.");
 if ((l<0)||(n<1)||(eta<0)||(eta>1))
     error("normT: bad arguments.");
```

```
 kR=rootT(l,n,eta);

 np=20+(int)kR/10; /* number of points for interpolation */

 if ( ((x=malloc(sizeof(double)*(np+1)))==NULL ) ||
      ((w=malloc(sizeof(double)*(np+1)))==NULL ) )
    error("normT: memory allocation error");

 gauleg(kR*eta,kR,x,w,np);

 for (m=1;m<np+1;m++)
  {
    y=(x[m]/kR-eta)/(1-eta);
    radT(l,n,y,&t,&dt,eta);
    norm+=x[m]*x[m]*y*t*t*w[m];
  }

 free(x); free(w);

 return sqrt((1.0/(l*(l+1)*norm));
}


double normP(int l, int n, double eta, double pr)
{
 double *x,*w,A,B,y,kR,norm=0;
 int m,np;

 if ((l<0)||(n<1)||(eta<0)||(eta>1))
     error("normT: bad arguments.");
 if (eta==1) return 0;

 kR=rootP(l,n,eta,pr);

 np=20+(int)kR/10; /* number of points for interpolation */

 if ( ((x=malloc(sizeof(double)*(np+1)))==NULL ) ||
```

```
      ((w=malloc(sizeof(double)*(np+1)))==NULL ) )
    error("normP: memory allocation error");

 gauleg(kR*eta,kR,x,w,np);

 for (m=1;m<np+1;m++)
  {
    y=(x[m]/kR-eta)/(1-eta);
    radP(l,kR,y,&A,&B,eta,pr);
    norm+=x[m]*x[m]*w[m]*(A*A+l*(l+1)*B*B);
  }

 free(x); free(w);

 return sqrt(1.0/norm);
}
```

- `cross`

  This function returns the dimensionless factor $(k_{n2}a_n^{h,s})^2$ giving the absorption cross–section of a spherical detector (cf. chapter 5). The calculation is performed simply using the definition given in the text.

```
double cross(int n, double eta, double pr)
{
  double nm, sig, p[3], v3=0, j, y, dj, dy, kR, qR;

  if (eta==1) return 0;

  nm=normP(2,n,eta,pr);
  weightsP(2,n,p,eta,pr);
  kR=rootP(2,n,eta,pr);
  qR=kR*sqrt((1-2*pr)/(2-2*pr));
  v3=pow(eta,3);
```

```
  sphbes(2,qR,&j,&y,&dj,&dy);
  sig=(j+p[1]*y);
  sphbes(2,kR,&j,&y,&dj,&dy);
  sig-=(3*(qR/kR)*(p[0]*j+p[2]*y));
  if (eta>0){
    v3=pow(eta,3);
    sphbes(2,qR*eta,&j,&y,&dj,&dy);
    sig-=v3*(j+p[1]*y);
    sphbes(2,kR*eta,&j,&y,&dj,&dy);
    sig+=(v3*3*(qR/kR)*(p[0]*j+p[2]*y));
  }

  sig*=nm;
  sig*=sig;
  sig*=pow(kR,3)*(2-2*pr)/((1-v3)*(1-2*pr));
  sig*=0.23873241446;  /* 3/4 pi=0.238 */

  return sig;
}
```

Bibliography

[1] A. Abramovici *et al*, *Science*, **256**, 325 (1992).

[2] *Handbook of Mathematical Functions*, edited by M. Abramowitz and I.A. Stegun, Dover, New York (1972).

[3] E. Amaldi and G. Pizzella, *Nuov. Cim.*, **C9**, 612 (1986).

[4] R. Arnowitt, S. Deser and C.W. Misner, *Phys. Rev.*, **121**, 1556 (1961).

[5] N. Ashby and J. Dreitlein, *Phys. Rev.*, **D12**, 336 (1975).

[6] P. Astone *et al*, *Europhys. Lett.*, **16**, 231 (1991).

[7] P. Astone *et al*, *Phys. Rev.*, **D47**, 362 (1993).

[8] P. Astone, J.A. Lobo and B. Schutz, *Class. Quant. Grav.*, **11**, 2093 (1994).

[9] P. Astone *et al*, in *Proceedings of the First Edoardo Amaldi Conference on Gravitational Wave Experiments*, edited by E. Coccia *et al*, World Scientific, Singapore (1995).

[10] J.G. Banker and E.G. Reineke, *ASM Handbook*, **6**, 303 (1993).

[11] J.F. Bennoun, *C.R. Acad. Sci. Paris*, **A259**, 3705 (1964).

[12] M. Bianchi, E. Coccia, C.N. Colacino, V. Fafone and F. Fucito, *Clas. Quant. Grav.*, **13**, 2865 (1996).

[13] K. Billing *et al*, *Lett. Nuov. Cim.*, **12**, 111 (1975).

[14] D. Blair, *Gravitational Radiation (Les Houches)*, edited by N. Deruelle and T. Piran, North–Holland, Amsterdam (1982).

[15] L. Blanchet and T. Damour, *Ann. Inst. Henri Poincaré*, **50**, 377 (1989).

[16] D.R. Bland, *The Theory of Linear Viscoelasticity*, Pergamon Press, Oxford (1960).

[17] H. Bondi, *Nature*, **179**, 1072 (1957).

[18] G. Breit and E.P. Wigner, *Phys. Rev.*, **34**, 510 (1936).

[19] D.R. Brill and J.B. Hartle, *Phys. Rev.*, **135**, B271 (1964).

[20] R. Brunstein, M. Gasperini, M. Giovannini and G. Veneziano, CERN–TH/95-144 preprint (1995).

[21] B. Carter, *Commun. Math. Phys.*, **30**, 261 (1973).

[22] B. Carter, *Gravitational Radiation (Les Houches)*, edited by N. Deruelle and T. Piran, North–Holland, Amsterdam (1982).

[23] B. Carter and H. Quintana, *Phys. Rev.*, **D16**, 2928 (1977).

[24] M. Cerdonio *et al*, in *Proceedings of the First Edoardo Amaldi Conference on Gravitational Wave Experiments*, edited by E. Coccia *et al*, World Scientific, Singapore (1995).

[25] M. Cerdonio, P. Fortini, A. Ortolan, G.A. Prodi and S. Vitale, *Phys. Rev. Lett.*, **71**, 4107 (1993).

[26] E. Coccia and V. Fafone, *Phys. Lett.*, **A213**, 16 (1996).

[27] E. Coccia, J.A. Lobo and J.A. Ortega, *Phys. Rev.*, **D52**, 3735 (1995).

[28] E. Coccia, V. Fafone and G. Frossati, in *Proceedings of the First Edoardo Amaldi Conference on Gravitational Wave Experiments*, edited by E. Coccia *et al*, World Scientific, Singapore (1995).

[29] E. Coccia *et al*, in *Proceedings of the First Edoardo Amaldi Conference on Gravitational Wave Experiments*, edited by E. Coccia *et al*, World Scientific, Singapore (1995).

[30] D.C. Champeney, *Fourier Transforms and their Physical Applications*, Academic Press, London (1988).

[31] R. Christensen, *Theory of Viscoelasticity*, Academic Press, New York (1971).

[32] G. Dahlquist and Å. Björk, *Numerical Methods*, Prentice Hall, Englewood Cliffs N.J. (1974).

[33] T. Damour and G. Esposito-Farèse, *Clas. Quant. Grav.*, **9**, 2093 (1992).

[34] R. Dautray and J.L. Lions (ed.), *Mathematical Analysis and Numerical Methods for Science and Technology, Volume 1: Physical Origins and Classical Methods*, Springer-Verlag, Berlin (1985).

[35] R. Dautray and J.L. Lions (ed.), *Mathematical Analysis and Numerical Methods for Science and Technology, Volume 2: Functional and Variational Methods*, Springer-Verlag, Berlin (1985).

[36] D.H. Douglas *et al*, *Phys. Rev. Lett.*, **35**, 480 (1975).

[37] S.V. Dhurandhar and M. Tinto, *Mon. Not. R. astr. Soc.*, **234**, 663 (1988).

[38] S.V. Dhurandhar and M. Tinto, *Mon. Not. R. astr. Soc.*, **236**, 621 (1989).

[39] F.J. Dyson, *Astrophys. J.*, **156**, 529 (1969).

[40] F.W. Dyson, A.S. Eddington and C. Davidson, *Phyl. Trans.*, **A220**, 291 (1920).

[41] D.L. Eardley, D.L. Lee and A.P. Lightman, *Phys. Rev.*, **D8**, 3308 (1973).

[42] A.S. Eddington, *The Mathematical Theory of General Relativity*, Cambridge University Press, Cambridge (1924).

[43] A.R. Edmonds, *Angular Momentum in Quantum Mechanics*, Princeton University, Princeton (1957).

[44] A. Einstein, *Annal. der Phys.*, **49** (1916). English translation in H.A. Lorentz *et al*, *The Principle of Relativity*, Dover, New York (1952).

[45] A. Einstein, *S.B. Preuss. Akad. Wiss.*, p.688 (1916).

[46] A. Einstein, *S.B. Preuss. Akad. Wiss.*, p.154 (1918).

[47] P.L. Fortini and C. Gualdi, *Nuov. Cim.*, **B71**, 37 (1982).

[48] R. Forward, *Gen. Rel. Grav.*, **2**, 149 (1971).

[49] R. Forward, *Phys. Rev.*, **D17**, 379 (1978).

[50] G. Frossati and E. Coccia, *Cryogenics*, **34**, 9 (1994).

[51] Y.C. Fung, *Solid Mechanics*, Prentice-Hall, Englewood Cliffs (1965).

[52] R.L. Garwin and J. Levine, *Phys. Rev. Lett.*, **31**, 176 (1973).

[53] A. Giazotto, *Phys. Rep.*, **182**, 6 (1989).

[54] G.W. Gibbons and S.W. Hawking, *Phys. Rev.*, **D4**, 2191 (1971).

[55] J. Gittus, *Creep, Viscoelasticity and Creep Fracture in Solids*, Wiley, New York (1975).

[56] R.P. Giffard, *Phys. Rev.*, **D14**, 2478 (1976).

[57] E.N. Glass and J. Winicour, *J. Math. Phys.*, **13**, 1934 (1972).

[58] D. Graffi, *Sem. Mat. Fis. Univ. Modena*, **9**, 21 (1971).

[59] D.R. Guo and Z.X. Wang, *Special Functions*, World Scientific, Singapore (1989).

[60] Y.M. Haddad, *Viscoleasticity of Engineering Materials*, Chapman & Hall, London (1995).

[61] W.C. Hernández, *Phys. Rev.*, **D1**, 1013 (1970).

[62] R.G. Hier and S.N. Rasband, *Astrophys. J.*, **195**, 507 (1975).

[63] R.A. Hulse and J.H. Taylor, *Astrophys. J.*, **195**, L51 (1975).

[64] R.A. Hulse, *Rev. Mod. Phys.*, **66**, 699 (1994).

[65] R.A. Isaacson, *Phys. Rev.*, **166**, 1263 (1968).

[66] R.A. Isaacson, *Phys. Rev.*, **166**, 1272 (1968).

[67] J.D. Jackson, *Classical Eletrodynamics*, Wiley, New York (1962).

[68] P. Jaerisch, *J.f. Math. (Crelle)* **Bd. 88** (1880).

[69] W. Johnson and S.M. Merkowitz, *Phys. Rev. Lett.*, **70**, 2367 (1993).

[70] B.W. Kernighan and D.M. Ritchie, *The C Programming Language*, Prentice Hall, Englewood Cliffs N.J. (1978).

[71] H. Lamb, *Proc. London Math. Soc.* **13** (1882).

[72] L.D. Landau and E.M. Lifshitz, *Theory of Elasticity*, Pergamon, Oxford (1970).

[73] L.D. Landau and E.M. Lifshitz, *The Classical Theory of Fields*, Pergamon, Oxford (1962).

[74] P. Lebrun, *Cryogenics*, (ICEC 15 supplement) (1994).

[75] L. Lindblom and S.L. Detweiler, *Astrophys. J. Suppl.*, **53**, 73 (1983).

[76] J.A. Lobo, *Phys. Rev.*, **D52**, 591 (1995).

[77] J.A. Lobo, in *General Relativity, Proceedings of SUSSP-46*, edited by G.S. Hall and J.R. Pulham, SSUSP Publications, Bristol (1996).

[78] J.A. Lobo and J.A. Ortega, submitted to *Phys. Rev.* (1997).

[79] J.A. Lobo and M.A. Serrano, *Europhys. Lett.*, **35**, 253 (1996).

[80] A.E.H. Love, *A treatise on the mathemathical theory of elasticity*, Dover, New York (1944).

[81] N.S. Magalhães *et al*, *Mon. Not. R. Astron. Soc.*, **274**, 670 (1995).

[82] F. Mainardi (ed), *Wave propagation in viscoelastic media*, Pitman, London (1982).

[83] F.K. Manasse and C.W. Misner, *J. Math. Phys.*, **4**, 735 (1963).

[84] K.P. Marzlin, *Phys. Rev.*, **D50**, 888 (1994).

[85] G.A. Maugin, *Gen. Rel. Grav.*, **4**, 241 (1973).

[86] G.A. Maugin, *Gen. Rel. Grav.*, **5**, 13 (1974).

[87] G.A. Maugin, *J. Math. Phys.*, **19**, 1212 (1978).

[88] S.M. Merkowitz, *Ph.D. thesis*, Lousiana State University (1995).

[89] S.M. Merkowitz and W.W. Johnson, *Phys. Rev.*, **D51**, 2546 (1995).

[90] P.F. Michelson, *Mon. Not. R. Astron. Soc.*, **227**, 933 (1987).

[91] P.F. Michelson and C.Z. Zhou, *Phys. Rev.*, **D51**, 2517 (1995).

[92] J.P.C. Miller, in *British Association for the Advancement of Science, Bessel functions, Part I*, Cambridge University Press, Cambridge (1950).

[93] C.W. Misner, K.S. Thorne and J.A. Wheeler, *Gravitation*, Freeman, San Francisco (1973).

[94] C. Moreno, *Ph.D. Thesis*, IAC La Laguna (1994).

[95] P.M. Morse and H. Feshbach, *Methods of Theoretical Physics*, McGraw Hill, New York (1953).

[96] G.V. Pallotino and V. Pizzella, *Nuov. Cim.*, **C4**, 237 (1981).

[97] A. Papapetrou, *Ann. Inst. Henri Poincaré*, **16**, 63 (1972).

[98] V.Z. Parton and P.I. Perlin, *Mathematical methods of the theory of elasticity*, University Press, Moscou (1984).

[99] W. Pauli, *The Theory of Relativity*, Pergamon Press, London (1921).

[100] R.V. Pound and G.A. Rebka, *Phys. Rev. Lett.*, **4**, 337 (1960).

[101] W.H. Press, S.A. Teukolsky, B.P. Flannery and W.T. Vetterling, *Numerical Recipes in C. The Art of Scientific Computing* (2d. edition), Cambridge University Press, Cambridge (1992).

[102] W.H. Press and K.S. Thorne, *Ann. Rev. Astron. Astrophys.*, **10**, 335 (1972).

[103] J.C. Price, *Phys. Rev.*, **D36**, 3555 (1987).

[104] S.N. Rasband, *J. Acoust. Soc. Am.*, **57**, 899 (1975).

[105] M. Rees, R. Ruffini and J.A. Wheeler, *Black Holes, Gravitational Waves and Cosmology*, Gordon & Breach, New York (1974).

[106] N. Robertson, in *General Relativity, Proceedings of SUSSP-46*, edited by G.S. Hall and J.R. Pulham, SSUSP Publications, Bristol (1996).

[107] N. Rosen, *Phys. Rev.*, **71**, 54 (1947).

[108] R. Ruffini and J.A. Wheeler, *Proceedings of the Conference on Space Physics*, European Space Research Organization, Paris (1971).

[109] G. Salzman and A.H. Taub, *Phys. Rev.*, **95**, 1659 (1959).

[110] B.F. Schutz, *Class. Quant. Grav.*, **6**, 1761 (1989).

[111] B.F.Schutz in *Proceedings of GR13, Córdoba, Argentina*, edited by R.J. Gleiser, C.N. Kozameh and O.M. Moreschi, IOP (1993).

[112] N. Solomonson, W.O. Hamilton, W.W. Johnson and B. Xu, *Rev. Sci. Instrum.*, **65**, 174 (1994).

[113] J.M. Souriau, *Géométrie et Relativité*, Hermann, Paris (1974).

[114] J.L. Synge, *Math. Z.*, **72**, 82 (1969).

[115] J.H. Taylor, *Rev. Mod. Phys.*, **66**, 711 (1994).

[116] K.S. Thorne, *Rev. Mod. Phys.*, **52**, 299 (1980).

[117] K.S. Thorne, *Three Hundred Years of Gravitation*, edited by S.W. Hawking and W. Israel, Cambridge University Press, Cambridge (1987).

[118] S. Vitale, M. Cerdonio, E. Coccia and A. Ortolan, to appear in the February'97 issue of *Phys. Rev. D.*

[119] R.V. Wagoner and H.J. Paik, *Proceedings of International Symposium on Experimental Gravitation, Pavia*, Accademia Nazionale dei Lincei, Roma (1976).

[120] R.V. Wagoner and C. Will, *Astrophys. J.*, **210**, 764 (1976).

[121] R.M. Wald,*General Relativity*, The University of Chicago Press, Chicago (1984).

[122] J. Weber, *Phys. Rev.*, **117**, 306 (1960).

[123] J. Weber, *General Relativity and Gravitational Waves*, Interscience, New York (1961).

[124] J. Weber, *Phys. Rev. Lett.*, **17**, 1228 (1966).

[125] J. Weber, *Phys. Rev. Lett.*, **20**, 1307 (1968).

[126] J. Weber, *Phys. Rev. Lett.*, **22**, 1320 (1969).

[127] S. Weinberg, *Gravitation and Cosmology*, Wiley, New York (1972).

[128] H. Weyl,*Space–Time–Matter*, Methuen, London (1922).

[129] C.M. Will, *Theory and Experiment in Gravitational Physics*, Cambridge University Press, Cambridge (1992).

[130] C. Zener, *Elasticity and Anelasticity of Metals*, The University of Chicago Press, Chicago (1948).